Politecnico di Milano

School of industrial and information engineering

A Thermal Balance Test Prediction For a Geostationary Satellite

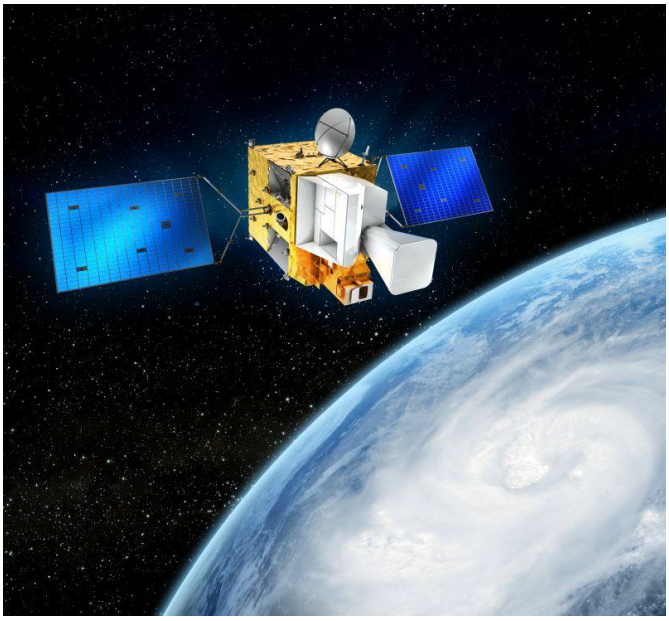

Supervisors : - Prof. Michèle Lavagna
- Dr.-Ing. Czupalla Markus

Fulvio Triberti - 804978

Academic Year 2014-2015

Acknowledgments

I would like to thank my parents that supported me through all my university career.

A big thanks to all the engineers at OHB that continuously shared with me their experience during the thesis development.

I am also grateful to all the professors of Politecnico di Milano, to whom I owe the knowledge gained in these years.

A special thanks goes to all my friends and colleagues, the best companions for this adventure.

Abstract

The Meteosat Third Generation (MTG) is the next European family of weather satellites born under the cooperation on meteorological missions between the European Space Agency and the European Organization for the Exploitation of Meteorological Satellites (EUMETSAT).

OHB AG was given the task to develop part of the satellite platform and an innovative payload, the InfraRed Sounder (IRS), which shall provide an increased accuracy in the temperature and humidity measurements, with respect to the actual state of the art of the weather satellites. Moreover, the IRS will introduce several improvements on the detection of the major air pollutants.

The development of the IRS includes the verification of the Thermal Control System (TCS) to be performed within a test campaign, that has to be designed and simulated with the aid of appropriate softwares before its physical execution. Part of this test campaign is the Thermal Balance Test (TBT), that will be executed in Noordwijk, Holland, inside of the Large Space Simulator (LSS), a test chamber part of the ESA thermal testing facilities.

The work of this thesis is the design and prediction of the Thermal Balance Test, which has as objectives the correlation of the Thermal Mathematical Model (TMM) with the physical model of the instrument, and the verification of the TCS suitability.

Chapter 1 presents a review of the most common techniques and devices for the thermal control, while in Chapter 2 a brief introduction to the ESA defined standard software for thermal analysis, ESATAN-TMS, is given. A basic knowledge of the IRS, useful to the comprehension of the thesis work, is provided in Chapter 3, focusing on the main characteristics of the thermal control architecture. Afterwards, Chapter 5 introduces the reader to the LSS, providing a description of its most important features. Chapter 6 explains the preparation work, by describing the set up of the test configuration. Core of the thesis is the description of the test phases, presented and analyzed in Chapter 7. Chapter 8 concludes the thesis work giving an outlook on the criticalities encountered and the open points left for the future developers of the Thermal Balance Test.

Contents

List of Figures

List of Tables

Chapter 1

Literature Review

1.1 Thermal Control System - Passive

Passive thermal control systems comprise all the solutions which do not imply the use neither of moving parts nor power consumptions. This makes them the simplest and cheapest way to protect the spacecraft from the environmental and internal heat fluxes, experienced in orbit by the spacecraft. In this section the most common solutions are presented.

1.1.1 Thermal Control Coatings

Outside Earth's atmosphere, the satellite is thermally coupled with the space environment exclusively through radiative exchange.

Direct solar radiation is the greatest source of heating, whose intensity is wavelength dependent and is approximately subdivided in 7% ultraviolet (UV), 46% visible and 47% near IR. Being all these wavelength intervals far enough from the IR energy emitted by a body at a near room temperature, one can distinguish the thermo-optical properties of a surface between the total solar absorptance α, and the total infrared emissivity ϵ. It follows immediately that these properties are considerably affecting the way the satellite reaches its thermal equilibrium.

An intuitive way to classify thermal control surfaces, shown in Figure 1.1, is to divide them into four basic types: solar absorber, flat absorber, flat reflector and solar reflector.

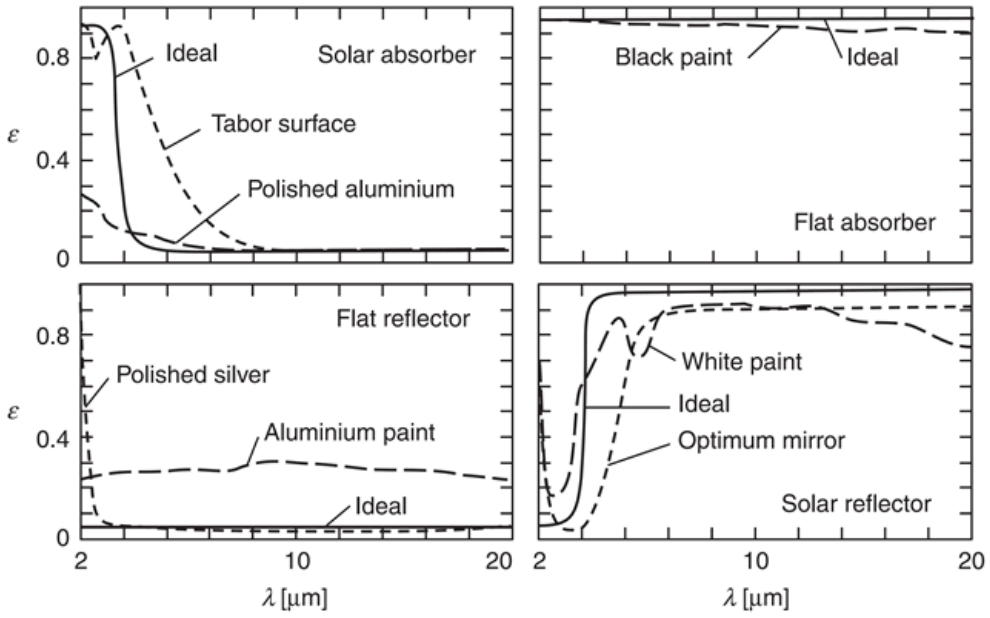

Figure 1.1: Spectral emissivity curves of the four ideal control surfaces types and of real substances (*Meseguer*).

All of the above mentioned types of surfaces are subject to degradation due to prolonged exposure to solar radiation, which increases the solar absorptance values (α), thus leading to a distinction between beginning of life (BOL) and end of life (EOL) properties. It follows that the EOL properties are normally used to define the hottest cases, while BOL thermo-optical properties are considered while considering the coldest cases calculations.

1.1.2 Multi-Layer-Insulation

One of the main insulation systems is the Multi-Layer-Insulation (MLI), consisting of numerous layers interposed to the heat flow. Their principal uses are to insulate the spacecraft from the outer radiation environment, or to achieve radiatively decoupled regions inside of it.

The inner layers are very thin (typically 15-25 layers of $7\mu m$) made of Kapton or Mylar and then coated with vapor deposited aluminium on both sides to guarantee a low emissivity and a high reflectivity, resulting in a lowering of the radiative heat flow. The outer cover, more important from the mechanical point of view, is usually a thicker layer ($125\mu m$) of Kapton and is aluminized only on its internal face to avoid degradation due to UV radiation. Should an improve of the mechanical properties be necessary, e.g. for micrometeoroids protection, materials such as beta-cloth offer a higher resistance.

Non-metallic low conductive spacers are placed at each layer's contact interface to avoid conduction with the spacecraft structure.

An electrostatic discharge is typically prevented through the presence of a bolt all along the thickness of the MLI, grounding the layers to the structure.

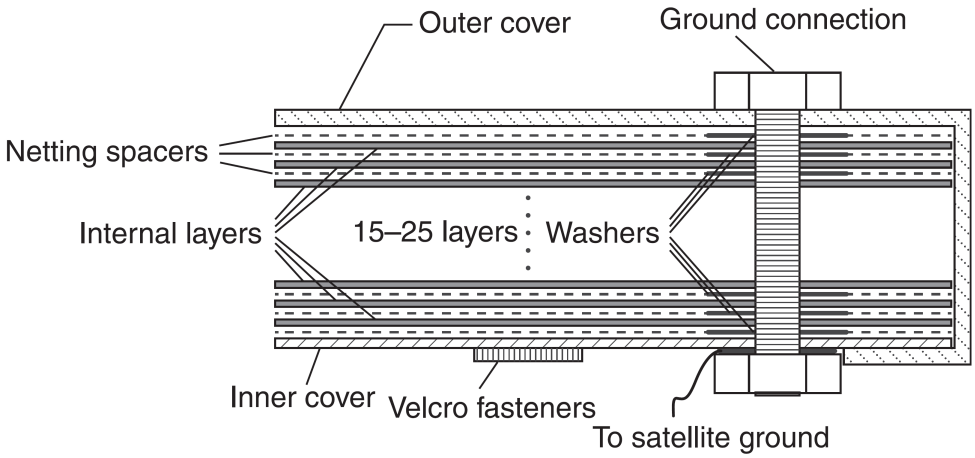

Figure 1.2: Typical multi-layer insulation configuration (*Meseguer*).

1.1.3 Heat Pipes

Heat pipes are heat-transfer devices which can transport high heat quantities. The functional scheme of a heat pipe, depicted in Figure 1.3, can be represented as a sealed structure, typically of cylindrical shape. It contains a working fluid, whose movement inside the structure allows the heat exchange at the two extremes of the heat pipe. The selection of the fluid is to be done on the basis of the desired operating temperature and of the chemical compatibility with the heat

pipe material. As heat is applied to the evaporator, the fluid in the wick start to evaporate letting the vapor fill the core region of the pipe, while on the opposite side the heat removed causes the vapor to condensate on the wick. The generation of the vapor at the evaporator and its depletion at the condenser create a pressure gradient which causes the motion of the vapor from the hot to the cold end of the pipe. Due to a combination of capillary effects and of the evaporation and depletion of the vapor, the pressure gradient inside the fluid generates a movement from the condenser towards the evaporator, thus closing the flow circuit.

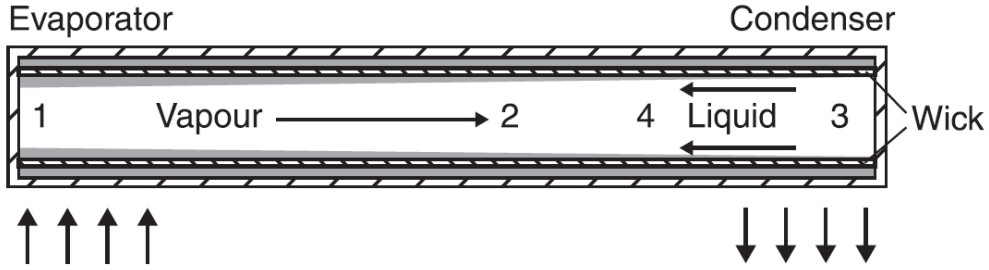

Figure 1.3: Heat pipe functional scheme (*Meseguer*).

A broadly affirmed variation of this device is the loop heat pipe, whose schematic is reported in Figure 1.4, and consists of a condenser, an evaporator, a compensation chamber reservoir, and two separate lines for the liquid and the vapor. Such devices are capable of heat transport performances one order of magnitude higher than those of ordinary heat pipes, allowing a quick heat removal from the source towards distant heat sinks, exploiting their slender transport lines.

1.1.4 Radiators

The design of the thermal control system of a satellite is macroscopically achieved by searching for the balance of the energy absorbed from the environment, the energy produced by the internal equipment and the energy emitted by the satellite. The waste heat is rejected to space by means of radiators, which are surfaces usually mounted on the exterior part of the satellite with the aim of taking the thermal energy in excess from the heat source and dispersing it through infrared radiation. The typical thermal coating for these components is characterized by a high infrared emissivity, to maximize the heat transfer towards space, and by a low solar absorptance, to limit heat absorption from both the sun and solar reflections on the spacecraft surface. According to the type of connection between them and

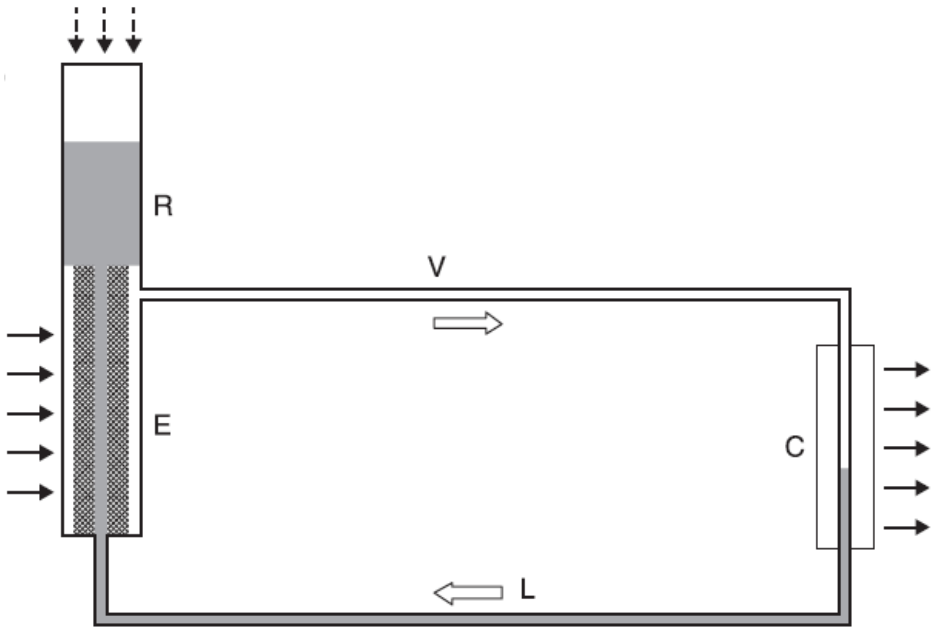

Figure 1.4: Loop heat pipe schematic: R, compensation chamber reservoir; E, evaporator; C, condenser; L, liquid line; V, vapor line. (*Meseguer*).

the heat source, radiators are often classified as passive or active. In the first case the connection is established either through direct contact or by means of heat pipes, while in the second case the thermal link is based on the use of fluid loops, which can sometimes be integrated with heat pipes.

When a heat pipe configuration is used for passive radiators, the condensers of the pipes are places in proximity of the heat source, while the evaporators are attached to the radiator. Within active radiators the working fluid is generally a two-phase fluid entering the radiator in vapor phase and leaving it as a liquid, while the inverse phase change happens at the heat source. When the link between the radiator and the heat source is created through a combination of fluid loops and heat pipes, the working fluid of the loop carries the heat from the source to the radiator, while the heat pipes are exploited as distributors of the heat along the radiator surface.

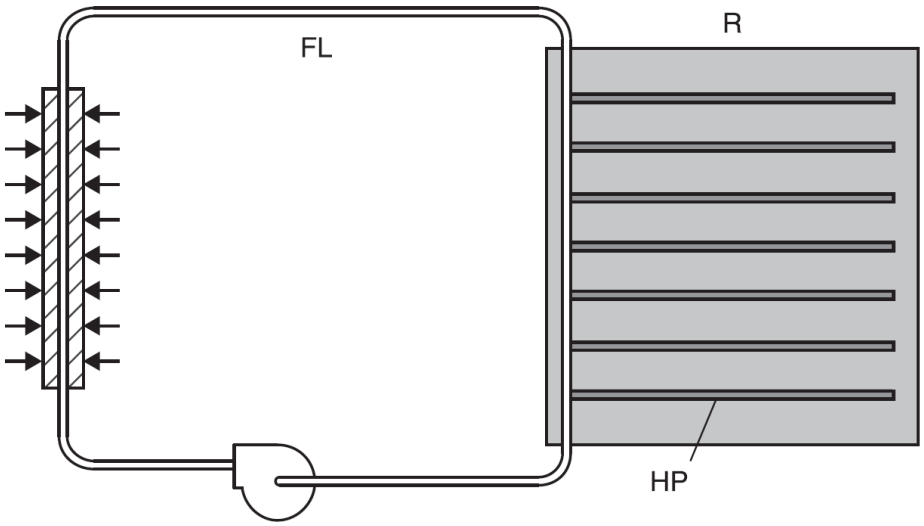

Figure 1.5: Typical radiator (R) configuration with fluid loop (FL) and heat pipes (HP) (*Meseguer*)

1.2 Thermal Control System - Active

Many different factors such as a non constant heat generating components, orbit and seasonal variations of the environmental fluxes, or the degradation of the surface finishes over the lifetime of the space vehicle would lead to temperature ranges impossible to be tolerated by every component. Because of this, an active thermal control sometimes has to be developed, of which some meaningful examples are here presented.

1.2.1 Heaters

When the attainment of specific temperature ranges of the spacecraft components implies a heat generation, installation of electrical heaters may be a valid solution to keep the components above their minimal operational or survival temperatures, or more generally to implement a desired temperature control. The most common type of these devices is the film heater, an electrical-resistance element included between two layers of electrically insulating material (Figure 1.6). Due to its thickness and flexibility, it can be installed on both curved and flat surfaces. The control of the power to be injected by the heater is achieved through thermostats

or solid-state controllers, responsible for the heat modulation depending on a preset temperature. Of course the exploitation of such devices is possible only provided the adequate power availability aboard, which in some cases may not be present.

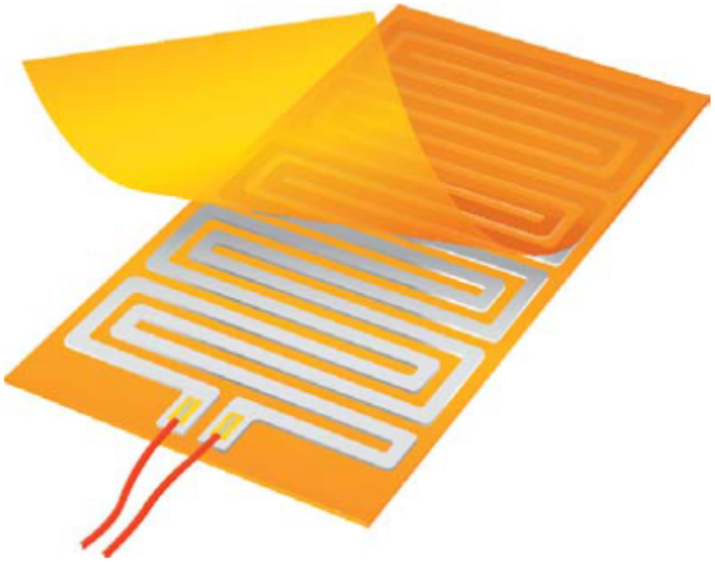

Figure 1.6: Example of a Flexible Film Heater (*minco.com*).

1.2.2 Cryogenic Systems

The performance of Earth observation instruments, such as IR telescopes, highly depends on the detector temperature, which needs to be stabilized at its design value, typically beneath 100 K, for the whole observation time. This task is achieved through cryogenic systems, responsible for evacuating the heat from a cold region, the detector, to a hot one, where the heat is then radiated to space. A cryocooler performs the cooling process following either an open loop or a closed loop cycle.

The first type involves the use of stored cryogenic materials, solid or liquid, which, through evaporation, act as a heat sink until the extinction of resources, which means a limited operational life depending on the quantity of cryogenic material stored.

Closed loop cryocoolers exploit moving parts such as compressors, so that

heat is extracted in proximity of the working fluid expansion, while at the compression region the heat is rejected. In this way the dependence on the on-board reservoirs can be avoided.

From a power budget point of view, open loop cryogenic systems do not need additional energy for their use, while closed cycle cryocoolers need a continuous work in order to extract thermal energy from a cold region to a hotter one.

In Figure 1.7 the black arrows represent the heat transfer direction in a space cooler, showing how the energy is directed from the detector to the radiator passing through the cold finger of the cryocooler at which the detector is attached.

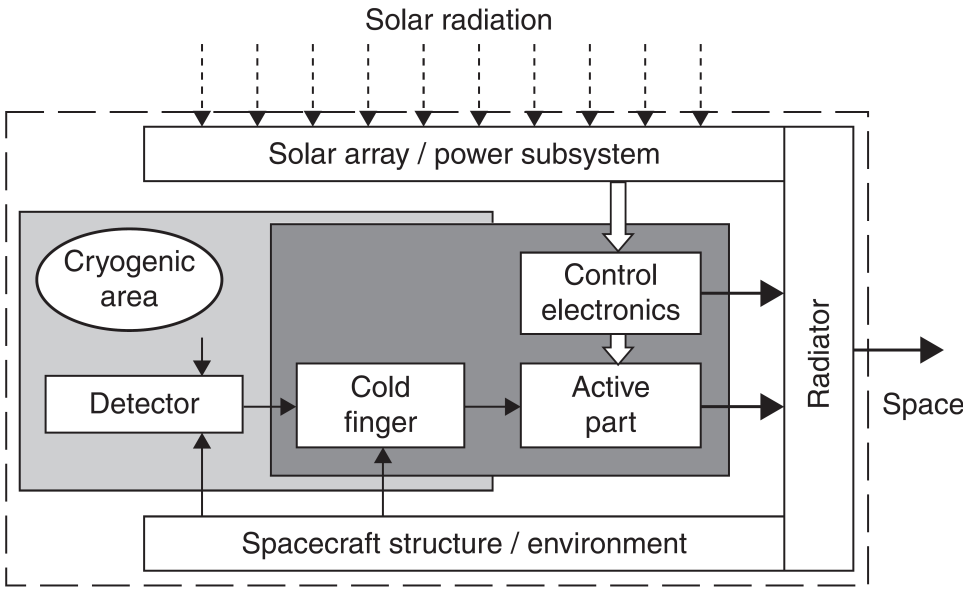

Figure 1.7: Closed cycle cryocooler block diagram (*Meseguer*)

Chapter 2

ESATAN-TMS

ESATAN-TMS, supplied by ITP Engines UK, is the ESA defined standard software tool for thermal modeling and analysis. Besides the conventional thermal calculations, the program is designed for space applications and it allows the user to perform orbital analysis simulating the space environment. The program adopts the so called *lumped parameter method*, where the geometry is divided into a discrete number of thermal nodes represented as points, onto which the thermal properties (heat capacity, heat fluxes, temperature, etc) are assumed to be concentrated.

The standard procedure for setting up and executing a thermal analysis in ESATAN-TMS consists of three steps, that contribute to form the two main models needed to complete an analysis: the Geometrical Mathematical Model (GMM) and the Thermal Mathematical Model (TMM).

1. **Spacecraft Geometry**. The user can decide to build the model either through the ESATAN-TMS GUI (Graphic User Interface) directly, or through the conversion of a meshed geometry created with a different software.

   What is typically asked to be defined in this step is the primitive geometry, the creation of a mesh, the bulk and thermo-optical properties, the activities of the nodes (which can be set as active or inactive from both a conductive and radiative point of view), while the typical outputs are the conductive couplings between nodes (GLs).

   Apart from the creation of a model hierarchy where the submodels can be organized, in this section it is also possible to define the presence of rela-

tive movements between different parts of the geometry, through built in functions called "*Assemblies*" in the ESATAN-TMS language.

2. **Radiative Case**. In this section the user is first asked to define the trajectory of the spacecraft which can be expressed either through orbital parameters, reduced arcs of interest, or through a matrix reflecting the positions and velocities of the orbit.

   The attitude of the spacecraft can also be taken into account, as well as celestial body properties such as the planet and Sun temperature, the albedo coefficient and the solar constant. As a second step the calculation types have to be stated, depending on which kind of results are needed.

   ESATAN-TMS allows one to calculate, among other things, View Factors (VFs), Radiative Exchange Factors (REFs) and SAFs (Solar Absorbed Fluxes), results that can be either static or time dependent, according to the chosen settings. Their calculation is performed by means of the MCRT (Monte Carlo Ray Tracing), a very powerful simulation method where a high number of rays is emitted by each node and then traced until complete absorption; in the radiative case many options are available to set the accuracy of this method, which as shown in Figure 2.2, is proportional to the square root of the number of rays fired. This last option allows the user to directly control the duration of the calculation, which decreases if a lower accuracy is selected.

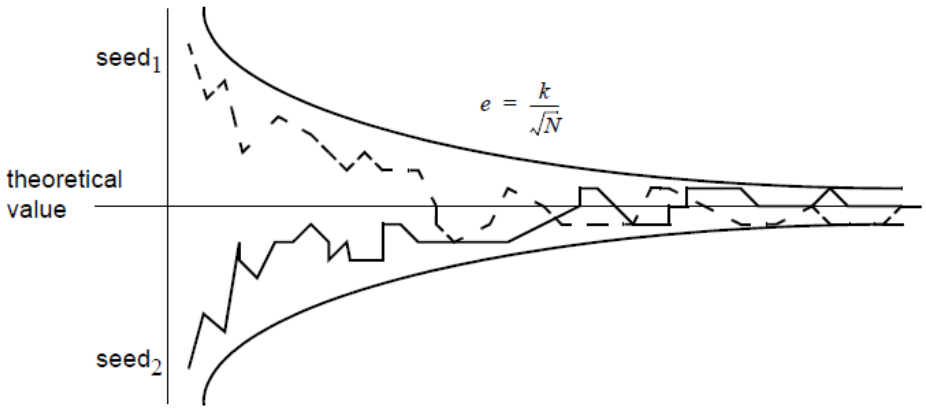

Figure 2.2: MCRT Error Evolution - e = error, N = number of rays fired, k = proportionality constant (*ITP Engines UK Ltd.*)

3. **Analysis Case (TMM)** . The final stage in the processing of a model is to

set up, solve and post-process the thermal analysis. The set up is specified within an "Analysis Case", where before solving the user can include:

- Node Data
- Group Definitions
- Boundary Conditions
- Conductive Couplings
- Radiative Exchange Factors
- Solar, Planet and Albedo Fluxes

A possibility is also given to specify the solution type and the preferred routine. It is worth mentioning the possibility to run the analysis in a batch-mode, where a source file containing the model definition in the standard ESATAN format is first manually edited and then read by the program. More specifically, the input source file contains two blocks of data, the *Data Blocks* which includes model topology, nodes, conductances and material properties, and the *Operation Blocks*, containing instructions to be performed on the model defined within the Data Blocks during the solution. The customization of these latter blocks, written in a language called *Mortran* (*M*ore F*ortran*, an extension of Fortran 77), allows a very high flexibility when complex or unconventional simulations have to be executed.

For the elaboration of the results ESATAN-TMS gives the possibility to graphically visualize some outputs directly on the model geometry, while the graphs and diagrams can be obtained through a built-in tool named ThermNV. Its use is not mandatory since the output result files can be post-processed by following alternative routes, for example by programming a Matlab® results reader.

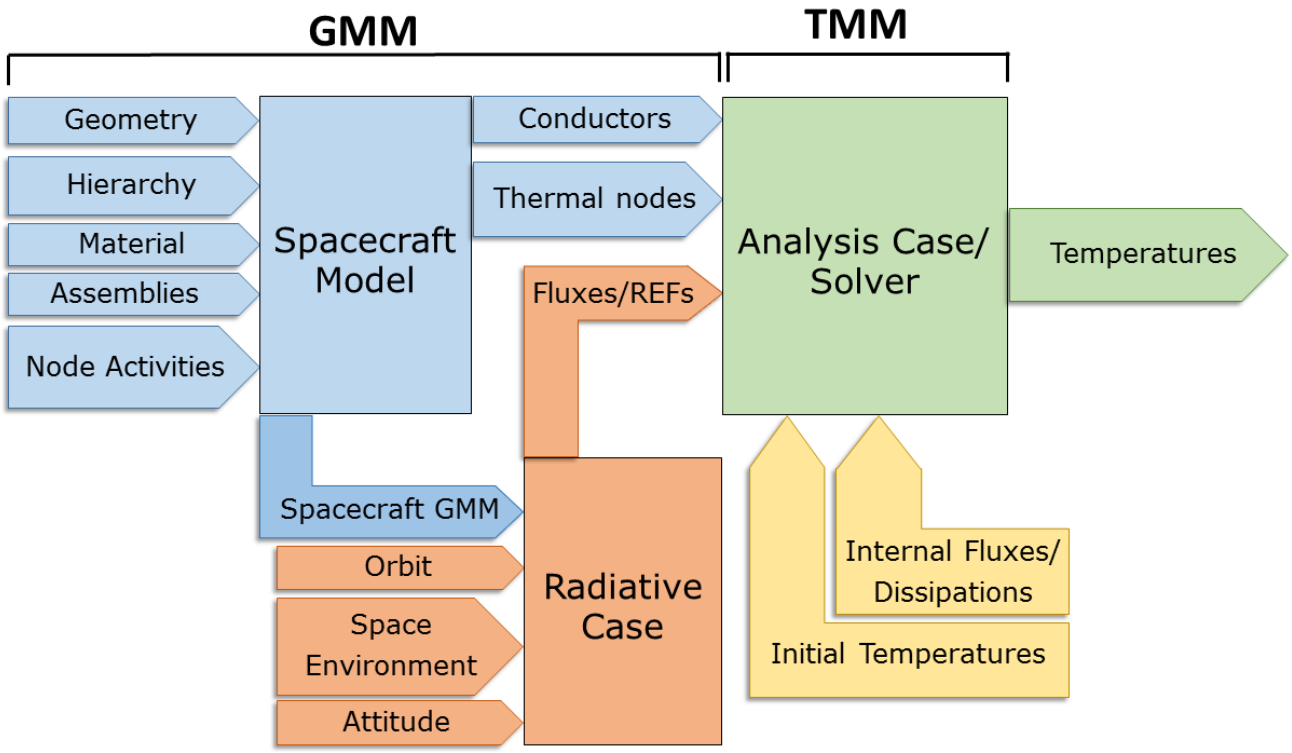

Figure 2.1: Flowchart of the Standard Procedure to complete a Thermal Analysis in ESATAN-TMS

Chapter 3

MTG

The Meteosat Third Generation program, established through cooperation between the European Organisation for the Exploitation of Meteorological Satellites (EUMETSAT) and the European Space Agency, comprises a twin satellite concept intended to provide accurate meteorological data for an overall duration of twenty years starting from 2017.

The platforms involved consist of four Imaging satellites (MTG-I) and two Sounding satellites (MTG-S), whose differences lie on the payloads carried on board. The imaging satellites will fly the Flexible Combined Imager (FCI), which will introduce improvements in the solar and infrared measurements, and the Lightning Imager (LI), an instrument that, through the observation of total lightning over the atmosphere, will produce sensible data to the short range detection of severe weather events and to the ozone conversion process and the acid rain generation. The sounding satellites will carry the Sentinel-4 instrument, a high resolution spectrometer taking measurements in the ultraviolet (305-400 nm), the visible (400-500 nm) and the near infrared (755-775 nm), and the Infrared Sounder (IRS), which will be better described in this chapter.

3.1 The Mission

The MTG-S is a geostationary satellite, whose orbit and attitude are defined by:

- Altitude: 35786 km
- Orbital Period 23.94 h
- Nominal Inclination: $0°/\pm 1°$

Local Vertical Local Horizontal Axis	From Autumnal to Spring equinox	From Spring to Autumnal equinox
Speed Vector (Roll)	$+X_{sc}$	$-X_{sc}$
South Direction (Pitch)	$+Y_{sc}$	$-Y_{sc}$
Nadir (Yaw)	$+Z_{sc}$	$+Z_{sc}$

Table 3.1: MTG-S Attitude

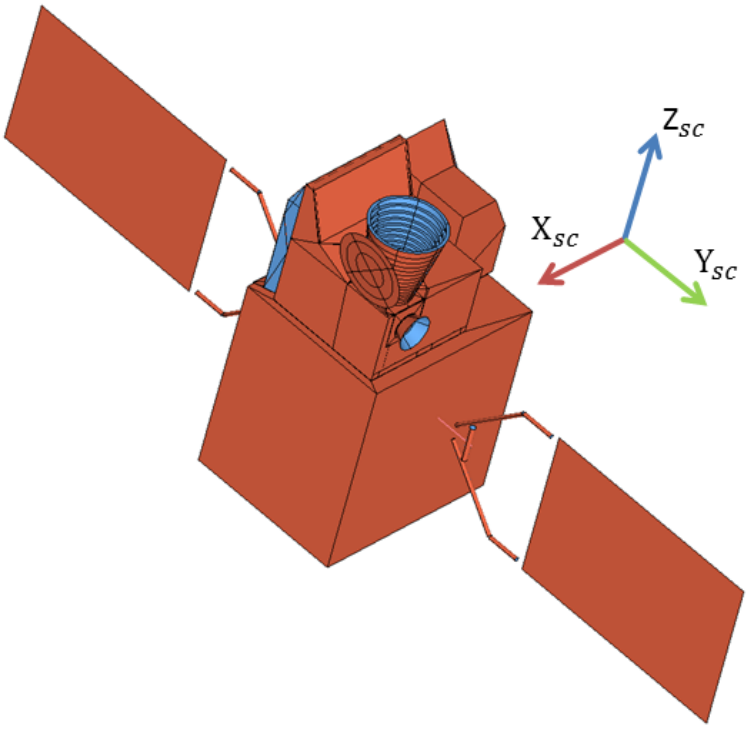

Figure 3.1: MTG Axis Orientation

The $+Z_{sc}$ axis is Earth pointed during operational modes, while, as understandable from Table 3.1, twice a year the attitude of the satellite shows a change, consisting in a yaw flip manoeuvre at each equinox season. Aim of this manoeuvre is to rotate the $+Ysc$ axis of 180° about the yaw axis, in order to ensure that the $-Ysc$ face of the satellite is not sun illuminated during nominal operations. The $-Ysc$ face of the satellite is in fact the one housing the majority of the radiators, an exception being the encoder radiator visible in Figure 3.1 directed in the $+Ysc$ axis and protected by a baffle.

During the Safe Mode the $-Z_{sc}$ face and the solar panels are sun pointed, thus keeping the solar baffle protected from the sun rays.

3.2 Infrared Sounder - IRS

The Infrared Sounder is based on an imaging interferometer (Fourier Transform Spectrometer) that will support, as a primary objective, the Numerical Weather Prediction by providing detailed horizontal, vertical and temporal profiles of temperature and humidity, with an increased spatial resolution and sampling frequency with respect to the actual availability. The IRS will take measurements in two bands, disposing of 800 spectral channels in the Long-Wave InfraRed (LWIR - from 14.3 to 8.3 μm) and 920 channels in the Mid-Wave InfraRed (MWIR - from 6.25 to 4.6 μm). As a secondary objective of the mission, the IRS will monitor atmospheric trace gases. The spectral range of acquisition of the IRS includes in fact the ozone and carbon monoxide absorption bands, offering information about the level of pollution below the free troposphere.

Figure 3.2 shows a functional sketch of the IRS, offering an overview of the different components of the instrument. Directly exposed to the Earth view is the Solar Baffle, protecting the inside from excessive solar intrusion. At the basis of the solar baffle is the Scanner, the first mirror encountered by the Earth's light, whose main function is to direct the screening action towards the selected area of interest. Its field of view is slightly wider than the Earth's disk, as understandable in Figure 3.5. All around the light path starting from the scanner, passing on the first optics M1 and arriving at the second mirror M2, is an inner baffle intended to absorb the incoming sunlight, avoiding undesired reflections on the mirrors. Between the second and the third optics M3 the Calibration and Obturation Mechanism (COM) operates as a trigger for sun avoidance solutions or for

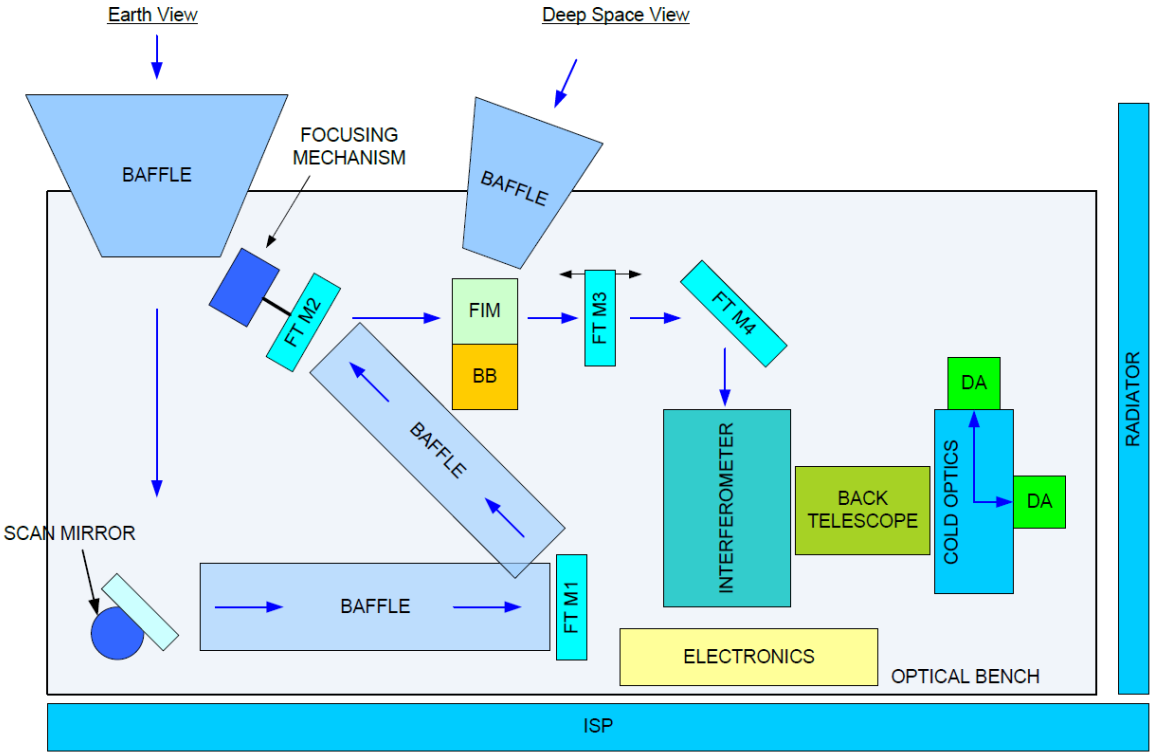

Figure 3.2: IRS Functional Skecth

calibration purposes. The COM consists of by the movable Flip In Mirror, and a Black Body (BB) of know temperature used for calibration purposes. Immediately after, the M4 directs the rays into the interferometer and then, through the Back Telescope Assembly (BTA), the rays finally reach the Detection Assembly (DA), where the two dimensional LWIR and MWIR detectors are thermally controlled by a cryocooler. All the mirrors and relevant optical systems are rigidly installed on to the Optical Bench Assembly (OBA), whose function is to provide a thermoelastic stable environment for the correct development of the optical path. On the outer part of the instrument several radiators are placed, among which the one dedicated to the cryocooler. Beneath the Optical Bench the Instrument Support Panel (ISP) is found, which provides the fixation of the payload to the rest of the platform.

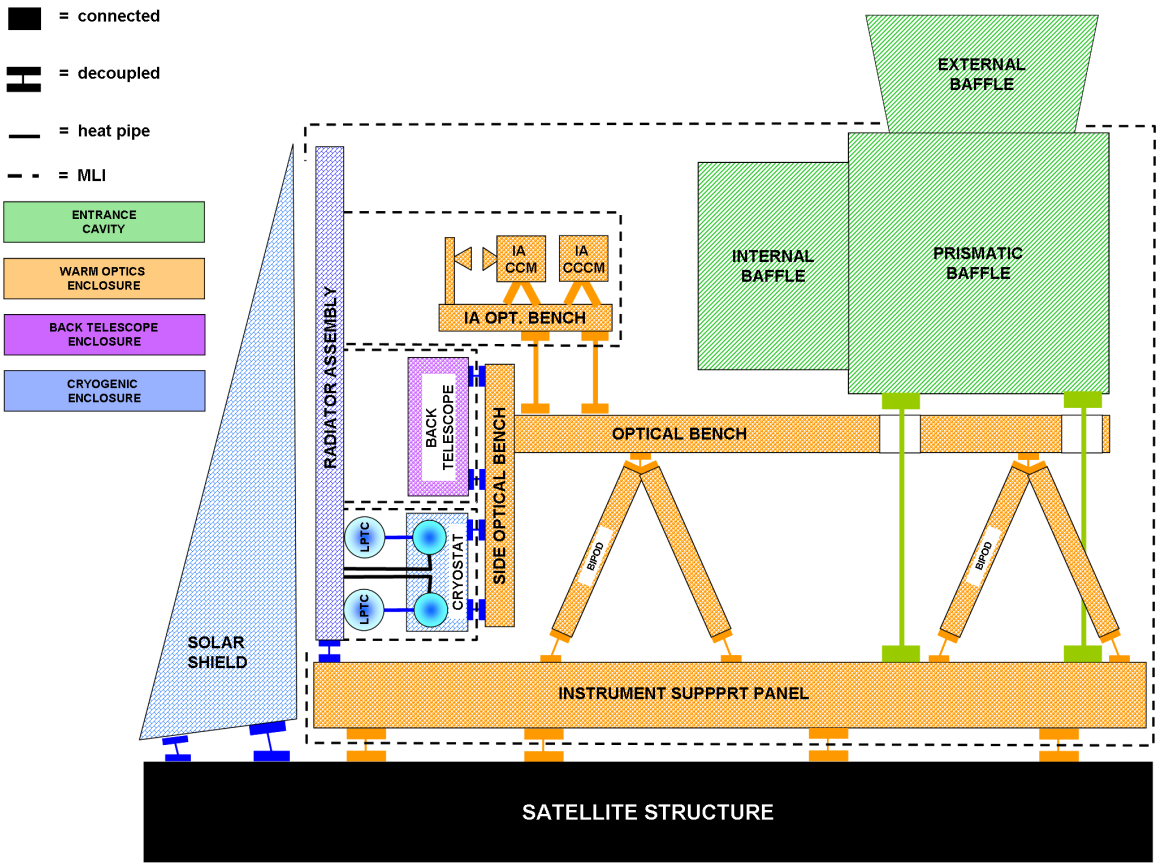

Figure 3.3: MTG Thermal Enclosures

3.3 Thermal Control Design of the Infrared Sounder

The IRS is thermally designed to guarantee the most stable thermal environment for the optical systems throughout the mission. The design concept of the IRS is such that the instrument is split into four thermal enclosures (Figure 3.3), decoupled from each other. The IRS itself is also disconnected from the satellite platform by means of thermal washers and MLI. The objectives of stability are met through a combined use of active and passive approaches.

The Entrance Baffling Assemblies (EBA) receive a high level of environmental fluxes, whose transport to the spacecraft and to the rest of instrument is avoided by means of the above mentioned decoupling of the enclosures and through supporting blades in titanium. The EBA has the task of preventing the external fluxes from

penetrating the inside of the instrument, a task that is achieved with the presence of vanes all along the baffles. With the exception of the solar baffle, which is white painted, and of the radiators, all the external elements of the instrument are covered with MLI. Another passive control strategy used on the IRS is represented by the radiators, installed on the $-Y_{sc}$ face of the spacecraft, which are used as a first basis in the control design of the payload.

Depending on the components, tighter ranges of temperatures are then achieved through an active thermal control. It consists firstly of a cooling system that keeps the detectors at their operational temperature range by means of a cryocooler and secondarily of the heating system that maintains several components of the instrument at their nominal temperature or above their survival limit.

The heating system makes use of two groups of heaters, the Operational and the Survival Thermal Lines (OTL and STL). The first group of thermal lines ensures stable temperatures during the operational modes of the instrument, and it is operated with proportional-integrative-derivative controllers. The second one is a survival heating system, whose aim is to maintain the temperatures above their switch-on limit during non-operational modes, and is operated through thermostats, meaning that their injected power has a fixed level when turned on, and it is zero when switched off. From a power budget point of view, the operational thermal lines are more numerous and have a higher total power than the survival ones, that dispose of a lower power availability but distributed between a smaller number of lines.

3.4 IRS Scanner

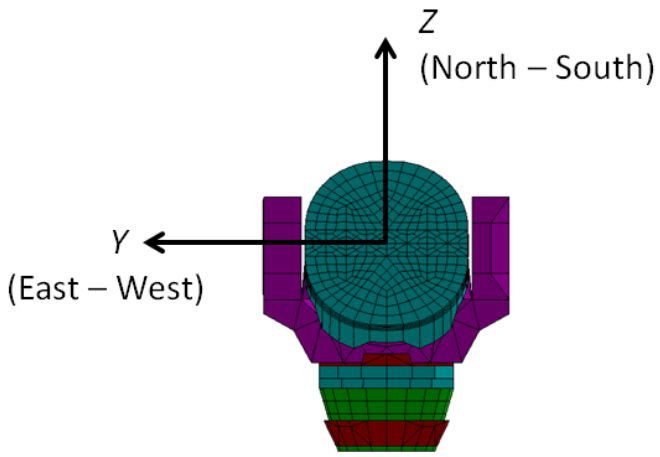

Figure 3.4: IRS Scanning Mirror

The first reflecting surface encountered by the light on its way to the detectors is the is the Scanner, also referred to as M0, and it plays a key role in the sun ray deviation inside the instrument, since it directs the measurements over different regions of the Earths disk. Within its screening action, it can rotate about Y and Z axes, shifting the observation along the North-South and East-West direction of the Earth respectively. Its maximum extensions are reported in Table 3.2.

Rotation	Angles Allowed
North-South (NS)	±9.7°
East-West (EW)	±5.4°

Table 3.2: Scanning Capacity of the M0

During the operational cases, its movement is dictated by a scan law, otherwise the scanner is left in its canonical position, corresponding to the values NS = ±0.0°, EW = ±0.0°, as happens for the safe mode configuration.

3.5 Thermal Sizing Cases

The defined load cases for the IRS are ten, and they differ from each other according to the optical properties, internal dissipations and solar heat fluxes (Earth infrared radiation and albedo are not considered in the analysis). In Table 3.3 are reported the most meaningful of them, that are also the ones considered for the thermal balance test.

Name	Optical Properties	Internal Dissipations	Solar Declination	Solar Constant
D56EOL	EOL	max	$-8.996°$	1398 W
EQBOL	BOL	min	$-0.0617°$	1371 W
SSBOL	BOL	min	$+23.45°$	1326 W
SAFE	BOL	none	$-0.0617°$	1371 W

Table 3.3: Selected Load Cases of the IRS

The name of the first case, D56EOL, stands for Day 56 End Of Life and it refers to the 56^{th} day of the orbit. This day is important because it is coincident with the longest time of residence of the sun in the Solar Baffle field of view. The sun declination in this day is such that the apparent movement of the sun describes a line tangent to the Earth's disc, impinging the front optics and the inner baffle for the longest time. The end-of-life condition is selected because it is the one which causes a higher income of environmental fluxes. EQBOL stands for EQuinox Beginning Of Life, referring to those two days during the year when the sun crosses the celestial equator. This special condition makes the eclipse last the longest, 72 minutes from a geostationary orbit, reason why Equinox is one of the cold cases for the IRS. SSBOL stands for Summer Solstice Beginning Of Life, and it indicates that day during the year when the sun declination is at its maximum and the solar radiation measured on the spacecraft surface is at its minimum.

The fact that the sun is maintained out of the field of view of the solar baffle makes the Summer Solstice another cold case to be analyzed. The last case is the SAFE mode, a non operational case where the solar baffle points towards outer space and an active temperature control exists only through the survival thermal

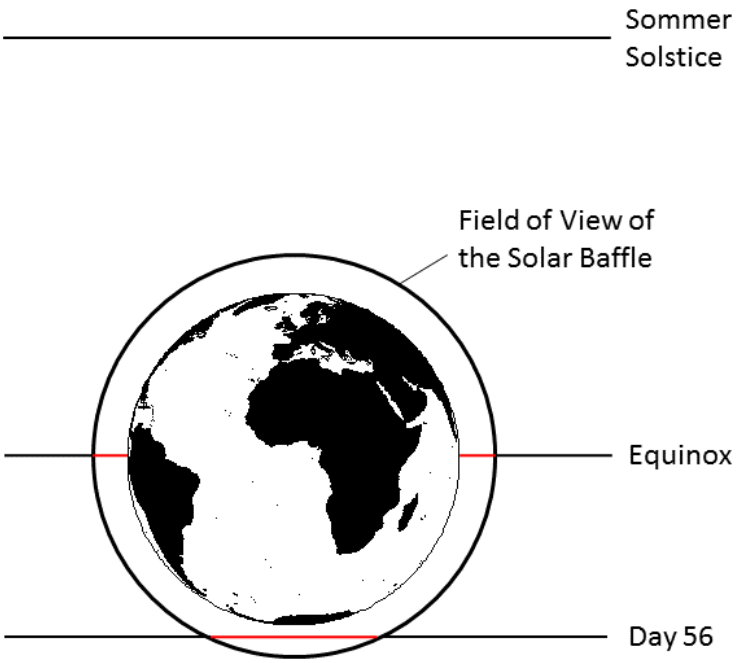

Figure 3.5: Sun Position and Sun Intrusion during the Main Load Cases. The red lines represent the Sun Intrusion into the Solar Baffle.

lines. The internal dissipations are either set to the maximum level for D56EOL, to the minimum for the cold cases, and not considered for the safe mode.

3.6 Dissipating Units

In Table 3.4 the dissipations of the components concurring to the load cases definition are reported. According to the test phases presented in Chapter 7, the internal dissipations will be set either to maximum, minimum or "OFF", where no dissipations are considered.

Unit	Maximum [W]	Minimum [W]
Instrument Control Unit (ICE)	20.0	10.0
Corner Cube (CC)	1.0	0.0
Receiver Assembly Unit (RAU)	2.4	1.2
Laser Assembly Unit	7.7	3.9
Front End Electronics	22.0	11.0
Scanner	6.5	4.4

Table 3.4: Internal Dissipations. Minimum and Maximum Values.

Chapter 4

Thermal Balance Test - TBT

Together with the Thermal Cycling, the Thermal Balance test is part of the thermal verification process to which a test object, normally at a high integration level such as a spacecraft or a payload modules, is subjected.

The objectives of such a test, as defined by the European Cooperation for Space Standardization (ECSS), are:

- To provide data for the verification of the numeric model of the test object. The information obtained from the test, for example temperature profiles, will be exploited to tune the parameters of the numeric model, in order to reach a satisfying adherence with the test results.
- To demonstrate the suitability of the thermal control system design. During the test the different control techniques are observed, and the quality of the choices made during the design phase is evaluated.
- To verify the performance of the hardware. The proper functioning of the thermal control system hardware is verified.
- To provide sensitivity data. The response of certain components of the thermal control system, for example the heaters power, is evaluated with respect to a change in some meaningful parameters, such as the heater set point temperature.

The reliability and the accuracy of the data to be provided by the test, which serve as an input to the numerical model correlation, are strictly connected to the congruence existing between the conditions of the real test and of the test simulation.

For this reason a correct modeling of the test chamber, together with a careful conduction of the predicted actions to be taken during the test, are two indispensable assumptions for a successful execution of the thermal balance test. According to the ECSS standard, the test shall include at least two steady state and one transient case. To these, more specific test cases are then added if a peculiar behavior of the test item has to be better observed, or if a higher number of cases is thought to be necessary for the test purposes.

A Thermal Balance Test has to be considered successful when the temperatures reached during the test are sufficiently close to the predicted ones. Typical values for the acceptance of these temperature deviations are defined by the ECSS standard, which indicates as satisfactory the values reported in Table 4.1.

Internal Units ΔT	5 K
External Units ΔT	10 K
Temperature Mean Deviation	2 K
Temperature Standard Deviation	3 K

Table 4.1: ECSS Defined Correlation Success Minimum Criteria

The temperature mean deviation (ΔT_{mean}) is the sum of the temperature differences between the measured and predicted values considered on comparable points of the numeric and real model, divided by the number of samples taken. It is defined as:

$$\Delta \mathrm{T}_{\mathrm{mean}} = \frac{1}{N} \sum_{i=1}^{N} (T_{Mi} - T_{Pi}) \tag{4.1}$$

The temperature standard deviation (σ) is a measure of the statistical dispersion of the temperature deviations, expressing how widely spread the values of temperature differences in a data set are. It is defined as:

$$\sigma = \sqrt{\frac{1}{N-1}\sum_{i=1}^{N}\left[(T_{Mi} - T_{Pi}) - \Delta T_{mean}\right]^2} \tag{4.2}$$

where T_{Mi} is the temperature acquired on the channel i , T_{Pi} is the predicted temperature on the correspondent node i, and N is the number of samples.

Chapter 5

LSS

Part of the ESTEC Test Centre of ESA, located in Noordwijk, Netherlands, the Large Space Simulator is a test facility well suited to conduct thermal balance and thermal vacuum tests on spacecrafts, and it comprises the following subsystems:

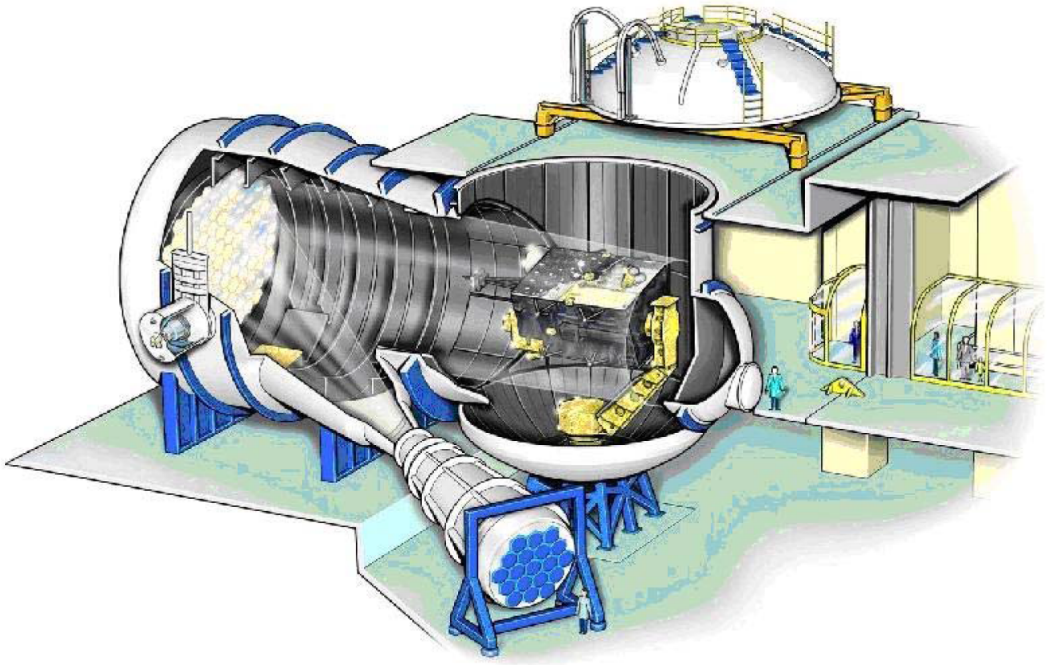

Figure 5.1: Large Space Simulator (Artistic view)

1. **LSS Chamber**. Depicted in Figure 5.1, it consists in turn of three main parts, the first of which is the *Main Vacuum Chamber*, a vertical cylinder where the satellite is placed during the test, the *Auxiliary Chamber*, a horizontal cylinder into which the mirror and the cryopumps are placed, and the *Seismic Block*, installed at the bottom of the Main Chamber with the aim to accommodate the interface structure to the satellite.

Main Chamber	
Diameter	9.5 m
Height	10 m
Auxiliary Chamber	
Diameter	$[8; 11.5]$ m
Height	14.5 m
Seismic Block	
Mass	90000 kg
Load Capability	60000 kg

Table 5.1: LSS Chamber dimensions

2. **Vacuum Pumping System**. The depressurization is achieved through a preliminary use of the Central Pumping System (CPS), which allows the chamber to reach a vacuum level of 2×10^{-2} $mbar$, followed by the start of the High Vacuum Pumping system (HVP), that lowers the pressure until 5×10^{-6} $mbar$. The HVP consists of:

   - 2× Liquid Nitrogen cooled cryopanels
   - 4× Turbo Molecular (TM) pumps and associated rotary pumps
   - 2× 20K - Cryopumps
   - 1× Helium Cryopump

   The typical duration for the depressurization and repressurization procedures are respectively of 16 and 10 hours.

3. **Shroud and Nitrogen Supply Equipment**.

   The LSS shroud temperature is controlled in the Main Chamber either in LN2 mode (Liquid Nitrogen), or in GN2 mode (Gaseous Nitrogen), while the shrouds of the Auxiliary Chamber are always controlled in the LN2 mode.

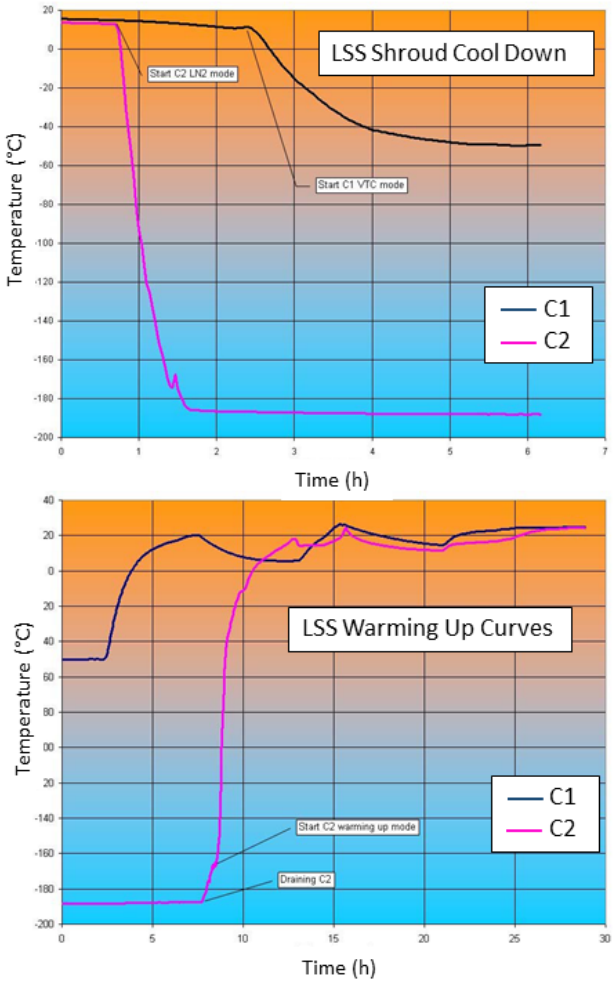

Figure 5.2: Cool Down and Warm Up Phases in the two Control Modes for the Main Chamber (C1) and the Auxiliary Chamber (C2)

4. **Sun Simulator**. It consists of 19 Xenon lamps whose radiation is projected through an optical integrator onto the collimation mirror placed in the Auxiliary Chamber. Its purpose is to provide a homogeneous parallel light beam in

Black wall surface temperature (LN2 mode)	$< 100\ K$
Black wall surface temperature (GN2 mode)	150 - 350 K
Thermal Coating	Chemglaze Z306
Infrared emissivity	0.90
Solar absorptivity	0.95

Table 5.2: Shrouds and Nitrogen Supply Equipment Characteristics

the test volume. The mirror structure is thermally controlled in GN2 mode between 26°C and 120°C to prevent contamination on its surface. The intensity level can be controlled in automatic or manual mode, and a shutter is available to simulate eclipses, acting between the Xenon lamps and the entrance to the Auxiliary Chamber. The test facility provides the possibility to synchronize the shuttering action with the motion system onto which the satellite is installed.

12 Lamps Intensity	1378 W/m^2
Maximum Intensity	2600 W/m^2
Stability	$\pm 0.5\%$
Mirror Infrared emissivity	0.015
Mirror Solar absorptivity	0.130

Table 5.3: Sun Simulator Main Characteristics

The presence of a sun simulator is particularly suited to test those items, such as the IRS optics, whose behavior is governed by the solar environment.

5. **Motion System**.It allows one to reproduce the attitude of the satellite with respect to the incoming solar beam, according to two possible configurations. The one used for the MTG-S thermal balance test is the Gimbal stand configuration, depicted in Figure 5.3, that permits the tilting of the test object with respect to the horizontal axis and the rotation around the vertical axis of the Main Chamber. The Spin box, situated between the satellite and the seismic structure, can be operated by controlling both the position and the velocity, and its main performance parameters are reported in Table 5.4 together with that of the Gimbal stand configuration.

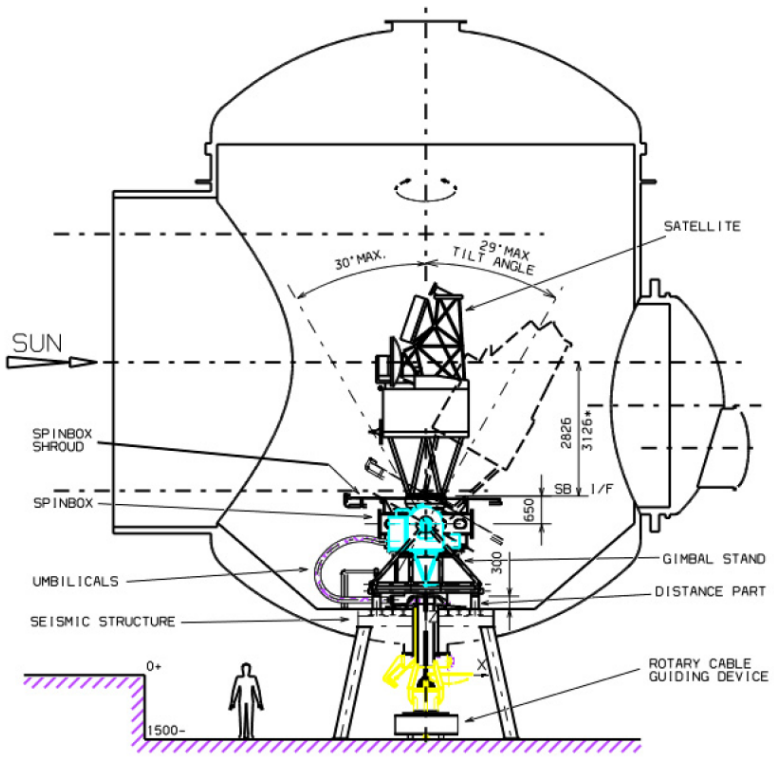

Figure 5.3: Gimbal Stand Configuration

Parameter	Spin Box	Tilt
Velocity Range	0.25 - 2160°/*min*	1 - 3°/*min*
Position Accuracy	±0.4°	±0.01°
Position Resolution	±0.1°	±0.01°
Max. Min. Extension	—	+30/ − 29°

Table 5.4: Gimbal Stand Configuration Performance Parameters

6. **Leveling System**. It is installed between the seismic block and the Gimbal stand structure, with the purpose of compensating a possible misalignment from the horizontal of the test object.

As for the ESATAN-TMS model of the Large Space Simulator, which is directly provided by ESA, it comprises the Main Chamber, the Auxiliary Chamber and

the spin box, onto which the satellite is installed. The furnished model is thought to be used to calculate the radiative couplings with the test object, whereas no mention is made about the conductive interactions within the chamber and to the satellite. The information contained in the numerical model is that concerning the geometry of the chamber and the optical properties of the different components. In the chamber model file a list of suggested temperatures is given, which will have to be included into the inputs for the TMM solution; they are reported in Table 5.5, and their values will be kept constant as soon as these temperatures are reached, as better explained during the test description.

Component	Temperature
Chamber Shrouds	$-180°C$
Spin Box	$-180°C$
Lamp Window	$+40°C$
Entrance Cone	$+20°C$
Mirror	$+25°C$
Vessel	$+20°C$
Auxiliary Panel	$-80°C$
Top Shroud	$-170°C$

Table 5.5: LSS model suggested temperatures

From now on the values reported in Table 5.5 will be used as settings for the test prediction, referring to them as "GN2/LN2" boundary temperatures.

Chapter 6

Preparation

6.1 Test Adapter

Before starting the test predictions it is necessary to consider how the model of the IRS is to be linked to the LSS model. OHB System AG has already designed an adapter, on the basis of two other tests of the campaign, the opto-thermo-mechanical and the thermal cycling test. Unfortunately its design does not completely meet the needs of the thermal balance test, therefore some modifications have been implemented. During the execution of the predictions it will be then understood if the new model of the adapter will fit to the test requirements. The drivers identified in the design of the adapter are:

- The capability to reproduce the Earths Deck temperatures. In orbit the Instrument Support Panel is connected to the satellite platform via the Earths Deck. This component assumes different temperatures according to the load cases considered: the connection between the adapter and the instrument shall be able to reproduce these temperatures.
- Allow the encoder radiator cryogenic environment. In order to respect the horizontality of the heat pipes, the instrument has to be installed into the chamber with the encoder radiator facing the bottom of the chamber. In this way the radiator would see the adapter legs, while in the orbital configuration it is always directed to space.

- Alignment of the instrument first optic with the center of the solar beam.

As for the possibility to reproduce the Earths Deck temperatures, the adapter alone will not be able to adjust its temperature to the one requested by the test requirements. The solution investigated foresees to cool down the interface plate by infrared heat exchange towards the cold shrouds, in order to achieve a range of low enough temperatures, that would give the possibility to better control its temperature by simple heating devices such as the heaters. During the discussion of the thesis, it will be verified if for each case the temperature profile of the interface plate does effectively allow the above mentioned thermal control. In the old model of the adapter the surface of the interface plate looking toward the shroud of the chamber is covered with MLI, fact that would not allow to fulfill the requirement on the temperature, since both solar and infrared heat exchange would be blocked between the adapter interface plate and the chamber. For this reason the MLI has been removed and the back surface has been white painted, to minimize the solar radiation while letting the heat exchange in the infrared band for the cooling.

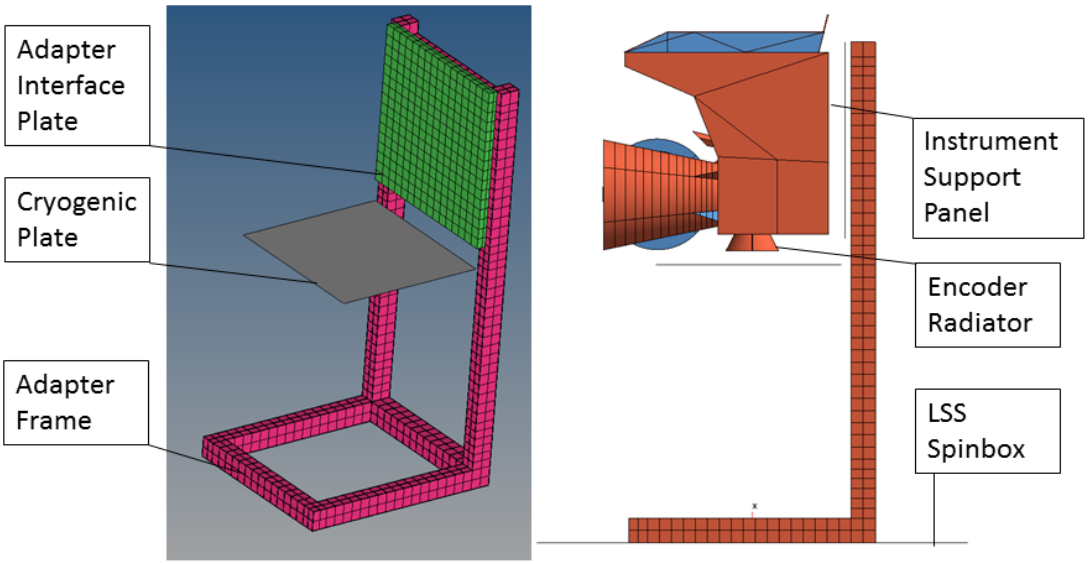

Figure 6.1: Adapter (left); Integration with the IRS and the LSS Spinbox (right)

Depicted in Figure 6.1, it can be noticed that a cryogenic plate has been inserted just below the instrument, to keep the encoder radiator at a sufficiently low temperature for the duration of the test. The aim of the encoder radiator is

to cool down the scanner, which is often exposed to solar irradiation: a lack of the radiator cooling down capacity would damage this mirror.

The legs of the adapter have been then enlarged in order to place the scanner, considered in its canonical position, in the center of the sun beam.

In Table 6.1 the main parameters of the adapter are presented.

Component	Thermal Coating / MLI	Material
Frame	Black MLI	Stainless Steel
Interface Plate	Internal: Black MLI	Aluminium
	External: White Paint	Aluminium
Cryogenic Plate	Upper: Black Paint	Aluminium
	Lower: Black MLI	Aluminium

Table 6.1: Adapter main characteristics

Finally the thermal couplings within the adapter are manually inserted, since ESATAN-TMS does not have the information necessary to automatically create them. Between the frame and the spinbox eight conductive couplings have been manually defined, approximating the entire thermal conductors between the two components by considering eight screwed connection of type M10 (0.04 W/K). The screws are disposed on the frame bottom by considering only one connection at the edges of the frame and two connections on each leg between them. The same principle has been adopted to connect the frame to the interface plate, while for the thermal link existing between the interface plate and the instrument support panel, a screw has been assumed to link the plate with the nodes of the ISP where the connection with the earth deck normally occurs, these nodes being called inserts.

The models of the adapter and of the instruments have then been placed inside the LSS, taking care of respecting the alignment of the first optic of the instrument with the center line of the solar beam. While merging the models, an assembly has been created within the LSS, which was chosen as a reference component, and the adapter and the instrument models, selected as moving components and fixed with each other. This has been done to allow the rotation of the

testing object inside the chamber, a necessary condition to dynamically represent the radiative couplings and the heat fluxes, thus allowing an orbital variation in the temperature profiles.

6.2 Solar Generator Workaround

As already stated, the lack of an optical model correctly describing the solar generator from the production of the radiation in the Xenon lamps, until the final reflection on the mirror, has led to a dedicated solution for the simulation of the solar fluxes. The whole test model, composed by the LSS, the adapter and the instrument, has been used to build a radiative case where a dummy heliocentric orbit was defined, whose parameters have been selected in order to generate the wished solar fluxes arrays.

Orbit Center	Sun
Sun Radius	6378.09 km
Perihelion	42164.169 km
Aphelion	42164.169 km
Solar Constant	1378 W/m^2

Table 6.2: Radiative Case Descriptive Parameters

By using the parameters reported in Table 6.2 to conduct a radiative case, the resulting heat fluxes will just respect the period of the geostationary orbit considered in the operational cases analysis, and the respective solar radiation for the hot case. Apart from the above mentioned parameters, the implemented attitude of the LSS is such that the center axis of the solar beam is constantly pointing towards the sun.

The side of the chamber facing the sun has been modified by introducing a hole on it, whose position and diameter have been chosen to create a correspondence with the solar beam, while the mirror has been deleted from the model being

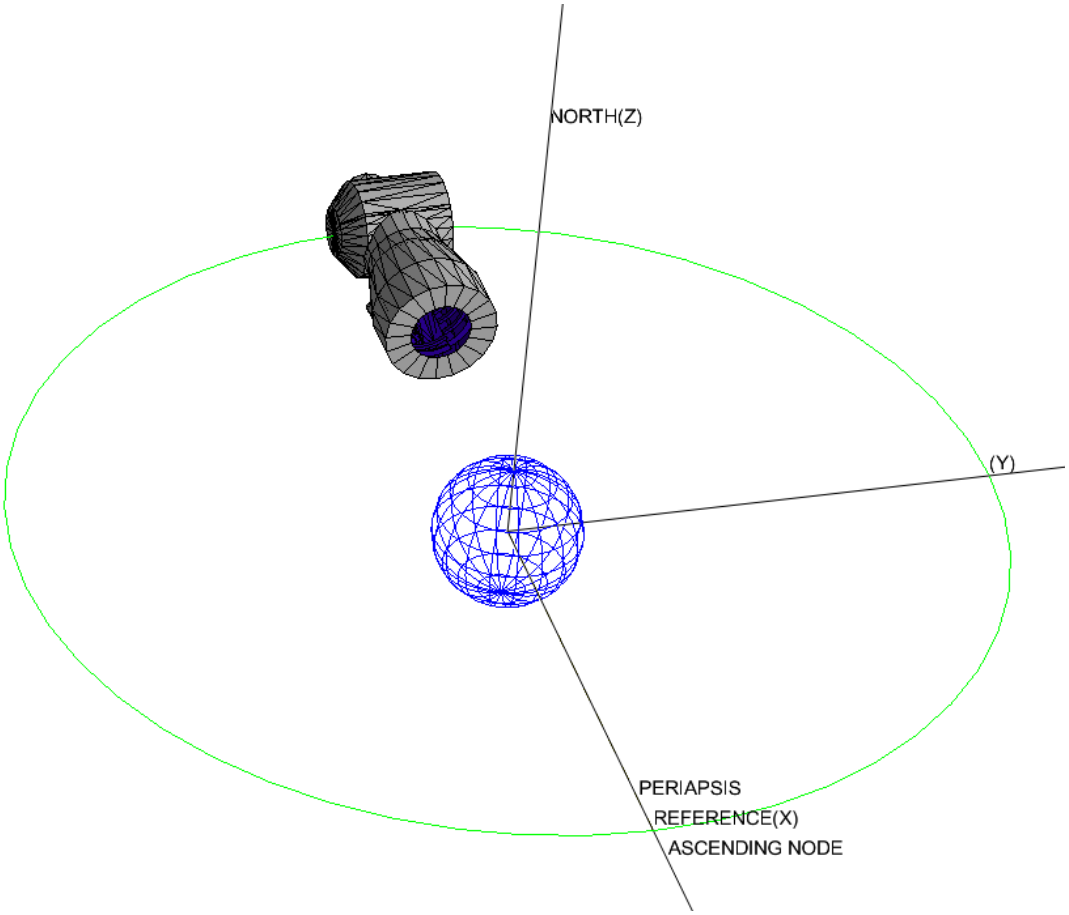

Figure 6.2: Large Space Simulator Dummy Orbit. The hole in the Auxiliary Chamber is always sun pointed.

it an obstacle for the sun ray's path. This procedure is exclusively dedicated to the obtainment of the solar fluxes, so it has to be thought of as a "simulation of the solar simulator" belonging to the real test chamber. If the model created to calculate the solar fluxes had been used to generate also the radiative couplings, the results would have not taken into account the presence of the mirror, which, as already reported in Table 5.5, is set to a much higher temperature than the one of the shrouds. In absence of the mirror, the resulting radiative couplings would have been instead calculated by considering the much lower temperature of outer space ($3\ K$). For this reason the fitting model to the radiative calculation is the original one, fact that leads to the necessity of running the two separated radiative cases for the solar fluxes and for the thermal couplings, every time that a simulation has to be performed. The possibility of conducting the two calculations together has been rejected after having set the solar transmissivity of the mirror and of the

disc vessel to one; the results showed that the way ESATAN-TMS interprets the transmission of the solar fluxes is highly dependent on the meshing precision of the transmitting nodes. Unfortunately it was observed that the transmitted fluxes were not converging to the desired intensity as the detail of the node mesh increased, thus leading to abandon the idea of exploiting such a solution.

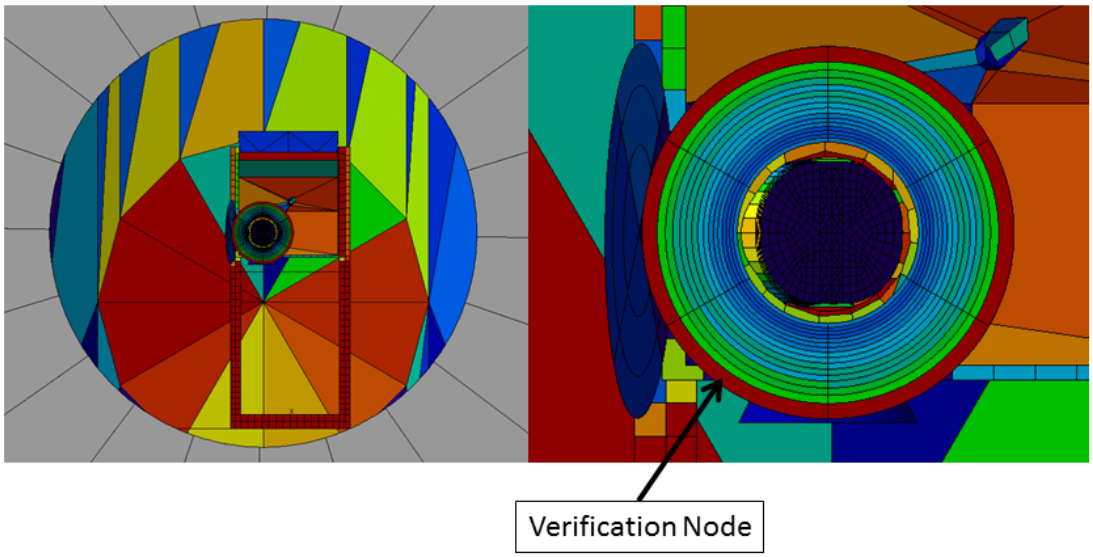

Figure 6.3: The IRS inside the LSS model (left), and a detail on the Solar Baffle and on the node used to the verification.

The correctness of the solar fluxes calculated through this method has been proven by modeling a known case and comparing it with the results obtained. Figure 6.3 presents the IRS and the Adapter models inside the LSS, indicating the reference node chosen for the verification. The verification node is part of the Solar Baffle, and for construction it is perpendicular to the incoming sun rays. It is then expected to measure on its surface the exact value of solar radiation defined in the calculation.

A rotation has been then given to the instrument inside the chamber, and the relative dynamical fluxes have been observed, also reported in Figure 6.4. In the graph it can be seen how the solar fluxes absorbed by the verification node increase until reaching the nominal value defined in the analysis settings. It can be also notice how the solar intensity decreases as soon as the incident angle between the sun rays and the node reaches the 90°. At the extreme region of the graphs a little noise is observable: this is due to the spurious reflections happening inside the chamber, not absorbing the shrouds wall the total solar irradiation.

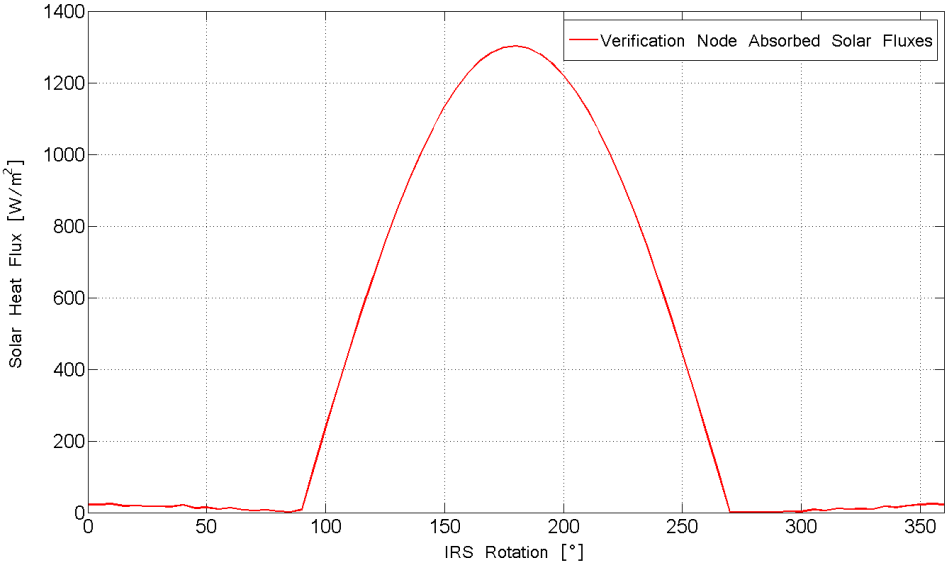

Figure 6.4: Heat Fluxes Profile on the Verification Node

Chapter 7

Test Phases

Referring to the objectives of the thermal balance test explained in Chapter 4, the test phases reported in Table 7.1 are performed to provide measurements for the correlation of the model, to verify the thermal control design, and to test the correct functionality of the hardware. In the test sequence the four load cases are recognizable (one hot case, two cold cases and the safe mode), while the other phases are inserted especially as a verification of the thermal design (e.g Heater Subcooling, Sun Intrusion) and of the hardware performance (Cryocooler cooling down sequence, Decontamination). As requested by the ECSS, phase 10 provides sensitivity data about the operational heater lines.

The test philosophy followed to guarantee a successful correlation foresees to clearly fix the test conditions (shrouds temperature, solar generator intensity, spinbox rotation, etc.), so that the effects of these settings will be comparable between the test and its simulation. As for the orbital simulations, an attempt was made to adjust the chamber and instrument settings in such a way to obtain the highest degree of similarity with the orbital conditions, while respecting the limits imposed by the chamber circumstances.

The sequence of the phases' conduction has been iteratively evaluated on the basis of the results obtained at each step of the development, and their order is a function of many different aspects that will be illustrated along the thesis. As a general rule, the test starts with the hot cases, being these the most suited cases to verify the cryogenic cooling of the detectors in a hot environment, which will be then kept operative until the decontamination case.

Phase	Name	Test Performed
1	Specimen Installation	General inspection - horizontality check
2	Pump Down	Check of test instrumentation
3	Shroud Cool Down	
4a	Hot Case - Cryocooler Cooling Down	Detectors cooling down
4b	Hot Case - ϵ effect isolation	In-depth mirrors thermal balance
5	Hot Case Operational - Day 56	Orbital Simulation
6	Heater Subcooling	Thermal control margin identification
7	Sun Intrusion	M2 design verification
8	Cold Case Operational - Equinox	Orbital Simulation
9	Cold Case Operational - Summer Solstice	Orbital Simulation
10	Heater Sensitivity	Power margin identification
11	Decontamination	Decontamination operations
12	Safe Mode	STL design verification
13	Safe OTL	OTL in safe mode design verification
14	Shroud Warm Up	
15	Pressure Recovery	
16	Specimen Inspection	General inspection

Table 7.1: Test Phases Sequence

All along the conduction of the phases, the solar generator intensity is gradually reduced, passing from the operational cold cases and arriving to the safe mode. The decontamination case, during which the detectors are re-brought to non-cryogenic temperatures, is placed just before the simulation of the safe mode, where the cryocooler is no longer operative and therefore does not need to be tested. In this chapter the design of the test phases will be discussed, and the predictions for the most meaningful components will be reported.

7.1 Specimen Installation & Pump Down

In this phase the instrument and the adapter are installed on the chamber spinbox, paying attention to the centering of the M0 with the solar beam, due to the spatial stability of the Xenon lamp of the LSS. Afterwards, a horizontality check has to be

performed, for two main reasons. The first one is to assure that the instrument is in a well known and measured orientation with respect to the chamber, in order to allow a coherent comparison between the test results and prediction. The second one is to guarantee that the heat pipes distributed on the radiators on the $-Y_{sc}$ face of the instrument are effectively horizontally oriented, since even a slight tilt of the adapter and the instrument with respect to the gravitational field would affect their correct functionality.

When the initial inspections have been finally concluded, the depressurization sequence begins, bringing the chamber pressure to 5×10^{-6} *mbar*. In the meanwhile a check of the test and flight heaters can be executed, together with the monitoring of the temperature sensors.

7.2 Shroud Cool Down

The last part of the initialization process foresees the cool down of the main and auxiliary chamber shrouds, whose cooling down process, as reported in Figure 5.2, differs in both duration and final temperature. The shrouds' cooling down have been linearly approximated, being their actual temperature profiles not relevant for testing purposes.

In Table 7.2 the main simulation variables are reported.

Simulation Variables	Value
Heater lines	ON - Operational mode
Instrument configuration	Scanner canonical position
Spinning system	$-Z_{sc}$ towards Chamber Mirror
LSS Boundary Temperatures	GN2 / LN2
Sun Simulator	0 $[W/m^2]$
Thermal Coating Properties	BOL
Units Dissipations	ON
Adapter Interface Plate	$+40°C$

Table 7.2: Shroud Cool Down Main Simulation Variables

Being this phase just an obliged step to the start of the test's core part, many settings can be chosen in order to facilitate and accelerate the start of the next one: the heater lines used are the operational ones, since their set point matches with the desired initial temperatures of the next phase, while the IRS is pointed in the opposite direction of the solar simulator, consistently with the initial orientation in space of the satellite operational phase. Again, to speed up the start of the next phase, the units are considered to dissipate at their maximum level.

The canonical position

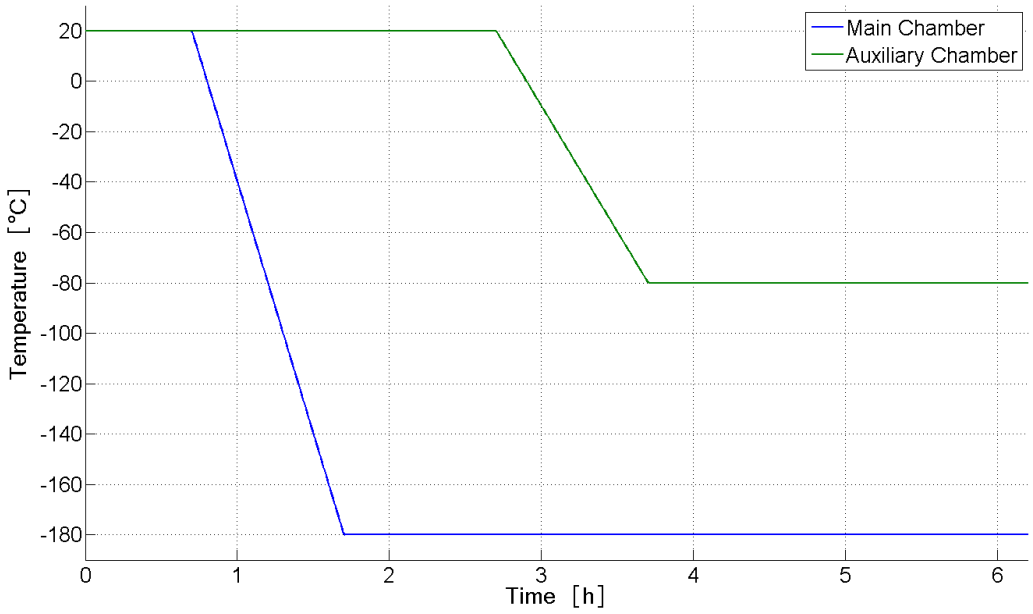

Figure 7.1: Main and Auxiliary Chambers Cooling Down

7.3 Hot Case

Immediately after the cooling down of the shrouds, the units of the instrument are switched on, together with the cryocooler, which will initialize the cooling process of the sensible items, bringing them to their operational cryogenic temperature. Therefore, before starting any simulation of the operational cases, the cooling chain of the cryocooler has to be monitored until stabilization, verifying as well its proper functioning. Being this process estimated to last slightly more than a day, an additional test has been included, supposed to be carried out simultaneously with the observation of the cryocooler cooling down sequence.

7.4 Cryocooler Cooling Down

The hot case is characterized by the most demanding and therefore most appropriate conditions to observe the cooling down sequence of the cryocooler, being the surrounding thermal environment at its hottest point. The aim of the observation is to measure the temperature and duration of stabilization, measured on both the MWIR and LWIR detector retinas. The first event which gives the start to the test phase is the switch on of the Xenon lamp, which is here assumed to reach immediately its nominal power intensity, fixed at the hot case value. As soon as this happens, the spinning mechanism is activated and adequately controlled to obtain a constant positive rotation of the instrument about the $-Ysc$ axis. The modulus of the spinning mechanism rotation is set to the orbital angular velocity, in order to let the solar beam impinge the spacecraft in the most adherent way to the operational condition.

As for the simulation of this phase, in Table 7.3 are listed the main variables set for the prediction.

It is important to notice that the coating properties have been set to beginning of life, which could appear as a contradiction within a hot case analysis since the resulting fluxes are lower than the ones that would have been obtained by

Simulation Variables	Value
Heater lines	ON - Operational mode
Instrument configuration	Scanner canonical position
Spinning system	+15.04 $[deg/hour]$
LSS Boundary Temperatures	GN2 / LN2
Sun Simulator	1398 $[W/m^2]$
Thermal Coating Properties	BOL
Units Dissipations	Maximum
Adapter Interface Plate	+40°C

Table 7.3: D56A Main Simulation Variables

setting the coating properties to end of life. The reason behind this is the impossibility to physically simulate the end of life properties, a condition of the material that could be replicated only through a direct exposure to the space environment for the entire duration of the mission.

The calculated temperature plots for the two detectors are reported in Figure 7.2, predicting a stabilization time of 35 hours, at a temperature of 53 K. These results are coherent with the ones provided by the developers of the detection assembly.

The settings given for the scanner configuration and the spinning system are valid during this phase until a change is requested during the conduction of the simultaneous phase explained below. Their variation will anyhow not sensibly affect the observation of the cooling down sequence.

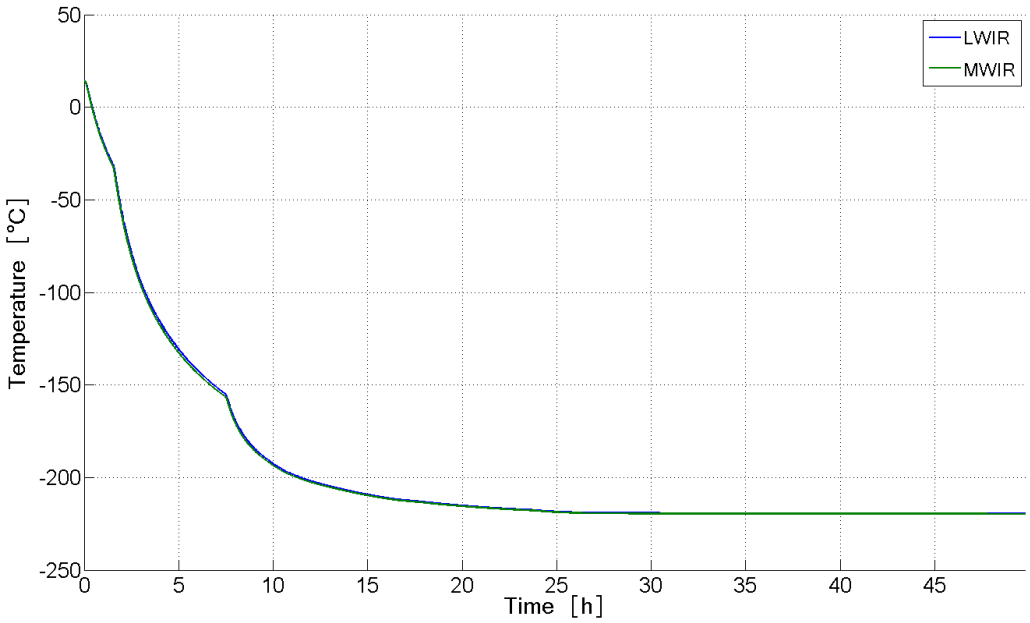

Figure 7.2: LWIR and MWIR Detectors Cooling Down Profile

7.5 Epsilon Effect Isolation

The objective of this phase is to isolate, identify and afterwards correlate the influence that the pure infrared emission of the Inner Baffle, heated up by the solar beam, has on the first two optics inside of it, M1 and M2, untouched by the solar fluxes. Figure 7.3 graphically clarifies the problem statement. This condition, if achieved, would allow a much faster and more precise correlation since it would be easier to identify the parameters to be tuned in the numerical model. This condition is also likely to be achieved within a steady state, that could guarantee a more accurate correlation of the model.

The variables that directly control the fluxes absorbed by the mirrors and the inner baffle have been recognized to be the IRS rotation inside of the chamber and the two degrees of freedom of the scanner. The problem addressed is the search for a configuration minimizing the solar fluxes absorbed by the mirrors, while having as a lower limit a sufficient solar irradiation on the inner baffle, in order to let the infrared effect be clearly visible on the mirrors temperature trend, and as an upper limit the maximum allowable temperatures of the optics that must never be exceeded. This configuration is intended to be fixed in time, in order to

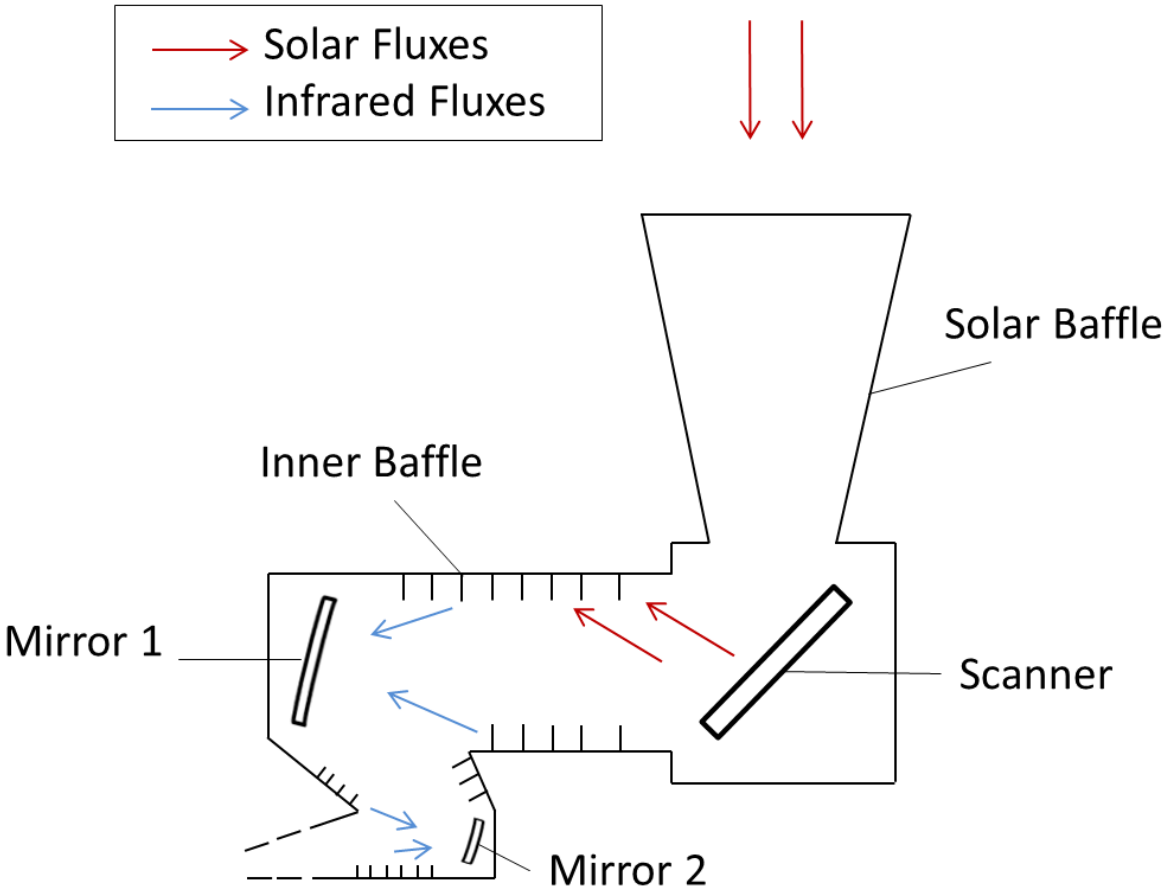

Figure 7.3: Inner Baffle Epsilon Effect Isolation: Functional Sketch

allow, if existing, the obtainment of a steady state condition. For this purpose a radiative case has been set up, in which, for each angular position of the IRS where the scanner is exposed to the solar beam, the absorbed solar fluxes have been calculated for nine orientations of the scanner, these having being recognized as extreme conditions in the deviation of the incoming radiation. These nine cases contain the nine combinations of the maximum, minimum and canonical angles of the M0 scanning capacity. The resulting fluxes have been then post-precessed and reordered according to each scanner configuration, producing nine different heat power trends on the components of interest, M1, M2 and the inner baffle, as the IRS angle changes. To the discovery of an adequate configuration,the exploitable band in terms of IRS angular position for each of these nine cases, an example of which is presented in Figure 7.4, is delineated by two factors. From one side by a

value such that the contribution of the IR radiation from the inner baffle remains orders of magnitude higher than the spurious solar irradiation on the mirrors. From the other side by an excessive power value on the first mirror.

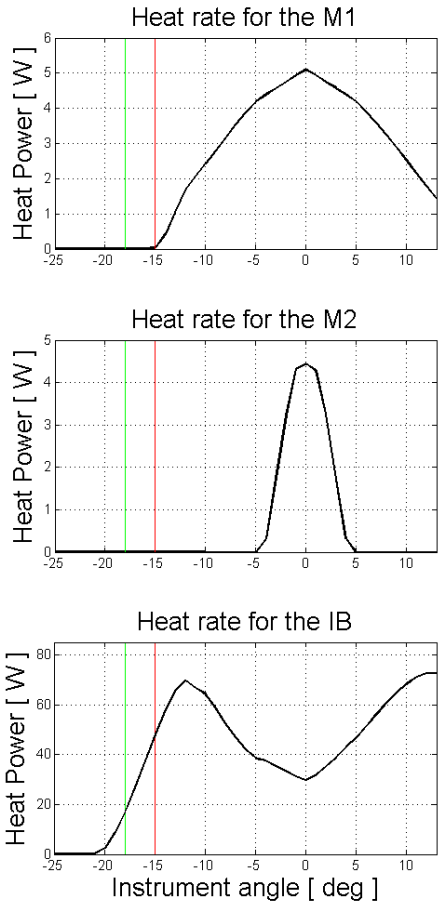

Figure 7.4: Solar Absorbed Fluxes vs IRS angle for the canonical configuration. The red vertical line represents the limit imposed by an excessive power on M1, while the green line is placed three degrees before this limit.

The band of interest is further restricted on the right by introducing a safety margin of 3 degrees to avoid excessive heating on the M1 for a prolongated period of time, being a long pause to be carried out in the configuration to be selected.

By taking as a starting point the IRS angle obtained after the introduction

of the safety margin, a steady state analysis has been solved for each of the nine cases characterized by a different orientation of the scanner, to quantify the stabilization time and temperature for the two mirrors. While in several cases the survival temperature of the mirrors has been overcome, after iteratively lowering the IRS angle a configuration minimizing the two parameters of interest has been found, thus allowing its implementation in the test flow. In Table 7.4 the results of the nine analyses is reported. On the basis of the case 3, which gave the most promising results, the fitting case was then identified by iteratively lowering the instrument angle, and is reported in Table 7.5,

CASE	IRS Angle[°]	NS/EW [°]	M1/M2 Solar Radiation [mW]	IB Solar Radiation [W]	M1/M2 Stab. Temp. [°C]
1	-18	0/0	7.4/0.39	17.12	>60/47
2	-13	0/5.4	45/0.17	7.13	>80/57
3	-22	0/-5.4	3.5/0.12	4.675	56/46
4	-17	9.7/0	7.8/0.3	21.46	>60/58
5	-11	9.7/5.4	14.1/0.7	47.6	>80/62
6	-21	9.7/-5.4	4.1/0.15	7.254	65/40
7	-18	-9.7/0	6.6/0.38	12.96	>60/45
8	-12	-9.7/5.4	12.2/0.5	44.83	>80/60
9	-21	-9.7/-5.4	4.5/0.17	7.14	63/51

Table 7.4: Stabilization Analysis for the Infrared Isolation

Case Parameter/Result	Value
IRS angle	$-23.0°$
North-South angle	$0.0°$
East-West angle	$-5.4°$
M1/M2 Stabilization Temperature	55°C/43°C
M1/M2 Stabilization Time	>100 [hours]

Table 7.5: ϵ effect isolation - Fitting Configuration Parameters

Even if the survival temperature is not overcome, the stabilization time remains excessive, which would make this single sub-phase last more than four days. For this reason, by knowing the stabilization temperature, the huge transient is skipped during the test by means of an opportune change in the heaters' set point temperature installed on the back of M1 and M2. Since the heaters are not exactly installed on the optics, the set point temperatures have been evaluated iteratively. The achievement of the steady state is performed significantly sooner in a heater-aided test configuration, and no additional instrumentation is required since the operational heater lines are exploited. Referring to the Figure 7.5 and 7.6 where the temperature profile for the two optics is reported, the heater lines are operative until approximately 10.5 hours in their ordinary configuration, where the set point is changed to the values needed to tune the two temperatures of the optics to their environment.

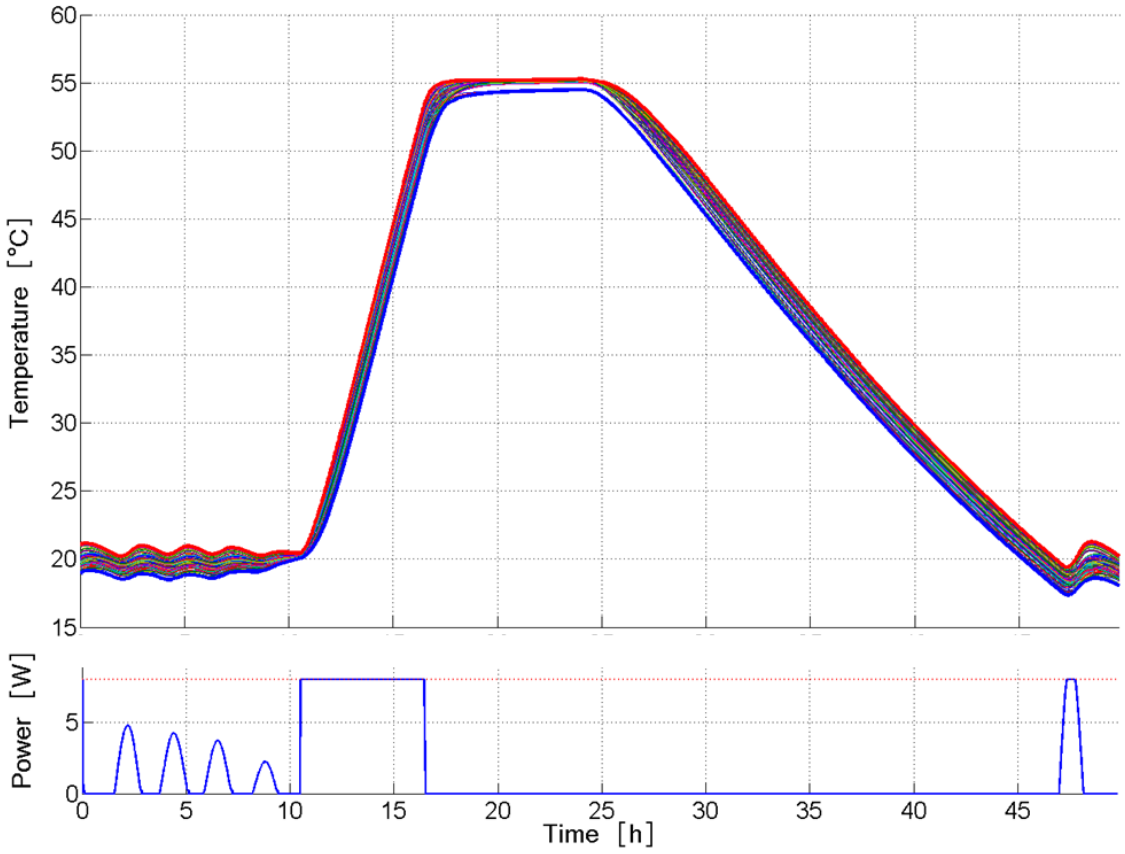

Figure 7.5: M1 Temperature and heater Power Profiles

After the controlled stabilization is reached, the heaters are this time reset to their original condition, thus letting their temperatures ultimately adjust to the

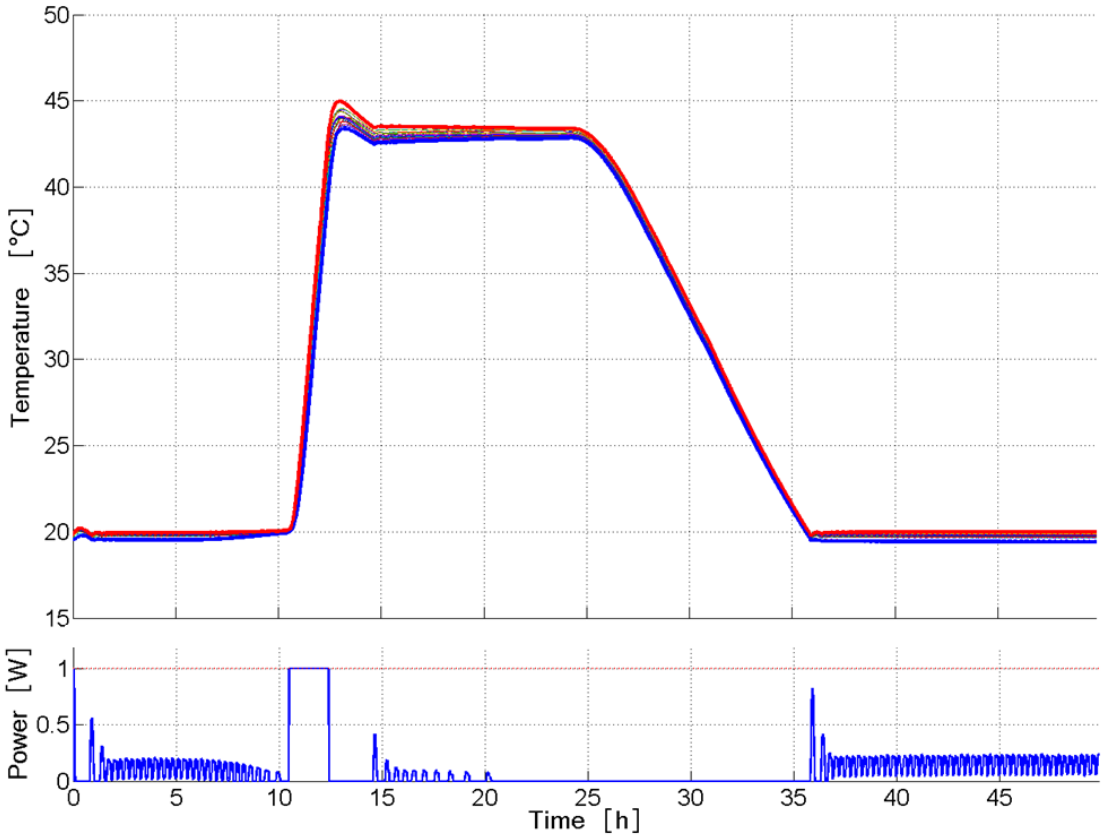

Figure 7.6: M2 Temperature and Heater Power Profiles

inner baffle for the period of time going from 20 to 25 hours, the convenient window for the static correlation. In Figure 7.7 the temperature profile of the inner baffle is presented: it is worth noticing here that the earliest opportunity to lower the heaters' set point and let the ϵ-effect be dominant, is as soon as the inner baffle reaches in turn the stability, that is assumed to happen at 20 hours.

After the acquisition in the steady state region, the spinning system is restarted to let the phase continue. A further IRS rotation in the already hot condition of the optics would inevitably warm them up above their survival limit, which has to be somehow avoided. Two options can be considered: the first one is a backward spin of the instrument to let the temperatures cool down before resetting the ordinary rotation, while the second option is to shut down the solar simulator of the facility and simply restore the original rotation avoiding a harmful sun intrusion on the optics. The latter option has been chosen due to the significant saving in terms of test duration that it introduces with respect to the first one.

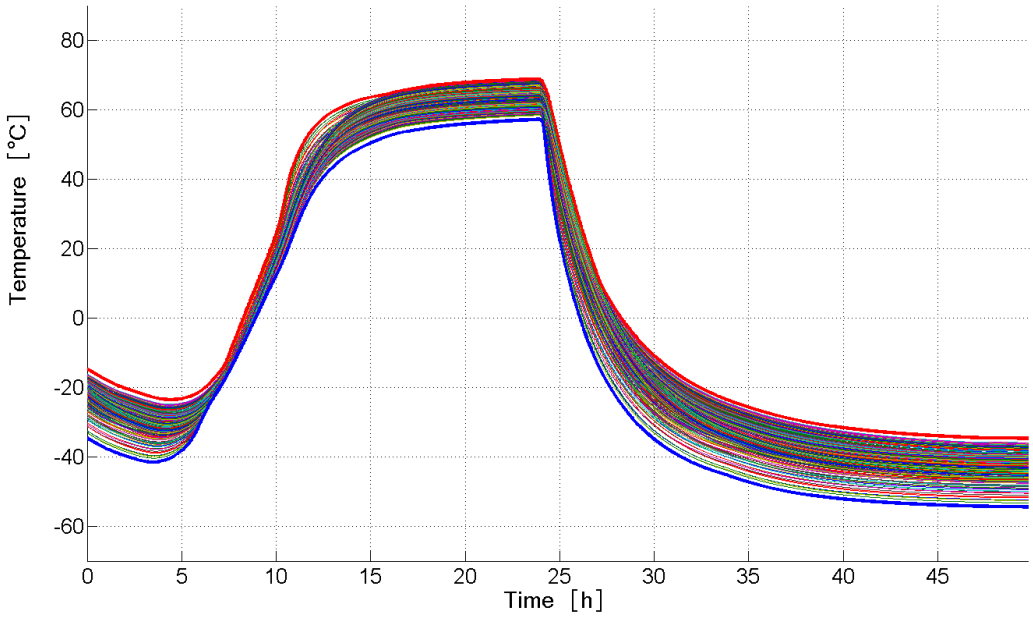

Figure 7.7: M2 Temperature Profile

From a simulation point of view special care has been taken for the solar fluxes' and radiative exchange factors inclusion in the source file driving the solution process. These quantities are generated under the form of many arrays of equal length, where each element represents the value of a heat rate (for the QS) or a radiative coupling (for the REFs) at every position index of the orbit considered into the radiative case definition. The way ESATAN-TMS handles them during the solution is through a time interpolation, obtaining consequentially a time-varying value between each element of the array. This is an unwanted behavior when it comes to describing a steady state condition, as it happens in this phase of the test. To allow a stationary case to be simulated a chained interpolation based on the angular position has been implemented. Firstly the IRS angles used to build the radiative case have been declared, as well as their correspondent times after having taken care of the pause needed for the ϵ-effect: these two arrays are used to express the IRS angle as a function of time. The last array constructed is made by the IRS angles to be coupled with the QSs and the REFs: the two IRS angle arrays are not identical since the first needs to give out as a result the pause position for a prolongated period of time, while the second identifies a unique QSs and REFs condition.

By looking now at the complete test phase, some consideration about the parallel testing must be done. It can be noticed that despite the presence of the eclipse, the main part of the cooling down chain of the cryocooler finds place during the application of the solar fluxes of Day 56, leaving its worst case environment untouched. Moreover, the contribution of the internal dissipations and the interface plate controlled temperature have never been touched during the test phase, fact that contributes to the feasibility of the simultaneous testing presented.

7.6 Operational Hot Case - Day 56

After having collected the information coming from the previous test phase regarding the IR influence of the inner baffle on the mirror, in this chapter attention will be focused on the effect that the solar radiation has on the mirrors temperature profile. As illustrated in Figures 7.8 and 7.9 , from the orbital simulations it is observed that the mirrors' behavior is characterized by many spikes in the central region of the orbit, when the sun rays are deviated by the M0 according to the scan law acting in that period of time.

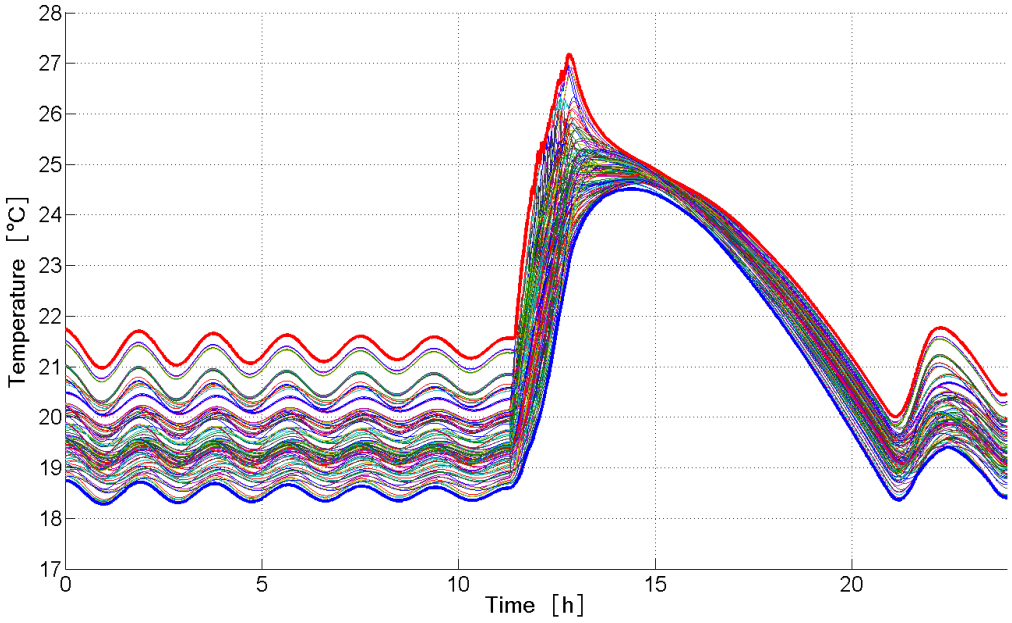

Figure 7.8: M1 Orbital Temperature Profile

Following the overall test philosophy, an attempt was made to fix the test condition as similar as possible to the orbital ones. As for the external part of the instrument, the test conditions are selected by setting the chamber parameters that best meet the space environment, while for the internal part the possibility of recreating the solar spikes has to be carefully investigated. The usage of the orbital scan law to replicate the temperature is not possible because of the different relative orientation between the instrument and the incident solar beam, which will not be reflected toward the optics in the same way as for the orbital case. While in the test chamber the sun declination is 0°, in the orbital case it is 8.9°. What is then searched for in this chapter, is a test scan law that, under the constrictions

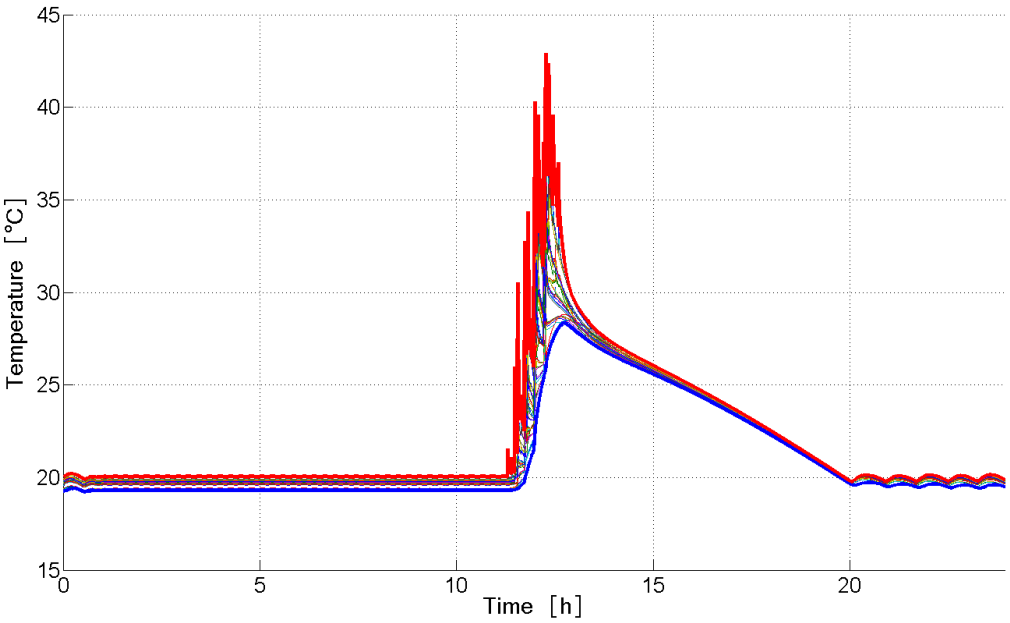

Figure 7.9: M2 Orbital Temperature Profile

of the test configuration, allows to achieve the most similar distribution of solar radiation in the inner part of the instrument, i.e. M1, M2 and the inner baffle.

The reference system used to face the problem is the one reported in Figure 7.10, with the origin into the center of the mirror, the Y-axis lying on the joints of the East-West rotation in its canonical configuration ($NS = 0$,$EW = 0$), the Z-axis directed as the North-South axis of rotation, and the X-axis perpendicular to the other two. The reference system is fixed with respect to M1, M2 and the inner baffle, but it is not with respect to the scanner. Being $\boldsymbol{v}_0$ the sun ray vector that would be incident on the mirror when the back of the instrument is directed towards the solar beam in the test configuration, the incident sun radiation vector in the test and in the orbital case can be expressed through:

$$\boldsymbol{v}_{in,test} = \mathrm{R}_\theta \boldsymbol{v}_0 \tag{7.1}$$

$$\boldsymbol{v}_{in,orbit} = \mathrm{R}_i \mathrm{R}_\theta \boldsymbol{v}_0 = \mathrm{R}_i \boldsymbol{v}_{in,test} \tag{7.2}$$

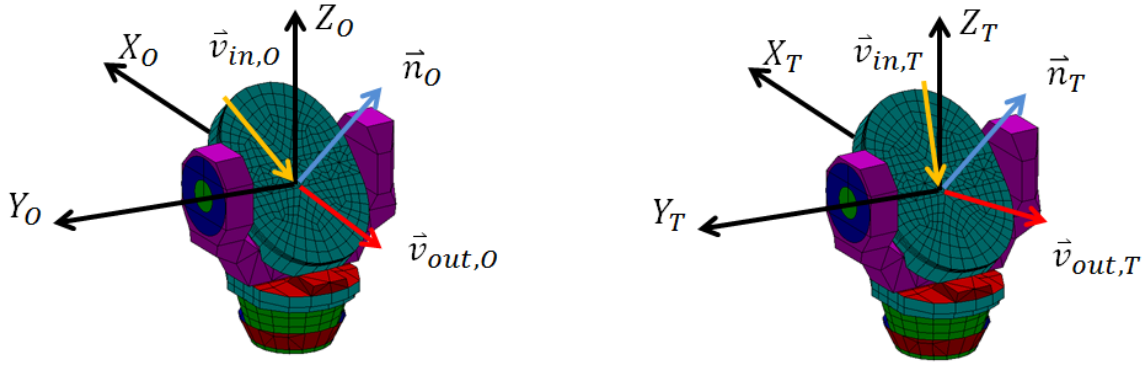

Figure 7.10: Orbital and Test Reference Systems

where R_θ and R_i identify respectively the rotation of an angle equal to the true anomaly θ about the Y-axis (thus meaning the orbital revolution for the orbit case and the spinning of the instrument inside the chamber for the test case), and the solar declination of 8.9°.

It is useful now to define the normal to the mirror in the orbital case, which depends on the scan law, identified by a series of North-South and East-West angles, the first one defined as a rotation about the Z-axis starting from the canonical position, the second one by a rotation around the Y-axis starting from a situation where the mirror is coplanar with the XY-plane. It is also important to underline that in the application of the two rotations, the EW one occurs before the NS one. Having clarified the definitions of the angles composing the scan law, it is immediate that the normal to the mirror when the two angles are both zero is coincident with the Z-axis, and by calling $\boldsymbol{n}_0$ the normal to the mirror in this particular condition it follows immediately that the normal in the orbital case as a function of the scan law has the form:

$$\boldsymbol{n}_{orbit} = R_{NS_{orbit}} R_{EW_{orbit}} \boldsymbol{n}_0 \tag{7.3}$$

where the matrices R_{NS} and R_{EW} are self-explanatory.

According to the specular reflection, the incident ray, the normal of the reflecting surface and the outgoing ray are coplanar: this very simple law allows to express the reflected radiation in the orbital case through:

$$\boldsymbol{v}_{out,orbit} = \mathrm{R}_{2\gamma_{orbit}} \boldsymbol{v}_{in,orbit} \tag{7.4}$$

where $\mathrm{R}_{2\gamma_{orbit}}$ is a matrix whose expressed rotation happens about:

$$\boldsymbol{p}_{orbit} = \boldsymbol{v}_{in,orbit} \wedge \boldsymbol{n}_{orbit} \tag{7.5}$$

orthogonal per construction to $\boldsymbol{v}_{in,orbit}$ and $\boldsymbol{n}_{orbit}$, thus also to $\boldsymbol{v}_{out,orbit}$ according to the specular reflection, of an angle $2\gamma_{orbit}$ where:

$$\gamma_{orbit} = \arccos(\boldsymbol{v}_{in,orbit} \cdot \boldsymbol{n}_{orbit}) \tag{7.6}$$

identifies the angle between the incident sun ray and the normal to the mirror. The best condition achievable to replicate the spikes on the mirrors in the test configuration happens where the test reflected ray is equal to the orbital one, which means:

$$\boldsymbol{v}_{out,test} = \boldsymbol{v}_{out,orbit} \tag{7.7}$$

It is possible now to express the normal to the mirror in the test conditions which respects the previous statement as:

$$\boldsymbol{n}_{test} = \mathrm{R}_{\gamma_{test}} \boldsymbol{v}_{in,test} \tag{7.8}$$

where $\mathrm{R}_{\gamma_{test}}$ is the matrix whose rotation axis is calculated as:

$$\boldsymbol{p}_{test} = \boldsymbol{v}_{in,test} \wedge \boldsymbol{v}_{out,test} \tag{7.9}$$

and whose angle of rotation is γ_{test} where:

$$2\gamma_{test} = \arccos(\boldsymbol{v}_{in,test} \cdot \boldsymbol{v}_{out,test}) \tag{7.10}$$

It is clear that per construction $\boldsymbol{n}_{test}$ is coplanar with the incident and the reflected rays and that the two angles between the two rays and $\boldsymbol{n}_{test}$ are equal, thus respecting the first principle of geometrical optics. What is now necessary in order to obtain a usable test scan law, is to express the normal to the mirror in the test configuration as a function of the two controlled angles of the scanner which will possibly not exceed the limits imposed by the hardware.

Similarly to the orbit case, the normal to the mirror in the test condition can be expressed as:

$$\boldsymbol{n}_{test} = \mathrm{R}_{NS_{test}}\mathrm{R}_{EW_{test}}\boldsymbol{n}_0 = \mathrm{R}_{test}\boldsymbol{n}_0 \tag{7.11}$$

where by expressing the product of the two rotation matrices with $\boldsymbol{n}_0$:

$$\begin{bmatrix} n_{test_x} \\ n_{test_y} \\ n_{test_z} \end{bmatrix} = \begin{bmatrix} \cos(NS)\cos(EW) & -\sin(NS) & \cos(NS)\sin(EW) \\ \sin(NS)\cos(EW) & \cos(NS) & \sin(NS)\sin(EW) \\ -\sin(EW) & 0 & \cos(EW) \end{bmatrix} \begin{bmatrix} 0 \\ 0 \\ n_{0_z} \end{bmatrix} \tag{7.12}$$

$$\begin{bmatrix} n_{test_x} \\ n_{test_y} \\ n_{test_z} \end{bmatrix} = \begin{bmatrix} \cos(NS)\sin(EW) \\ \sin(NS)\sin(EW) \\ \cos(EW) \end{bmatrix} \tag{7.13}$$

the two desired angles are found:

$$\mathrm{EW} = -\arccos(n_{test_z}) \tag{7.14}$$

$$\mathrm{NS} = \arctan\left(\frac{n_{test_y}}{n_{test_x}}\right) \tag{7.15}$$

where for the EW angle, being the codomain of the arccosine defined only between $[0, \pi]$, a minus has been added to let the solution be coherent with the geometry of the problem since EW is always negative defined. From the approach followed, it has been seen that only a single ray has been considered, hitting the scanner in its center where also the reference system has its origin, while in the reality a beam of ray is impinging the scanner and then being reflected. The discussion held until here for a single ray can be easily extended to an entire beam due to the fact that the scanner is flat and no focusing happens at the first stage of the reflections. Under these circumstances, and by assuming that the rays composing the solar beam are all parallel with each other, any ray hitting the scanner in a different position of the surface will encounter the same normal and will therefore be reflected creating a beam of rays all parallel with $\boldsymbol{v}_{out,test}$. Having found the values of the scan law starting from a single pair of angles NS_{orbit} and EW_{orbit}, the function has been implemented in Matlab® to obtain a test scan law for the period of time when the inner part of the instrument is exposed to the solar beam. The resulting maximum and minimum values of the two angles reached during the test scan law derived through the explained method has been checked not to exceed the limits of the hardware, proof that gave positive results as shown in Table 7.6

Angle	Maximum reached	Maximum Allowed	Minimum Reached	Minimum Allowed
NS	$+7.46°$	$+9.70°$	$-1.01°$	$-9.70°$
EW	$-40.88°$	$-39.60°$	$-49.09°$	$-51.40°$

Table 7.6: Limits of the Scan Law and Reached Values in the Test Configuration

Having verified the possibility of theoretically execute the test scan law, it was necessary to verify the validity of the method since the computation time for the scan law radiative cases for a single model takes approximately from seven to nine days if carried out on a single computer. The way identified to verify the goodness of the method makes use of a ESATAN-TMS built in function, named *solar ray propagation*, which allows, under the correct settings of the necessary parameters, to visualize the absorbed solar fluxes by tracing the incoming rays from the first reflections until a defined face of the model. Ideally it would be requested to visually check the whole sequence of reflections from the scanner

until M2, but unfortunately as previously explained the heat fluxes distribution in time is sparse, making it difficult to draw a configuration such that the ray tracing can be visible until M2. For this reason a dedicated disc shell has been included in the model between the first and the second mirror, constantly impinged by solar radiation, and selected as the end face of the reflections to be traced. A random position of the scan law has been chosen, whose values are reported in Table 7.7, and the images of the traced rays have been roughly compared.

Parameter	Orbital Case	Test Case
NS	$-6.14°$	$1.88°$
EW	$-45.21°$	$-44.75°$
True Anomaly/IRS Rotation	$174.14°$	$-5.86°$

Table 7.7: Random check for the Scan Law Transformation

The values of the true anomaly and IRS rotation are shifted of 180°, due to a difference in the conventions taken. At the initial orbit position, where the true anomaly equals 0°, the back of the instrument faces the sun, while the correspondent situation in the test chamber happens when the IRS angle equals 180°

In Figure 7.11 the two propagations are compared, showing an overall similarity of the beam shape. In the images at the top the different scanner orientation is recognizable, while in the lowest images the colors have been altered to show the similarity of the beam shape detected on the disc node.

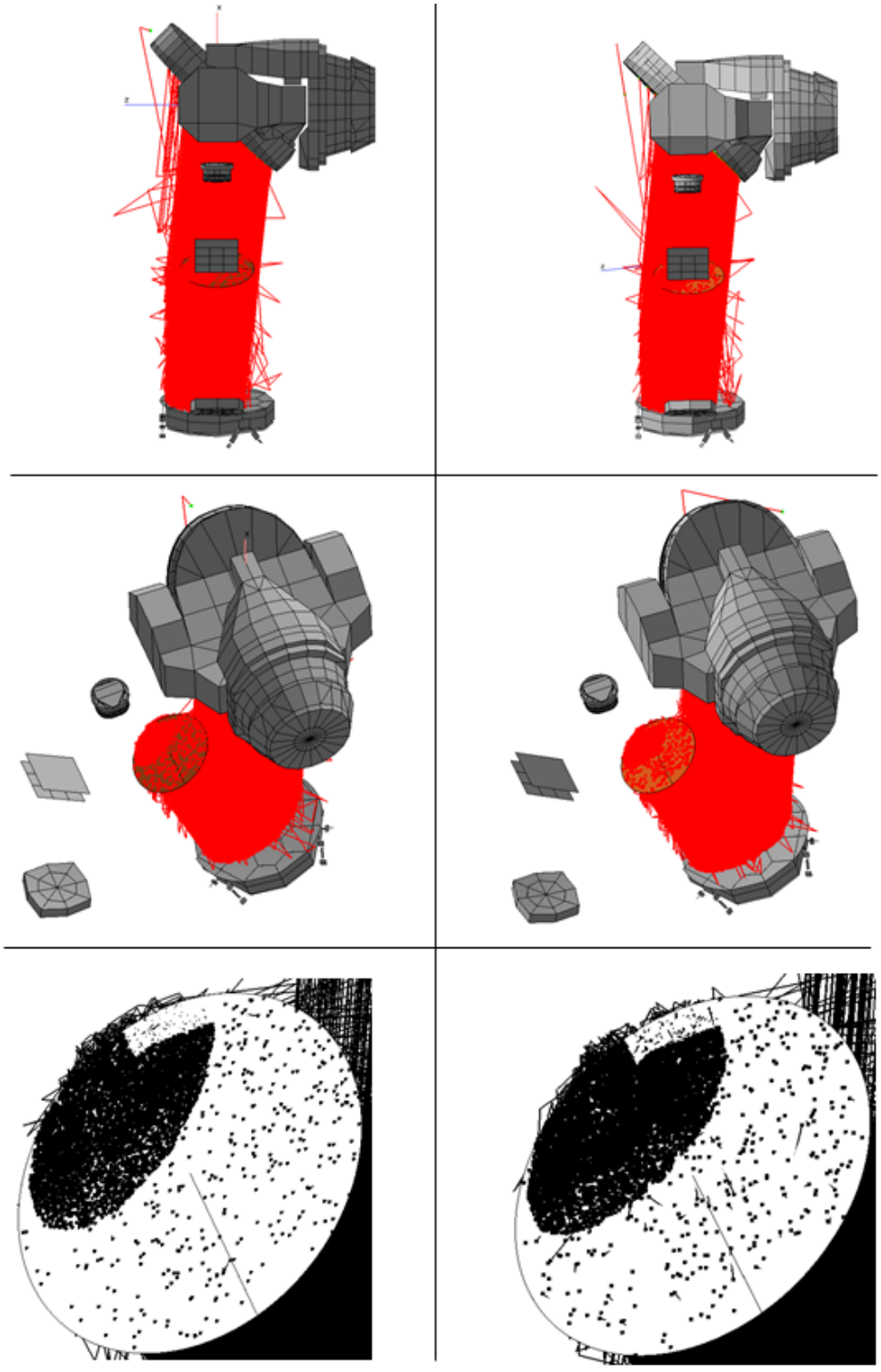

Figure 7.11: Solar Ray Propagation For the Orbital Case (left), and the Test Case (right)

Being the results of the visual check promising, the radiative cases have been executed, obtaining as an output the heat fluxes for the three different arcs of the scan law for each model.

From Figures 7.12 and 7.13 it is observable that the test scan law is capable of respecting the form of the orbital one, meaning that the geometrical transformation is valid, while for the test case higher values of the fluxes are registered, this finding an explanation in the higher incident angle between the scanner and the sun rays.

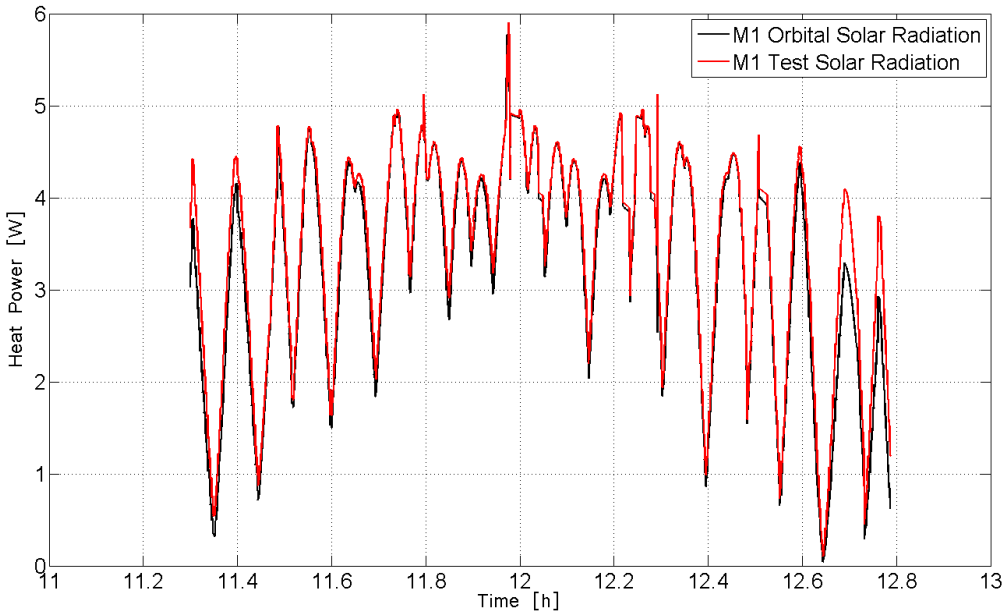

Figure 7.12: Comparison of the Solar Radiation Acting on M1 in the Orbital and the Test Case, over the Sun Intrusion Period

It can also be observed an expansion of the error at the start and at the end of the scan law: to that an explanation is found by looking at the rotation of the solar baffle during the scanner period of exposure to the sun in the two models. Due to the different inclination of the whole instrument with respect to the incoming solar rays, the solar baffle in the orbital case will begin later to uncover the scanner, and it will start sooner to cover it, of course causing a decrease in the absorbed power for the orbital case.

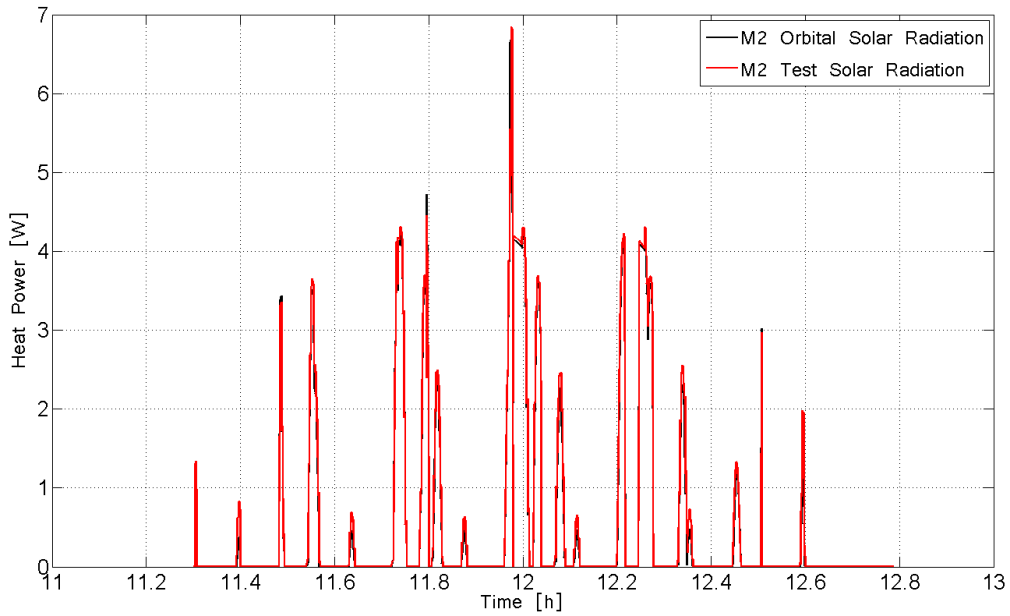

Figure 7.13: Comparison of the Solar Radiation Acting on M2 in the Orbital and the Test Case, over the Sun Intrusion Period

It is also to be reported that the radiative case have been carried out with a very poor value for the calculation accuracy (100 vs 10000 normal), this being another source, even if smaller, of the non perfect adherence of the two results.

Having now the heat fluxes available, the final stage of the phase simulation is the execution and the post processing of TMM, by paying particular attention to the way the different heat fluxes are considered during the calculation, and to the time step used according to the fluxes . Due to the low limit of memory storage for the ESATAN-TMS solver, the strategy adopted sees a dedicated usage of the M1, M2 and inner baffle scan law fluxes for the three arcs where the scan law is considered (three arcs with 1790 positions), while for the rest of the instrument the ordinary flues have been used (73 orbital positions) for the whole simulation time.

The results of the simulation in the test chamber are reported in Figures 7.14 and 7.15, showing a good reproducibility of the mirrors temperatures profile.

For what concern M1, the maximum temperatures in the two cases differ

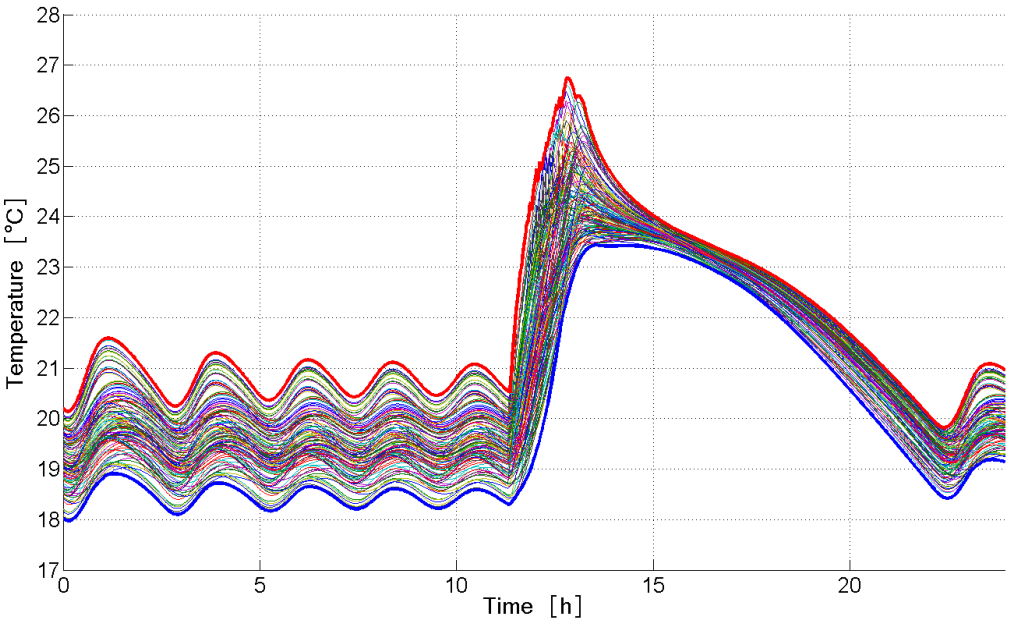

Figure 7.14: M1 Hot Case Test Temperature Profile

only of 0.1°C, and the minor spikes in the central region of the orbit are present as well. The main difference lies in the final stabilization phase, which appears to be greater for the test case: this is an expected result and its reason is in a different environmental temperature, which in the LSS reach −180°C, whereas for the orbital calculations it was set to −270°C. By looking at M2 it is immediately clear how the spikes of the solar intrusion have been satisfactorily obtained, their position in time is overall respected, while the single peak temperature are not perfectly matching due to the different solar fluxes used.

The main simulation paramenters are listed in Table 7.8.

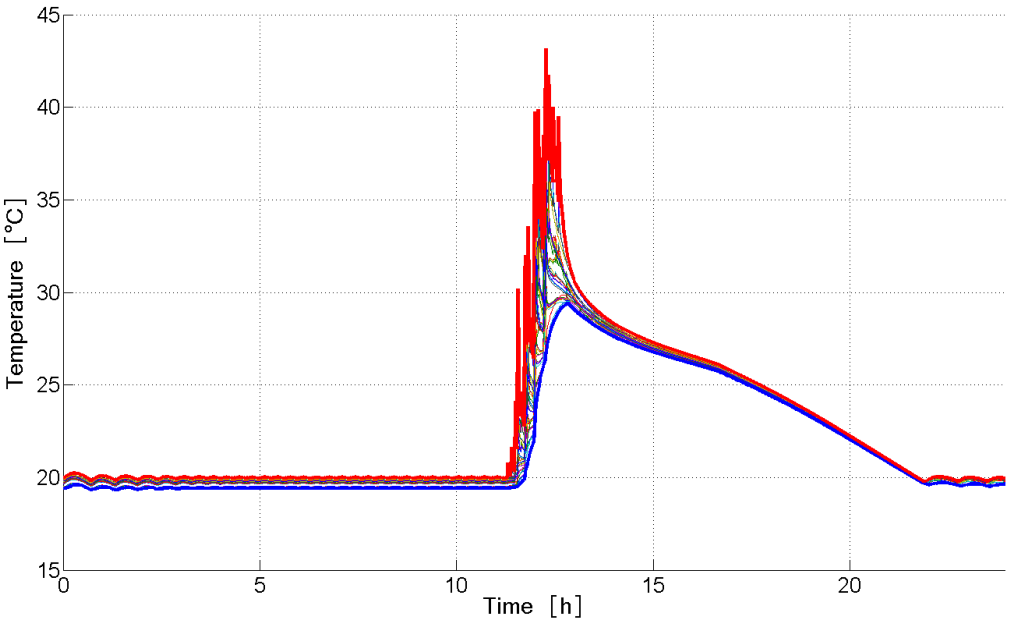

Figure 7.15: M2 Hot Case Test Temperature Profile

Simulation Variables	Value
Heater lines	ON - Operational mode
Instrument configuration	Transformed Scan Law
Spinning system	+15.04 $[deg/min]$
LSS Boundary Temperatures	GN2 / LN2
Sun Simulator	1398 $[W/m^2]$
Thermal Coating Properties	BOL
Units Dissipations	Maximum
Adapter Interface Plate	+40°C

Table 7.8: D56C Main Simulation Variables

7.7 Heaters Subcooling

The heater subcooling is a procedure designed for the verification of the thermal control goodness by means of the operational heaters. The name subcooling refers to the cooling down of the heater measured nodes as a consequence of their shutdown. In fact during these phase the heaters are turned off in a manner that will be here presented, and the deviation between the temperature achieved and the heater set point will registered.

This deviation has a particular meaning, because it is an indicator of how large is the margin for the controllability of the point where the heater is installed. The idea is in fact to verify that the uncontrolled temperature of the measure point remains far enough from the designed set point, so that if an error smaller or equal to the remaining error shall arise, the point would be still controllable.

Actually this check is not done on the single heater but on a subsystem level, meaning that the shut down of the heaters operating on the same component are executed simultaneously. In this way an information about the magnitude of the margin is gained at a subsystem level. It must be clarified that such a procedure could not be applied to the single heater, otherwise a cross-talking between heaters would arise: with cross-talking is indicated the reaction of the heaters that would answer with an increase of injected power as a consequence of the deactivation of the heater nearby. In case of cross-talking, the measurement taken in correspondence of the inactive heater would be affected by the reaction of the surrounding heaters, and the temperature profile registered would show a smaller gap from the set point temperature, with respect to the one that would be obtained by shutting down all the heaters of the subsystem.

This test phase investigates the controllability related to the entire subsystem, measured on the single nodes. In this sense it turns out to be important to define heater groups, in such a way that they can be the most independent as possible with each other, or in other words, to group the heaters influencing each other together, in order to ideally avoid cross-talking between subsystems.

in Table 7.9 the groups chosen are reported. It must be said that a perfect decoupling between them can not be reached, since every subsystem of the instrument is somehow thermally connected with the others, either radiatively or conductively. Therefore it was tried to obtain a sufficient degree of decoupling between groups.

Group Number	Group Name	Heaters
1	Electronic Boxes	OTL15 - LAU (Laser Assembly Unit)
		OTL16 - ICE (Instrument Control Electronic)
		OTL34 - FEEs (Front End Electronics)
2	Instrument Support	OTL23 - ISP Interface
	Panel	OTL30 - ISP 2
		OTL31 - ISP 3
		OTL36 - ISP 4
3	Mirrors	OTL2 - M1 Mirror
		OTL3 - M2 Mirror
		OTL4 - M1 Support
		OTL5 - M2 Support
		OTL6 - M3
		OTL7 - M4
		OTL26 - M3 Support
4	Back Telescope	OTL19 - Back Telescope Mirror Support
		OTL20 - Back Telescope Bench
5	Side Optical Bench	OTL21 - Side Optical Bench
		OTL22 - Side Optical Bench
		OTL29 - Side Optical Bench
6	Optical Bench	OTL8 - OB Around Azimuth Motor
		OTL9 - Optical Bench center -Y
		OTL10 - Optical Bench Center mX
		OTL11 - Optical Bench Center
		OTL12 - Optical Bench Center pX
		OTL13 - Optical Bench +Y
7	Interferometer	OTL14 - IA Bench (BS area)
		OTL27 - IA Bench (RAU)
		OTL28 - IA Bench (CC)
8	Radiators	OTL18 - Cold Finger Radiator
		OTL17 - Compressor Radiator
9	Scanner	Radiative Plate
		East-West Encoder
		North-South Encoder
		Interface Plate

Table 7.9: Heater Subcooling Operational Thermal Line Groups

For instance it can be immediately observed a strong coupling of the Instrument Support Panel with the Optical Bench Assembly and the Electronic boxes, and between the Mirrors and the Optical Bench.

Figure 7.16 shows the temperature profile of Side Optical Bench heater, part of the fifth group that has been shut down. During its period of deactivation, from 97 to 121 hours in the phase time, it can be observed how the heater power is set to zero, and how the temperature consistently drops from the set point. What is observed is a relative maximum at approximately 12 hours from the deactivation: such a result meets exactly the expectations, since it is coherent with the spinning of the satellite inside the chamber, that starting with its back directed to the solar simulator, slowly turns until the Sun fluxes are able to penetrate the inside of the instrument defining the hottest period of time during the orbit (or likewise during the rotation inside the chamber).

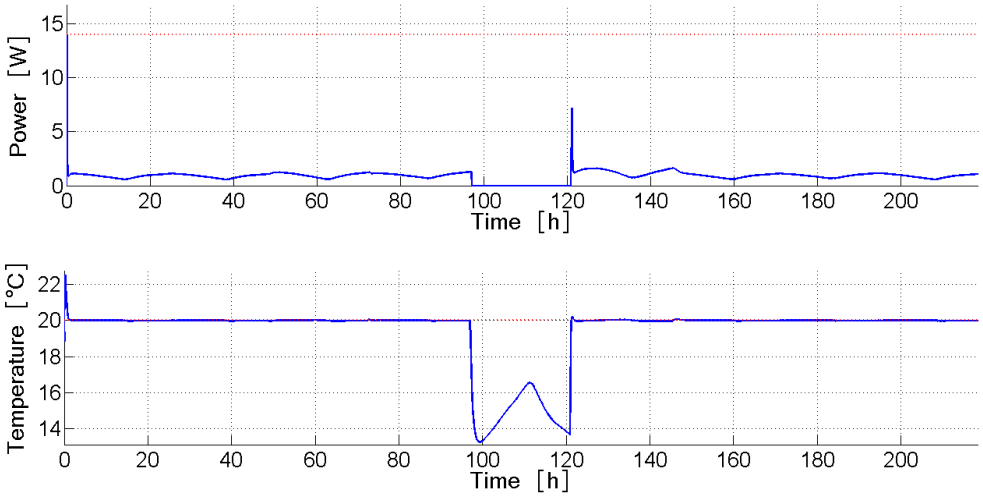

Figure 7.16: OTL21 - Side Optical Bench - Power and Temperature Profiles

It is exactly from this relative maximum that an information about the thermal control robustness is derived, as this peak is the worst case to add an uncertainty to.

In Figure 7.17 and 7.18 the behavior of two other heaters is reported. The presence of a relative maximum can be once again observed for the OTL14 of the Interferometer Assembly group, while for the OTL3 heater placed on the M2 Mirror of the third group another type of consideration has to be made.

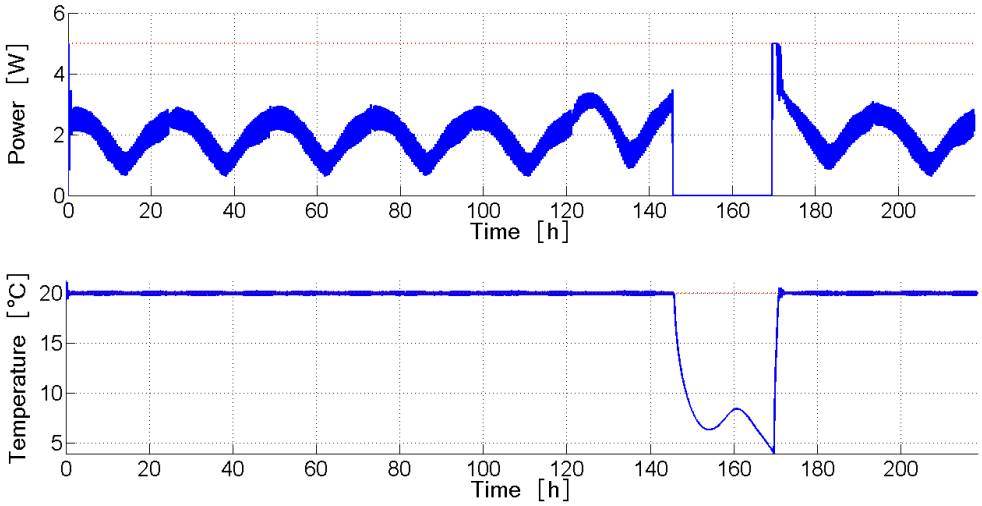

Figure 7.17: OTL14 IA Bench - Power and Temperature Profiles

The same principle at the basis of the relative minimum arising in the first two heaters presented, is the cause for the OTL3 of the Sun intrusion. For the second mirror an excessive Sun heating is not avoidable, leading to an undesired deviation from the stability condition at which they find themselves during the rest of the orbit period. In this case the estimation of the margin can not be done by measuring the gap between the relative maximum during the shutdown period and the set point, since it would be negative. The margin is instead considered by looking at that difference between the maximum of the temperature profile corresponding to the region of the orbit that is normally controlled, thus just before, or after, the Sun intrusion. This margin would then tell how far is the component, having not considered the uncertainties, to the set point in a region of controllability, having accepted the impossibility to control the component in the overheated region.

Table 7.10 presents the margin obtain by the test phase prediction for the different heaters, presented as positive when measured in a normally controlled

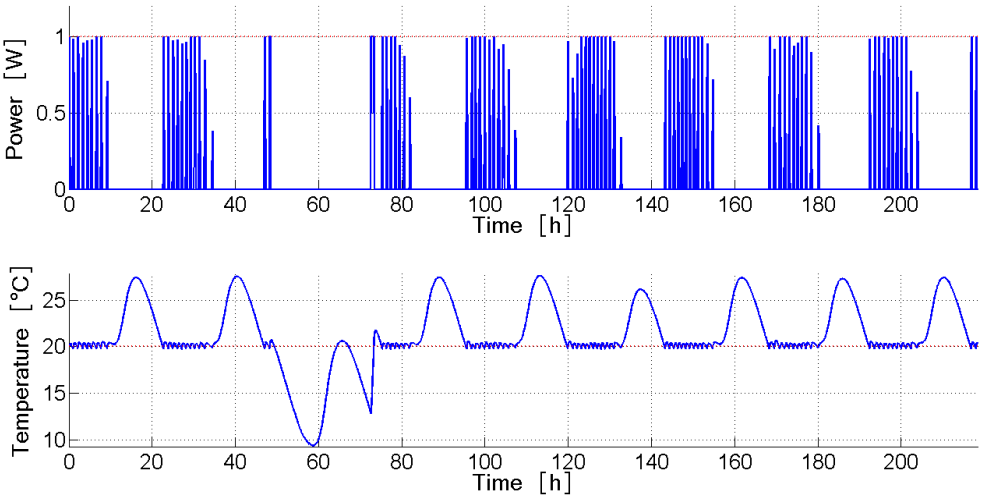

Figure 7.18: OTL3 M2 Mirror - Power and Temperature Profiles

region, and as negative when Sun intrusion is spotted.

Group Number	Deactivation Time	Heater	Positive Margin	Negative Margin
1	0-24 [h]	OTL15	5.5°C	- - -
		OTL16	8°C	- - -
		OTL34	0.5°C	9°C
2	24.26-48.26 [h]	OTL23	1°C	2°C
		OTL30	3°C	2°C
		OTL31	4°C	6°C
		OTL36	6°C	4°C
3	48.54-72.54 [h]	OTL2	5°C	1°C
		OTL3	7°C	0.5°C
		OTL4	9°C	2°C
		OTL5	12°C	2°C
		OTL6	2.5°C	- - -
		OTL7	8°C	1.5°C
		OTL26	0.2°C	- - -
4	72.8-96.8 [h]	OTL19	10°C	- - -
		OTL20	10°C	- - -
5	97.06-121.06 [h]	OTL21	3.5°C	- - -
		OTL22	3.5°C	- - -
		OTL29	1.5°C	- - -
6	121.32-145.32 [h]	OTL8	19°C	3°C
		OTL9	3°C	- - -
		OTL10	1°C	- - -
		OTL11	19°C	1°C
		OTL12	2°C	- - -
		OTL13	19°C	1°C
7	145.58-169.59 [h]	OTL14	12°C	- - -
		OTL27	12°C	- - -
		OTL28	11.5°C	- - -
8	169.85-193.86 [h]	OTL18	33°C	- - -
		OTL17	14°C	- - -
9	194.12-218.12 [h]	Radiative Plate	10°C	- - -
		East-West Encoder	10°C	- - -
		North-South Encoder	45°C	- - -
		Interface Plate	11.5°C	- - -

Table 7.10: Heater Subcooling Operational Thermal Line Groups

In Table 7.11 are reported the main simulation parameters for the phase. The sequence used to the deactivation of the heaters groups is from one to nine, during which the instrument is spinning to reproduce the orbital environments, each of this phases being preceded and followed by a stabilization period of ten hours during which the instrument is fixed in a position corresponding to the initial condition of the orbit. A stabilization is needed, otherwise each shutdown phase would be contaminated by the effects of the precedent one.

The fluxes are set to a hot case level due to the aim of this phase: since the objective is to observe the gap between the inactive heater temperature and its set point, the situation in which this gap is the shortest is when the spacecraft is heated the most, which is the most probable case in which an uncertainty could lead to an increase of temperature; the same can be said for the dissipation level, which has been set to the maximum.

Simulation Variables	Value
Heater lines	ON - shut down by groups
Instrument configuration	$NS = -9.7°$; $EW = 0.0°$
Spinning system	+15.04 / 0.0 $[deg/min]$
LSS Boundary Temperatures	GN2 / LN2
Sun Simulator	1398 $[W/m^2]$
Thermal Coating Properties	BOL
Units Dissipations	Maximum

Table 7.11: Heater Subcooling Main Simulation Variables

The scanner configuration has been selected after the arising of extreme temperatures on the optics. This phases in fact foresees a long exposure of the solar baffle and the scanner to the direct solar radiation: in such a condition the canonical configuration of the scanner would reflect the rays directly to M1 and M2 causing an unbearable increase of temperature. The selected configuration of the scanner instead, guarantees a deviation sufficient to direct most of the solar fluxes to the inner baffle allowing an indirect and gentler heating of the optics. It has to be underlined that not only the scanner is responsible for the temperature increase of M1 and M2, but a big role is also played by the flip in mirror. According to its position, the FIM makes the radiation either continue its path to the detectors

(causing the M3 and M4 to experience high temperatures), or reflect it black to M2 and M1 (practically doubling the heating on these mirrors), or deviate it towards the chamber shrouds. The latter one is the best condition to the protection of the optics, but has been found not to be sufficient to maintain the internal components at a reasonable temperature, reason why the above mentioned configuration of the scanner was chosen.

7.8 Sun Intrusion - Half Cone Angle

The Half Cone Angle identifies a possible scenario of the spacecraft orientation, representing a particular stressing condition for the optics. A previous analysis of this case was performed by OHB AG, that found a critical range of incident angles when the Sun lies on the X_{sc}, Y_{sc} plane, and its rays are impinging the spacecraft with an inclination of less than 5.5° with respect to the Z_{sc} axis. This situation where the Sun is exactly in front of the field of view of the solar baffle, is possibly damaging for the optics if the canonical position of the scanner is considered (e.g. detumbling operations). By considering an exposure period of 180 seconds, representing the requested duration for the instrument depointing from a Sun intrusion condition to a safer one, where the solar baffle is pointed to the deep space, a sample of the angles between the 0° and 5.5° is tested. The most stressed component during this scenario is the M2, onto which the analysis is focused. Two parts of the mirror are considered, differing in the temperature limits: the front of the mirror, with an admissible temperature of 58°C, and the so called "glue line", the link between the mirror and its support, with an allowed calculated temperature of 43°C. The designed test phase has then as objective the verification of the M2 design, which is suppose to survive the here defined Sun intrusion for a period of time necessary to execute a depointing.

Simulation Variables	Value
Heater lines	ON - Survival mode
Instrument configuration	Scanner canonical position FIM in Black Body Configuration
$+Z_{sc}$ - Sun Beam Incident Angles	0°, 1°, 2°, 3°, 4°
LSS Boundary Temperatures	GN2 / LN2
Sun Simulator	0 - 1371 $[W/m^2]$
Thermal Coating Properties	BOL
Units Dissipations	OFF

Table 7.12: Half Cone Angle Main Simulation Variables

Due to the several increases of temperature expected, the phase design kept as a driver the minimization of the stabilization periods between each sun expo-

sure. To this aim the external conditions of the chamber and of the instrument were adjusted consequentially, as noticeable in Table 7.12, by turning off the dissipating units, using the survival thermal lines and activating the solar simulator exclusively during the three minutes of exposure useful for the generation of the desired behavior.

The limited number of incident angles considered is due to the stabilization of the mirror requested after each exposure in order to regain the initial condition to test the next one; a finer investigation would lead to a substantial increase of the phase duration, while a restriction in the number of the angles considered can still give a good indication of the mirror's behavior.

For what concerns of the Flip In Mirror, its configuration has been set to Black Body to avoid possibly damaging reflections on the M2, and to protect the rest of the mirrors that would have been hit by the solar radiation if the FIM would have been left open.

In Figures 7.19 and 7.20 the results for the M2 front and glue line are presented, predicting the capability of the M2 to undergo these particular loads.

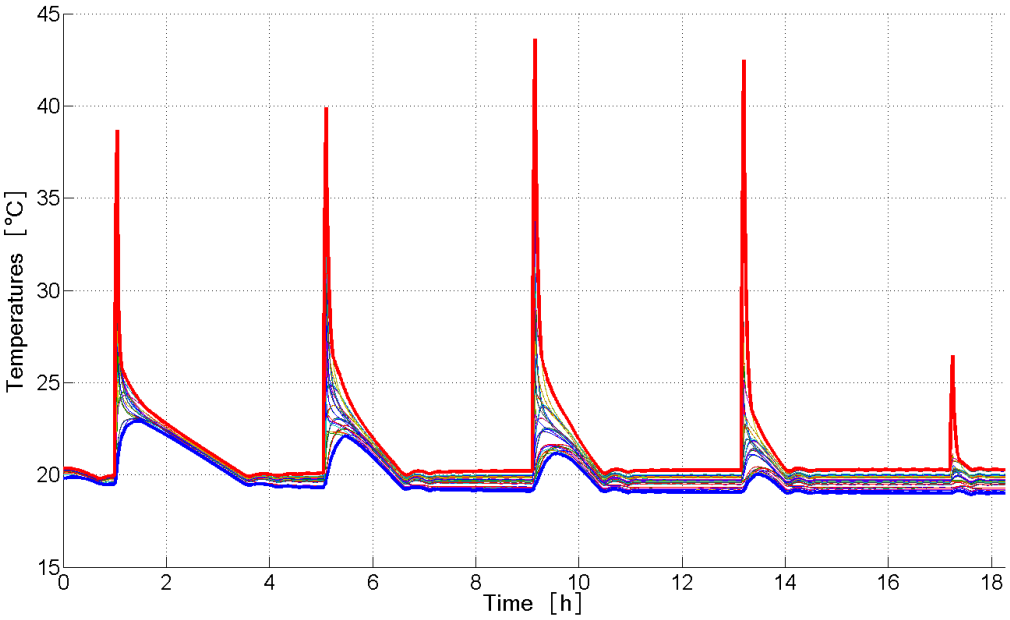

Figure 7.19: M2 Mirror Temperature Profile at different incident angles with the solar beam

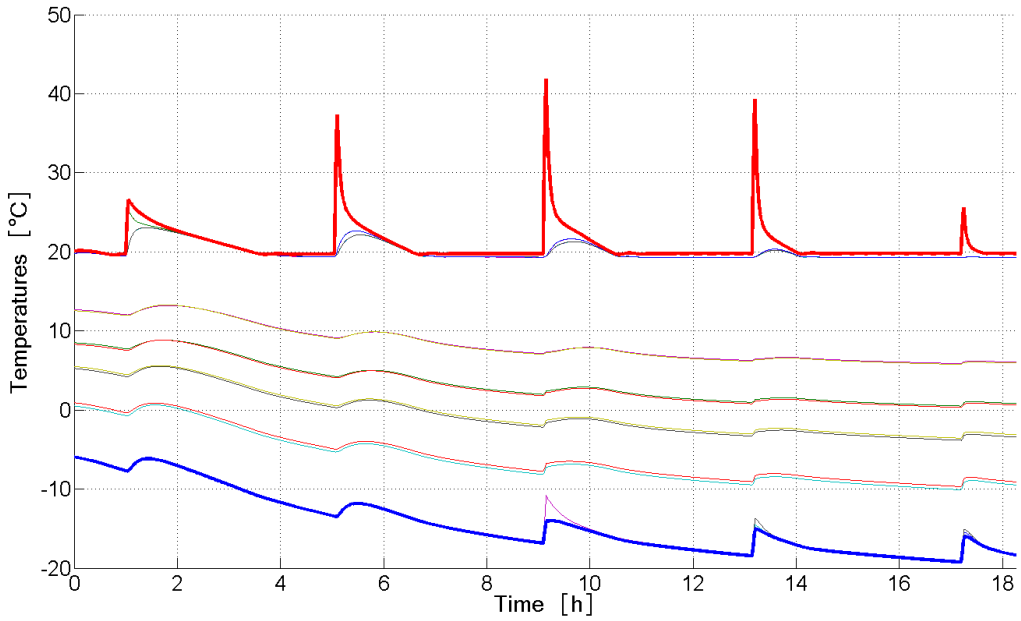

Figure 7.20: M2 Glue Line Temperature Profile at different incident angles with the solar beam

By looking at the spikes for the different incident angles, a general trend can be identified, according to which the third exposure experienced by M2 results to be the most critical, corresponding to an incident angle of 2°.

7.9 Operational Cold Case - Equinox

One of the most important load cases is the Equinox, which is the sizing cold case for many components and therefore needs to be tested. The peculiarity of this case lies into the long eclipse experienced by the satellite, starting at 11 hours and 23 minutes and ending at 12 hours and 32 minutes from the beginning of the orbit. The absence of solar fluxes in that period of time will strongly influence the temperature profiles of the optics, and an abrupt decrease of temperature is expected during that period of time. In Figures 7.21 and 7.22 are reported the orbital temperature profiles for M1 and M2, which are consistent with the external condition of the eclipse.

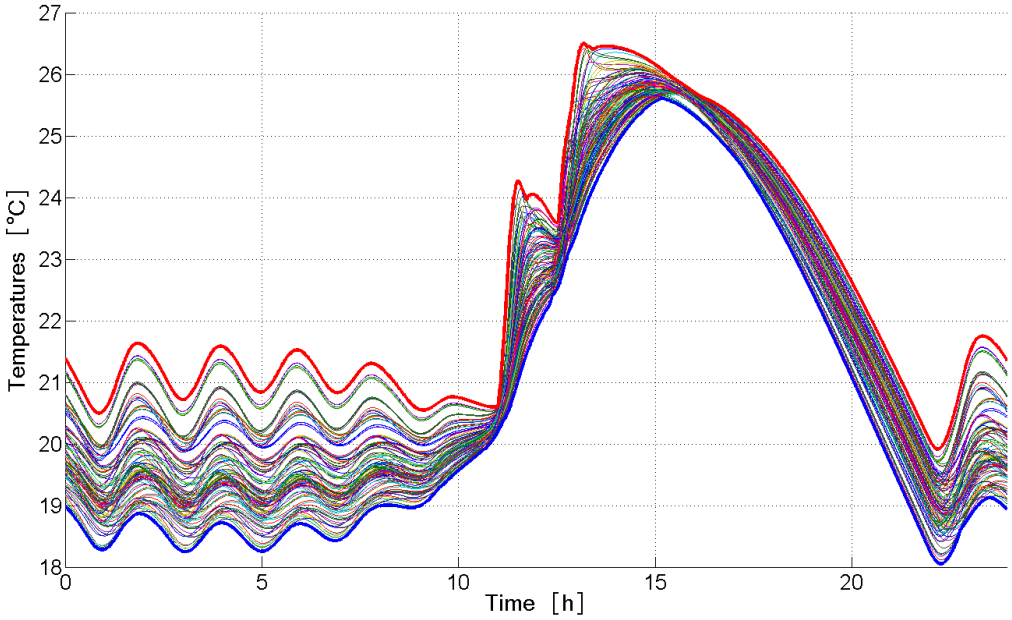

Figure 7.21: M1 Equinox Orbital Temperature Profile

It is possible to notice in the temperature profile of M1 the fast cooling down due to start of the eclipse, which last until the temperature immediately increases in proximity of the end of it. This dynamics is less marked on M2, but the effect of the eclipse is still observable in the two slight changes of the temperature slope coinciding with the start and the end of the eclipse. A thermal analysis carried out by considering the solar fluxes generated in presence of a scan law showed a minimal difference with respect to the results obtained with the scanner fixed in canonical position. Being the variations minimal between the two cases, it was

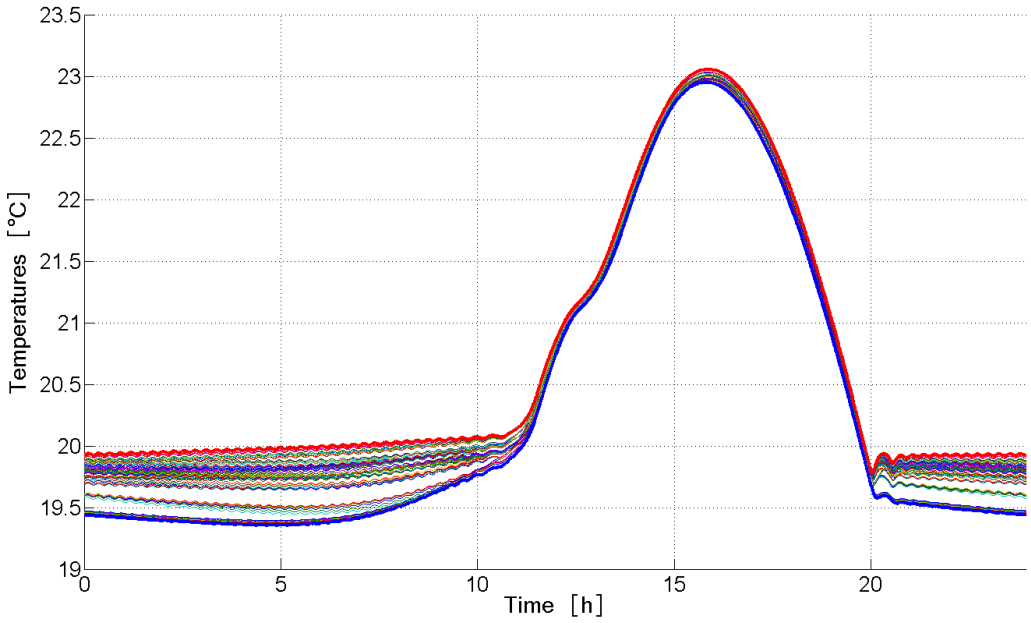

Figure 7.22: M2 Equinox Orbital Temperature Profile

decided to opt for a conduction of the test phase with the scanner kept in its canonical position, giving the precedence to the simplicity of execution.

In Table 7.13 the main simulation parameters are reported.

Simulation Variables	Value
Heater lines	ON - Operational mode
Instrument configuration	Scanner canonical position
Spinning system	+15.04 $[deg/min]$
LSS Boundary Temperatures	GN2 / LN2
Sun Simulator	1371 $[W/m^2]$
Thermal Coating Properties	BOL
Units Dissipations	Minimum
Adapter Interface Plate	$-10°C$

Table 7.13: Equinox Main Simulation Variables

It can be noticed that since EQBOL is an operational case, the heaters used are the OTLs, and that this time the optical properties effectively meet the ones experienced in orbit, since the simulated phase represents a cold case. The Sun Simulator power is lowered to the equinoctial value, and the dissipations are set to the minimum to be compliant with the cold nature of the case.

The results of the simulation are reported in Figures 7.23 and 7.24, showing an overall similarity with the orbital profiles. The duration of the eclipse with its position in the orbit and the shape of the temperature profiles are satisfactorily similar, and the maximal temperatures for M1 and M2 differ respectively 0.5°C and 1.0°C only.

A small difference is observable in the M1 profiles between the orbital and the test case, where a more pronounced spike arises at the beginning of the eclipse. The reason behind this deviation is to be founded in the different ways in which the eclipse was modeled. In the test prediction the an abrupt interruption and reactivation of the solar fluxes has been implemented respectively at the beginning and at the end of the darkening, while the way ESATAN-TMS interprets an eclipse in an orbital simulation consists in a linear decrease and increase of the fluxes within the start and the end of the eclipse respectively.

A further approach to the orbital conditions was not searched in the test phase development, since principal objective of the test simulation is to set the parameters used in the prediction as similar as possible to the conditions that are going to be encountered during the real test, fact that has an unbreakable priority on the adherence to the orbital conditions. Due to this reason and to the lack of information about the shuttering mechanism of the Large Space Simulator, the choice taken was to leave the approximation of the eclipse as an instantaneous stop and restoring of the fluxes. This implementation will work as a basis for a finer modeling as soon as a better knowledge of the shuttering mechanism will be gained.

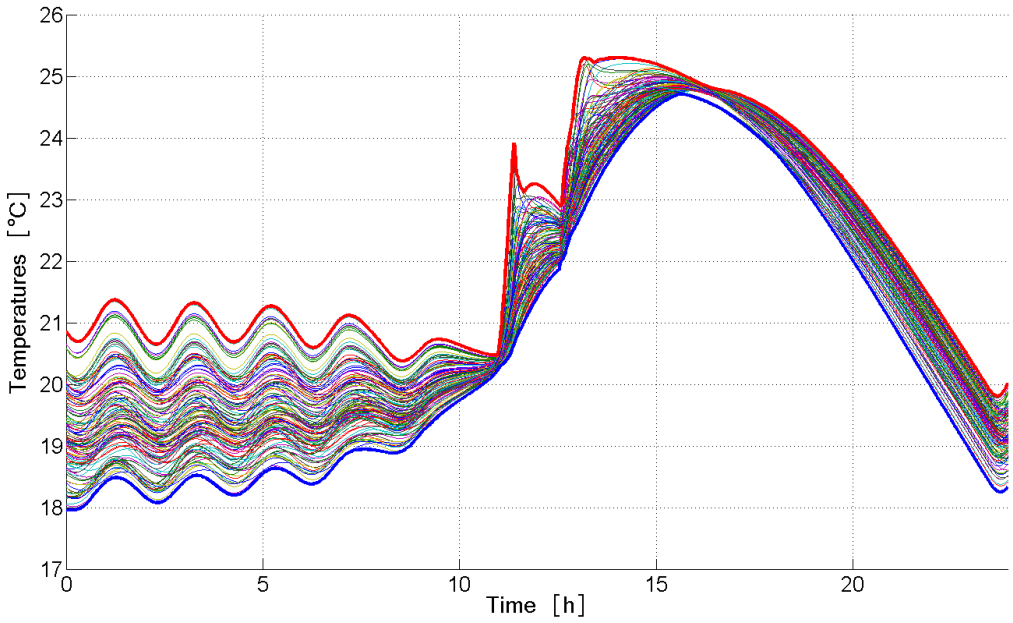

Figure 7.23: M1 Equinox Test Temperature Profile

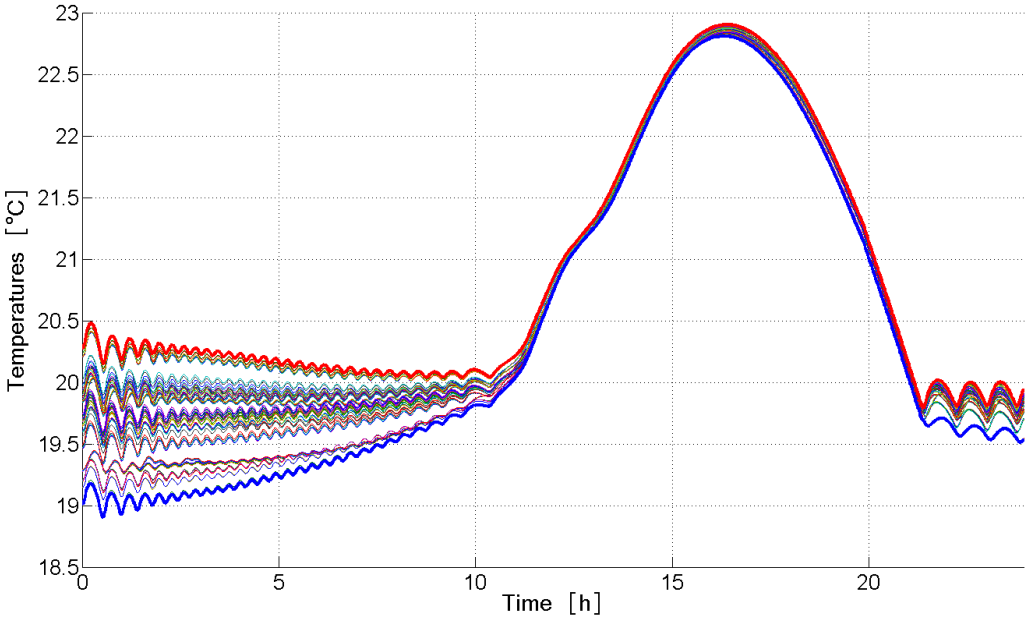

Figure 7.24: M2 Equinox Test Temperature Profile

A second difference identified lies in the slower cool down to the set point temperature of the heaters installed of both the mirrors. Behind this discrepancy, which happens when the inside of the instrument is no longer reached by the Sun rays, an explanation is found in the diversity of environments in the two simulations: in the orbital analysis the outer space is modeled as a black body at 3K, while for the test simulation the environment presents many higher temperatures, the coldest of them being 93K. The fact that the test environment is 90K hotter than the orbital one, makes the maximal test temperatures be slightly above the orbital ones.

7.10 Cold Case - Summer Solstice

This phase objective is to test the Summer Solstice cold case, where the solar declination is fixed at 23.5°, thus not letting the solar radiation fully penetrate inside in the of the instrument.

As already explained the instrument can not be tilted inside the test chamber due to the heat pipe presence, that would otherwise not function. For this reason an alternative way of testing the Summer Solstice case was investigated, making use of the scanner to deviate the incoming ray in a horizontal configuration of the instrument.

Similarly to what it was done for the Day56B test phase, a minimization of the solar fluxes on M1 and M2 was searched, with the only exception that this time not only a single orientation of the instrument was considered, but rather the minimization was searched for the whole period of time when the scanner is exposed to the solar radiation. As a first step a radiative case has been run, by considering once again each of the nine orientation of the scanner, as similarly done in the first hot phase development, and calculating the absorbed fluxes for each orientation of the inner instrument during Sun exposure.

After post processing the results, an optimal motion for the scanner was found, which is reported in Table 7.14, and which was finally used to calculate the fluxes for the solution.

IRS angle	From −180° to −359°	From 0° to 180°
North-South	−9.7°	−9.7°
Easth-West	+5.4°	−5.4°

Table 7.14: Summer Solstice Fluxes Minimization Configuration

In Table 7.15 the main simulation parameters are reported.

Simulation Variables	Value
Heater lines	ON - Operational mode
Instrument configuration	Fluxes Minimization
Spinning system	+15.04 [$deg/hour$]
LSS Boundary Temperatures	GN2 / LN2
Sun Simulator	1326 [W/m^2]
Thermal Coating Properties	BOL
Units Dissipations	Minimum
Adapter Interface Plate	$-10°C$

Table 7.15: Summer Solstice Main Simulation Variables

The results obtained through the test prediction are in this case consistently divergent from the orbital calculations. M1 presents a temperature deviation of almost 6°C, while the difference for M2 is slightly lower than 5°C. Moreover, the different orientation of the scanner causes a sensible anticipation of the temperature maximum, which in the test case happens two hours sooner than in the orbital case.

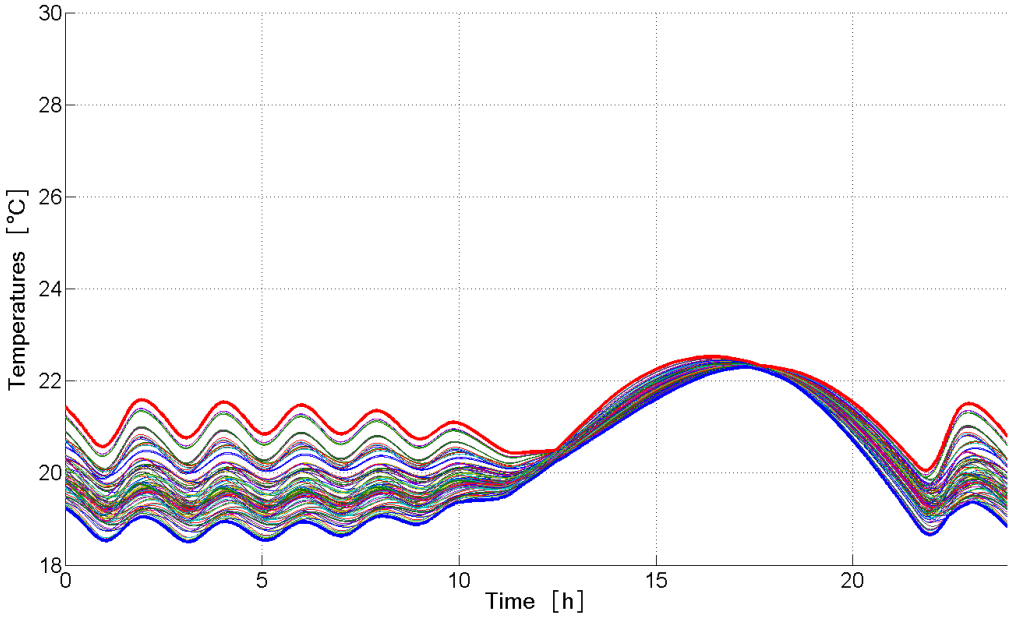

Figure 7.25: Summer Solstice M1 Orbital Temperature Profile

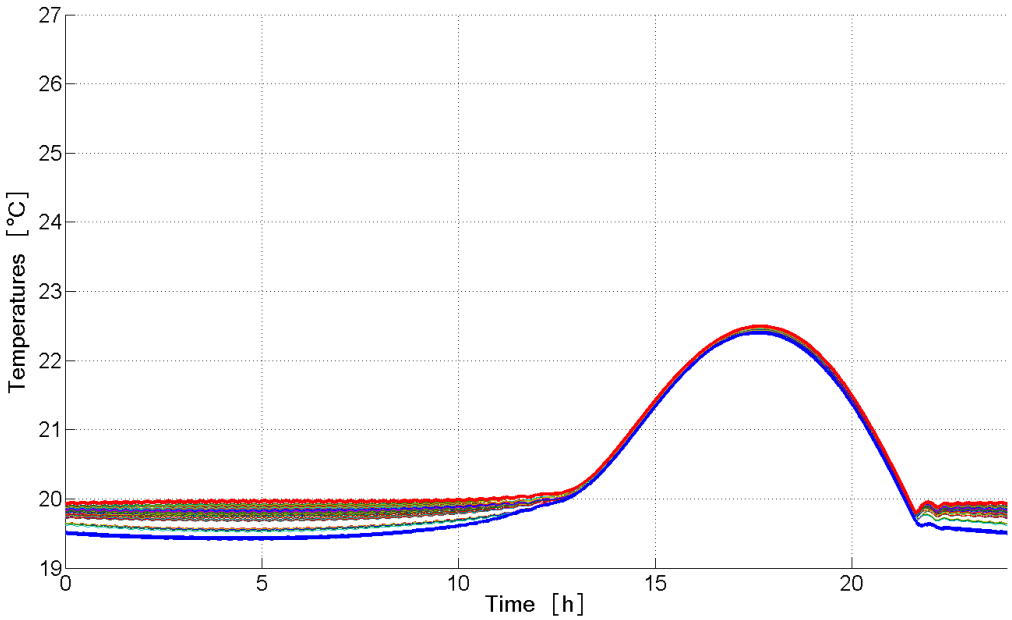

Figure 7.26: Summer Solstice M2 Orbital Temperature Profile

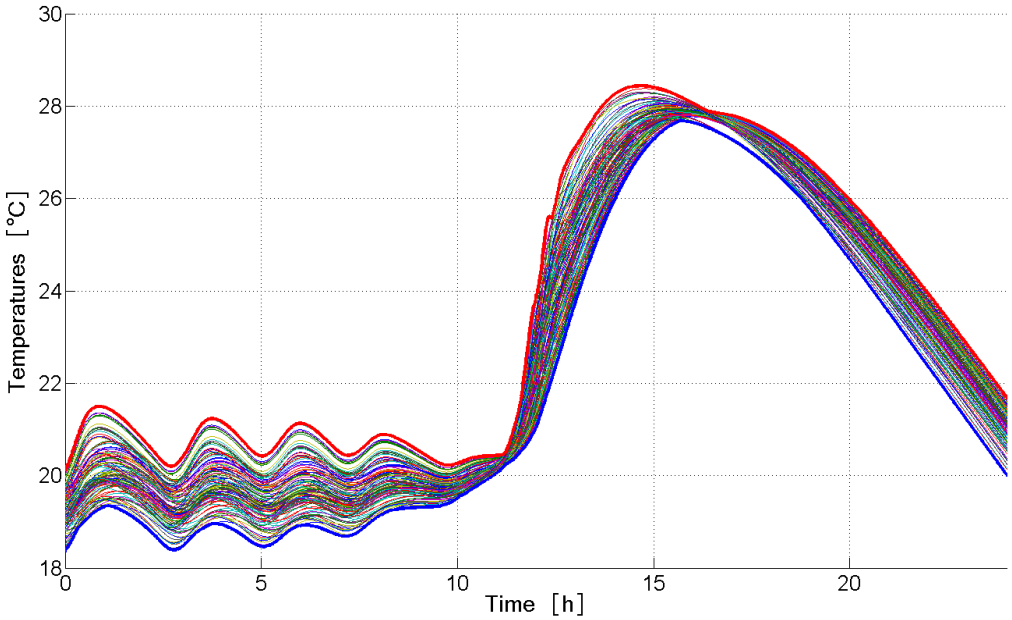

Figure 7.27: Summer Solstice M1 Test Temperature Profile

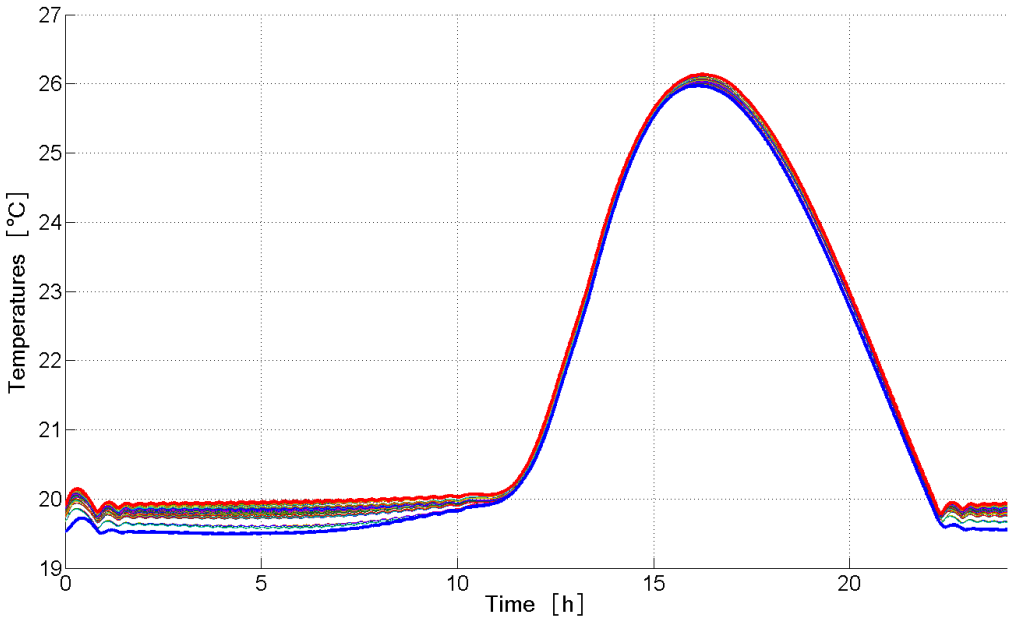

Figure 7.28: Summer Solstice M2 Test Temperature Profile

7.11 Heater Sensitivity

Coherently with the indications received from the ECSS, the present phase has been designed with the objective of gaining sensitivity data about the thermal control of the spacecraft. As the name suggests, the phase will focus on the observation of the heater performances in case of an increase of the set points, which will be risen of the expected model uncertainty of 3K, while the needed power will be read and stored.

Ideally it would be necessary to perform this procedure one heater line per time, unfortunately the big amount of lines, together with a needed stabilization period in between, would lead to a very long duration of the phase. The approach followed is once again based on the definition of groups.

Differently from the heater subcooling phase, for this sensitivity analysis the groups have been selected in order to contain heaters independent with each other, so that when their set point will be simultaneously raised, no mutual heating will occur. It is interesting to notice that by following this procedure, the heaters in the surrounding will have no influence on the ones currently tested, since they would not be able nor to increase or decrease the temperature of their controlled points. The reference condition to determine the power variation can not be taken inside of those sub-phases where a heater group is always being tested, since the injected power in the surrounding heaters will constantly vary in relation to the set point just increased. As reported in Table 7.16, the simulation parameters has been set identical to those valid during the Summer Solstice, with the only difference on the groups set point that are step by step risen up for the duration of an orbit time.

Between each of these sub-phases, a stabilization phase has been introduced in order to re-cool down of the heaters measured points that have just been tested, and to regain the initial condition needed to the start of the next phases. The stabilization phases are executed by keeping the satellite fixed in its safe mode orientation ($-Z_{sc}$ facing the solar simulator), which is the starting point for each orbital simulation. This stabilizations phases are based on a "Go/no go" principle, where the "go" condition is reached once all the sensors of the heater lines respected the stabilization criteria of showing a maximal temperature change of 1K in 1 hour, or once three hours have passed from the start of the sub-phase. The "no go" condition is true until the last heater line reaches its stabilization criteria or until three hours passed from the start of the sub-phase.

Simulation Variables	Value
Heater lines	ON - Operational mode
Instrument configuration	Fluxes Minimization
Spinning system	+15.04 [$deg/hour$]
LSS Boundary Temperatures	GN2 / LN2
Sun Simulator	1326 [W/m^2]
Thermal Coating Properties	BOL
Units Dissipations	Minimum
Adapter Interface Plate	$-10°C$

Table 7.16: Heater Sensitivity Main Simulation Variables (core phases only)

In Figure 7.29 the first group is presented as an example. The heaters independence has been searched by considering components distant from each other, and attention has been paid while considering the conductive and radiative couplings between them. As a general rule, it was tried to select heaters belonging to different thermal enclosures. Taking as reference the first group, it can be noticed how the heaters chosen are parts of different components way distant one from the other, and how a none of them directly sees the others nor conductively or radiatively: the first mirror has no direct coupling with nor the Laser Assembly Unit or the Cold Finger Radiator, and the radiative coupling with Back Telescope Assembly is "filtered out" by the Inner Baffle, not showed in the image.

In Figure 7.30 is observable the typical power and temperature profile achieved by the heaters in this phase. From 3 to 27 hours the the controlled point is kept 3° above its nominal temperature, which corresponds to a thickening of the power trend. In Table 7.17 the results of the different phases are presented. The heaters placed on the Optical Bench have been separately tested, since this subsystem, placed in the middle of the instrument, has a non-negligible influence on all the rest of the components. For what concerns the OTL34 does not show a power difference since the calculation was executed with a heater related to an old and problematic model of the Front End Electronics, which was in the meanwhile replaced.

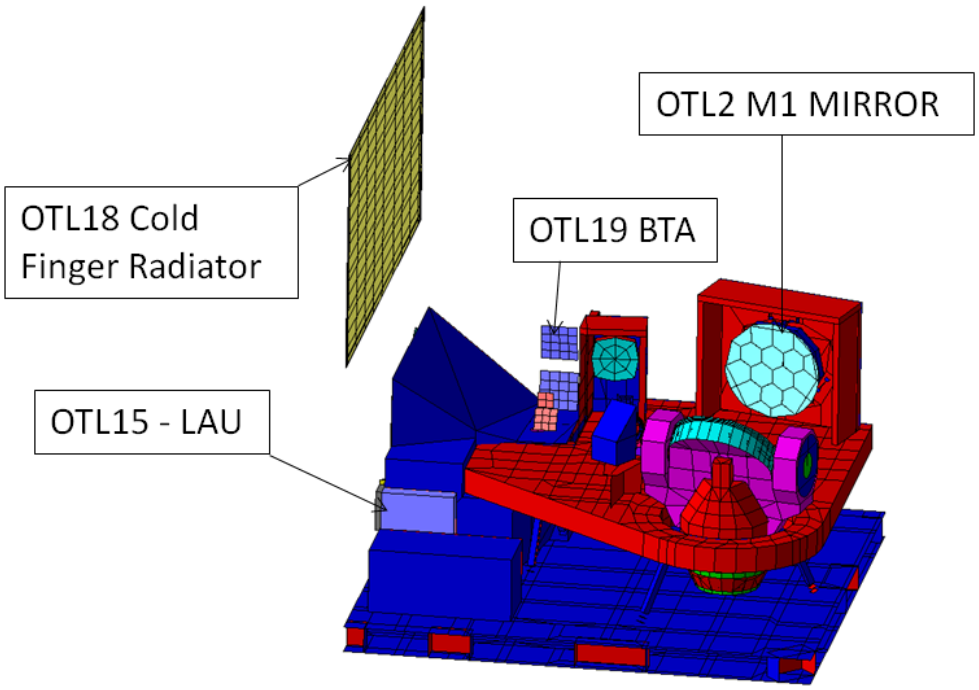

Figure 7.29: Heater Sensitivity 1^{st} Group of Independent Heaters

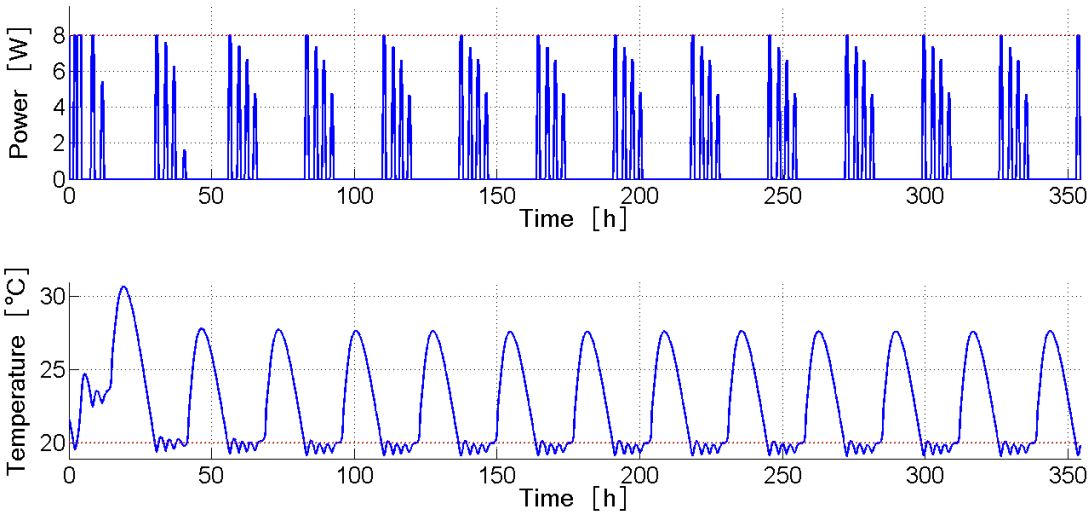

Figure 7.30: OTL2 Heater of the 1^{st} Group Temperature and Power Profile

Group	OTL Heater	Location	Set Point [From/To] [°C]	Power Difference [W]
1	OTL2	M1 - Mirror	20/23	0.25
	OTL15	Laser Assembly Unit	16/19	4.51
	OTL18	Cold Finger Radiator	-12.5/-9.5	11.89
	OTL19	Back Telescope Mirror Support	0/3	0.46
2	OTL4	M1 - Support	20/23	1.15
	OTL7	M4 - Mirror	20/23	0.24
	OTL16	Instrument Control Electronics	18/21	5.00
	OTL20	Back Telescope Bench	0/3	1.40
3	OTL3	M2 - Mirror	20/23	0.03
	OTL28	Interferometer CC	20/23	2.91
	OTL29	Side Optical Bench	20/23	1.98
	OTL31	Instrument Support Panel	20/23	1.43
4	SCA2	East-West Encoder	20/23	2.89
	OTL5	M2 - Support	20/23	0.63
	OTL14	Interferometer Bench	20/23	2.95
	OTL17	Compressor Radiator	-10/-7	10.33
	OTL21	Side Optical Bench	20/23	0.68
	OTL30	Instrument Support Panel	20/23	0.65
5	SCA1	Radiative Plate	20/23	0.21
	OTL6	M3 - Mirror	20/23	0.11
	OTL23	Instrument Support Panel	20/23	1.03
	OTL27	Interferometer RAU	20/23	4.99
6	SCA4	North-South Encoder	20/23	1
	OTL22	Side Optical Bench	20/23	0.78
	OTL36	Instrument Support Panel	20/23	4.32
7	SCA3	Interface Plate	20/23	1.07
	OTL26	M3 - Support	20/23	0.49
	OTL34	Front End Electronics	18/21	0.00*
8	OTL8	Main Optical Bench	20/23	3.35
9	OTL9	Optical Bench Center - Y	20/23	2.28
10	OTL10	Optical Bench Center mx	20/23	3.80
11	OTL11	Optical Bench Center	20/23	2.24
12	OTL12	Optical Bench Center px	20/23	2.06
13	OTL13	Optical Bench Center +Y	20/23	2.98

Table 7.17: Heater Sensitivity Phase Results

7.12 Decontamination Case

The Detection and Electronics Assembly (DEA) is supposed to undergo through a decontamination operation, during which the sensitive items such as the LWIR and MWIR detectors, the cold optics and the cold box are brought to a sufficiently high temperature to get rid of the contaminants which are expelled through a vacuum pipe. The operational decontamination, which is enabled whenever ice forming thickness allocation is reached during in-orbit life, consists of the following operations:

- Warm-up: an increase of the sensitive items temperature from their operational to the decontamination temperature. The success criteria to determine the correctness of application of this operation is the achievement of all sensitive items at a temperature greater than 200K.
- Stabilization: the sensitive items should not fall below the decontamination limit temperature of 200K during two hours.
- Cooling down: the operational temperature is recovered.

Following a conservative approach with regards to the sequence duration, the warm up and stabilization phases should be performed in a safe mode (Table 7.19), while the opposite is true for the execution of the cooling down phase, which is likely to be tested in a hot case condition. If the decontamination operations would be carried out by following their standard order, a change in the external conditions (e.g. solar fluxes and internal dissipations) should find place just between the stabilization and the cooling down phase, causing an increase in the duration of execution and adding complicatedness to the test. Due to this reason, and since the cooling down of the detectors was already tested into the first hot case, in this phase only the warm up and stabilization operations will be performed.

The Warm-up is executed by means of an operational heater, whose main characteristics are reported in 7.18.

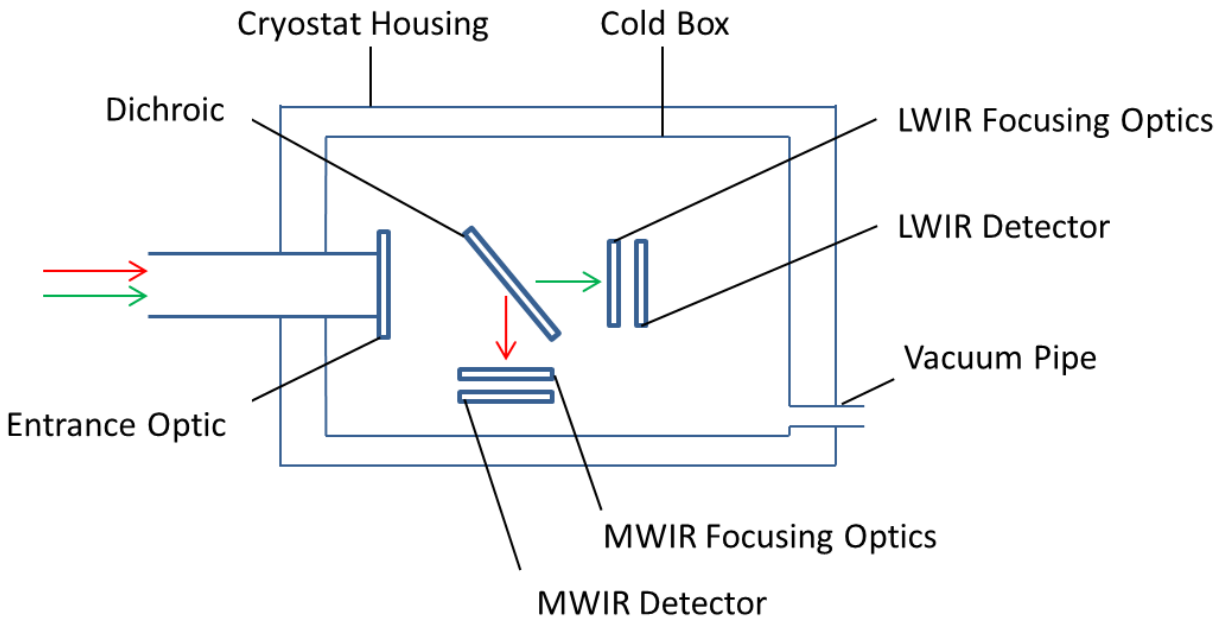

Figure 7.31: Detection Assembly Functional Sketch

Parameter	Value
Proportional Gain	10.0
Maximum Power	13.0 W
Set Point	$20K$
Control Node Location	Cryostat Housing

Table 7.18: Decontamination Heater Characteristics

The process defined by the DEA subcontractor foresees the decontamination heater to warm up the cryostat housing, which in turns heats up passively the cold box and the sensible items.

In Figures 7.32 and 7.33 the test prediction of the decontamination phase is presented, showing the overcoming of the aimed temperature after 20 hours from its initialization, whose start happen itself at 20 hours from the beginning of the phase. During this initial time the interface plate is brought from its previous temperature of $-10°C$, to the $-40°C$ proper of a safe mode simulation. As soon as this happen, the cryocooler is shut down and the decontamination process can finally begin. At the end of the phase, a margin of three hours was added to the two requested by the requirements on the stabilization.

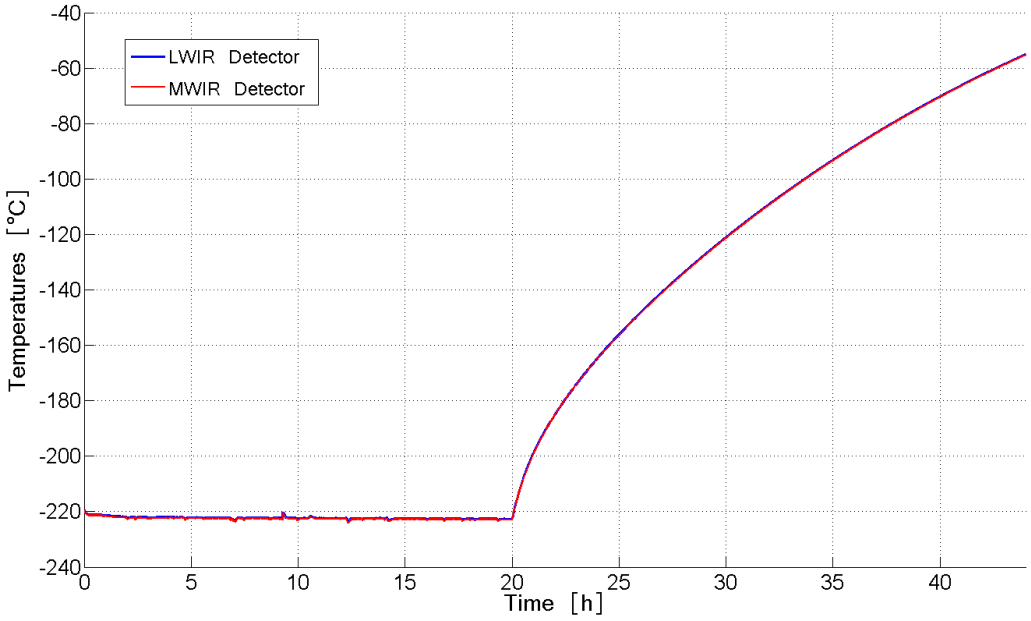

Figure 7.32: LWIR & MWIR Detectors Decontamination Curves

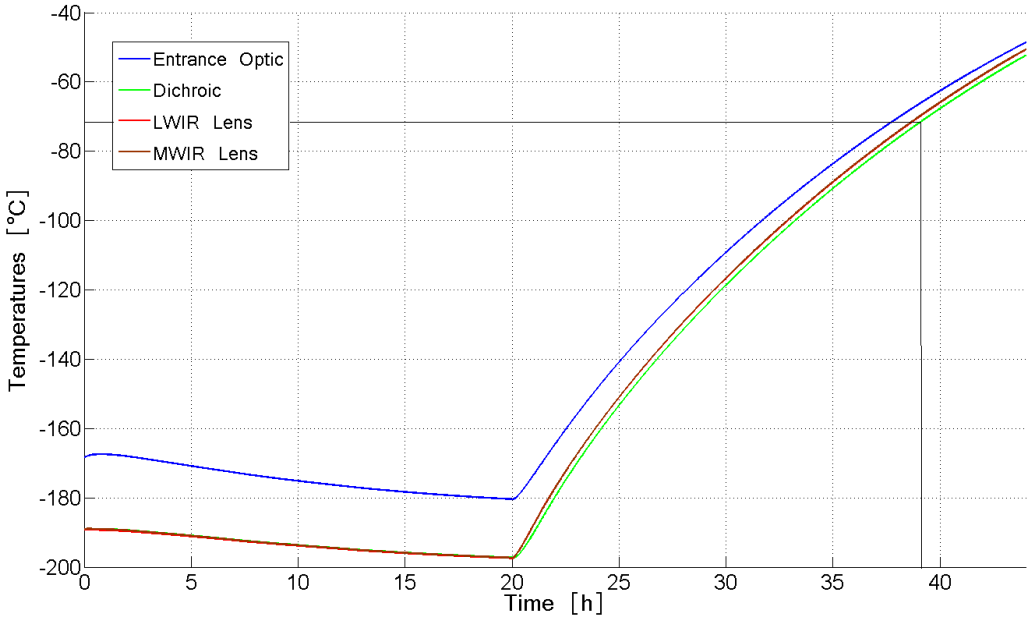

Figure 7.33: Cold Optics Decontamination Curves

Simulation Variables	Value
Heater lines	ON - Survival mode
Instrument configuration	Scanner canonical position $-Z_{sc}$ to Solar Simulator
LSS Boundary Temperatures	GN2 / LN2
Sun Simulator	0 $[W/m^2]$
Thermal Coating Properties	BOL
Units Dissipations	OFF
Interface Plate	$-40°C$

Table 7.19: Decontamination Main Simulation Variables

7.13 Safe Mode

Aim of this test phase is the verification of the safe mode thermal control design. The observation focuses on the correct functioning of the survival thermal lines in terms of controlled temperatures and heaters power as a validation of the goodness of the design. The survival thermal lines are fed by an independent subunit of the Instrument Control Unit (ICU) with respect to the operational lines. During the safe mode the subsystems' components are maintained above their survival temperatures, while the electronics are kept above their lowest switch on temperature. The safe mode sees the solar baffle directed to deep space, and the coldest condition is considered, thus in absence of solar radiation. From Table 7.20, where the descriptive parameters of the test phase configuration are reported, it can be noticed that the solar baffle is facing the shroud of the main chamber opposite to the mirror. This configuration allows the solar baffle and the instrument optics to see the coldest environment possible, while the back of the IRS, which is thermally controlled at -40°C, is not affected by the presence of the hotter mirror.

Simulation Variables	Value
Heater lines	ON - Survival mode
Instrument configuration	Scanner canonical position $-Z_{sc}$ to Solar Simulator
LSS Boundary Temperatures	GN2 / LN2
Sun Simulator	0 $[W/m^2]$
Thermal Coating Properties	BOL
Units Dissipations	OFF
Interface Plate	$-40°C$

Table 7.20: Safe Mode Main Simulation Variables

As understandable, the Sun simulator is assumed to be turned off, as well as the dissipating units inside the instrument.

STL Heater	Location	Set Point [°C]	Power Installed [W]	Power Average [W]
SCA1	Radiative Plate	2	25	2.87
SCA2	East-West Encoder	2	25	0.03
SCA3	Interface Plate	2	25	1.76
SCA4	North-South Encoder	2	25	3.53
STL2	M1 - Mirror	2	6	2.48
STL3	M2 - Mirror	2	1	0.18
STL4	M1 - Support	2	1	0.34
STL5	M2 - Support	2	1	0.88
STL6	M3 - Mirror	2	15.3	12.24
STL7	M4 - Mirror	2	24	23.77
STL8	Main Optical Bench	2	17	13.25
STL9	Optical Bench Center - Y	2	8.4	6.25
STL10	Optical Bench Center mx	-18	20	17.08
STL11	Optical Bench Center	-38	60	36.58
STL12	Optical Bench Center px	-38	100	78.44
STL13	Optical Bench Center +Y	2	10	9.52
STL14	Interferometer Bench	2	24	7.15
STL16	Instrument Control Electronics	-38	40	19.73
STL17	Compressor Radiator	-38	24	4.60
STL18	Cold Finger Radiator	2	80	37.87
STL26	M3 - Support	-18	8	5.59
STL27	Interferometer RAU	2	13	4.47
STL28	Interferometer CC	-18	15	13.21
SUM			**567.7**	**301.82**

Table 7.21: Survival Thermal Lines Results

The safe mode test prediction results, presented in Table 7.21, confirm the proper functioning of the survival thermal lines, which already showed a stabilization within the first hours of the simulation, thus allowing to lighten the test duration by considering this phase to only last six hours.

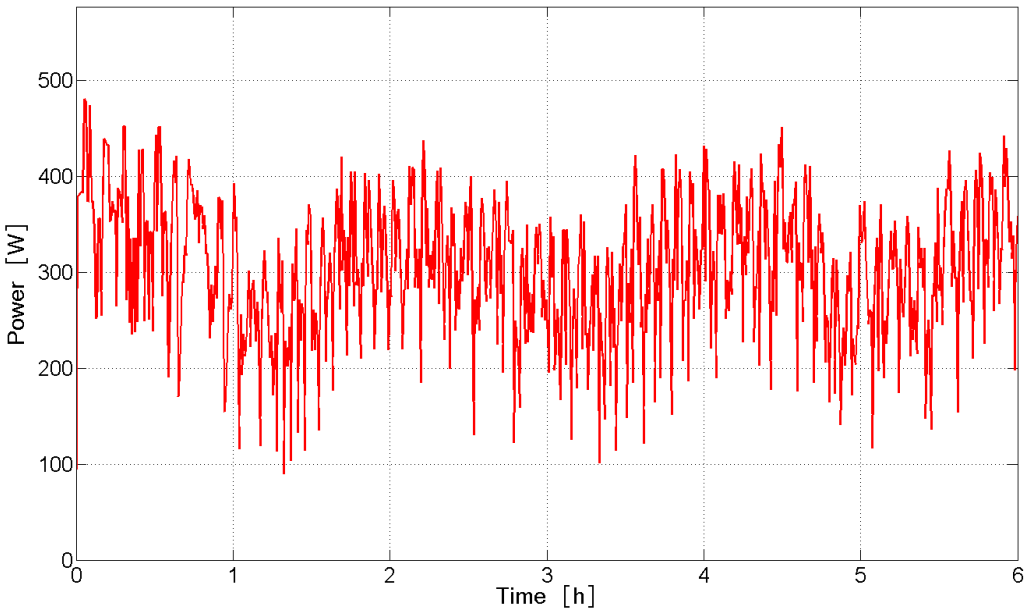

Figure 7.34: Safe Mode Total Heater Power vs. Time

7.14 Safe OTL

The operational heater lines have been designed including the ability of keeping all units above their minimum switch-ON temperature, without the aid of the survival lines. This peculiarity of the design finds its utility during the passage from the safe mode to an operational mode, where the units need to be switched on, as well as the operational heater lines. The STLs and OTLs in fact, can not be operated simultaneously by the Instrument Control Unit and the OTLs need to maintain the survival set point in order to guarantee the passage to the operational mode. The Safe OTL test phase is included to verify this capability of the operational thermal lines, which dispose of a higher total power, but distributed among a bigger amount of lines with respect to the survival ones. The test configuration, whose main parameters are presented in Table 7.22, is substantially equal to the safe mode one, with the only exception of the operating heater lines used.

Simulation Variables	Value
Heater lines	ON - Survival mode
Instrument configuration	Scanner canonical position
Spinning system	$-Z_{sc}$ to Solar Simulator
LSS Boundary Temperatures	GN2 / LN2
Sun Simulator	0 $[W/m^2]$
Thermal Coating Properties	BOL
Units Dissipations	OFF
Interface Plate	$-40°C$

Table 7.22: Safe OTL Main Simulation Variables

Once again, the results are listed in form of a table (7.23), where the heater average has been monitored in order to get an useful information for the battery sizing. As for the safe mode, the heater power and temperature stability is achieved in only six hours.

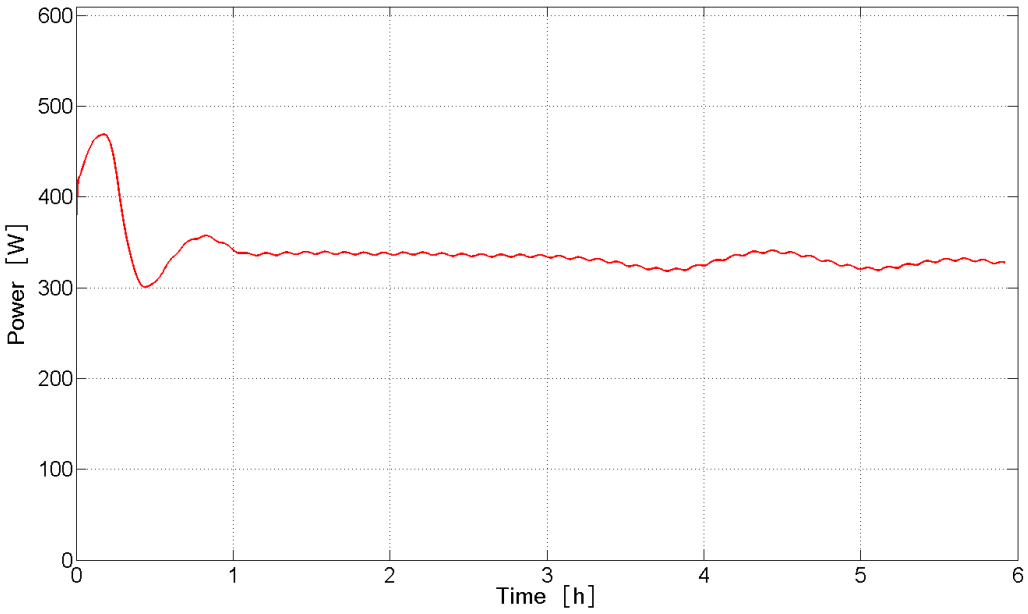

Figure 7.35: Safe OTL 5 Minutes Power

0TL Heater	Location	Set Point [°C]	Power Installed [W]	Power Average [W]
SCA1	Radiative Plate	2	25	2.87
SCA2	East-West Encoder	2	25	2.86
SCA3	Interface Plate	2	25	1.89
SCA4	North-South Encoder	2	25	3.90
OTL2	M1 - Mirror	2	8	2.36
OTL3	M2 - Mirror	2	1	0.13
OTL4	M1 - Support	2	5	4.71
OTL5	M2 - Support	2	5	4.99
OTL6	M3 - Mirror	2	1	0.16
OTL7	M4 - Mirror	2	1	0.84
OTL8	Main Optical Bench	2	12	9.49
OTL9	Optical Bench Center - Y	2	10	7.21
OTL10	Optical Bench Center mx	2	16	9.87
OTL11	Optical Bench Center	2	10	5.19
OTL12	Optical Bench Center px	2	8	5.35
OTL13	Optical Bench Center +Y	2	15	10.30
OTL14	Interferometer Bench	2	5	2.68
OTL15	Laser Assembly Unit	-18	10	5.38
OTL16	Instrument Control Electronics	-18	20	14.85
OTL17	Compressor Radiator	-38	40	36.57
OTL18	Cold Finger Radiator	-38	240	122.25
OTL19	Back Telescope Mirror Support	2	6	2.84
OTL20	Back Telescope Bench	2	4	3.34
OTL21	Side Optical Bench	2	14	0.64
OTL22	Side Optical Bench	2	14	0.71
OTL23	Instrument Support Panel	2	20	17.12
OTL26	M3 - Support	2	7.5	0.59
OTL27	Interferometer RAU	2	5	0.41
OTL28	Interferometer CC	2	5	3.20
OTL29	Side Optical Bench	2	14	1.91
OTL30	Instrument Support Panel	2	15	10.08
OTL31	Instrument Support Panel	2	20	18.56
OTL34	Front End Electronics	2	15	13.96
OTL36	Instrument Support Panel	2	20	10.70
SUM			**666.5**	**337.9**

Table 7.23: Safe OTL Results

7.15 Shroud Warm Up, Pressure Recovery & Specimen Inspection

At the end of the test the shrouds are brought back to the ambient temperatures, following the curves previously reported in Figure 5.2. Once again the shrouds warm up process has been linearly approximated, being their actual temperature profiles not relevant for correlation purposes.

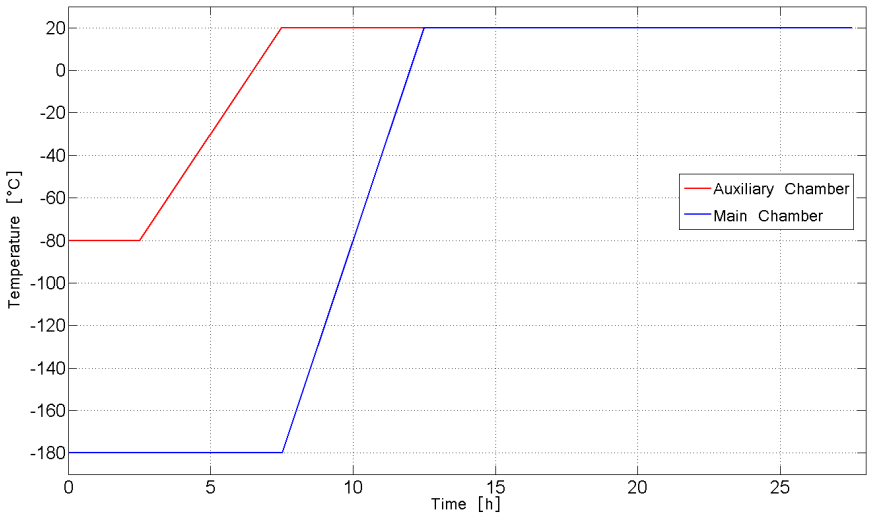

Figure 7.36: Main and Auxiliary Chambers Approximated Warm Up Profiles

Afterwards, the recovery of the pressure can be started, which is here assume to conclude after ten hours, leaving space to the final specimen installation.

Simulation Variables	Value
Heater lines	ON - Operational mode
Instrument configuration	Scanner canonical position
Spinning system	$-Z_{sc}$ to Solar Simulator
LSS Boundary Temperatures	Warm Up
Sun Simulator	0 $[W/m^2]$
Thermal Coating Properties	BOL
Units Dissipations	ON
Adapter Interface Plate	$+40°C$

Table 7.24: Shroud Cool Down Main Simulation Variables

Chapter 8

Conclusions

In this chapter the conclusions of the thesis are presented under the form of test duration, criticalities encountered and the future work expected on the way of the thermal balance test preparation.

8.1 Test Duration

Figure 8.1 reports the phases duration, while the overall test was found to last 34.3 days. It can be noticed that the most time demanding phases are those regarding the verification of the thermal control systems: Heater Subcooling and Heater Sensitivity.

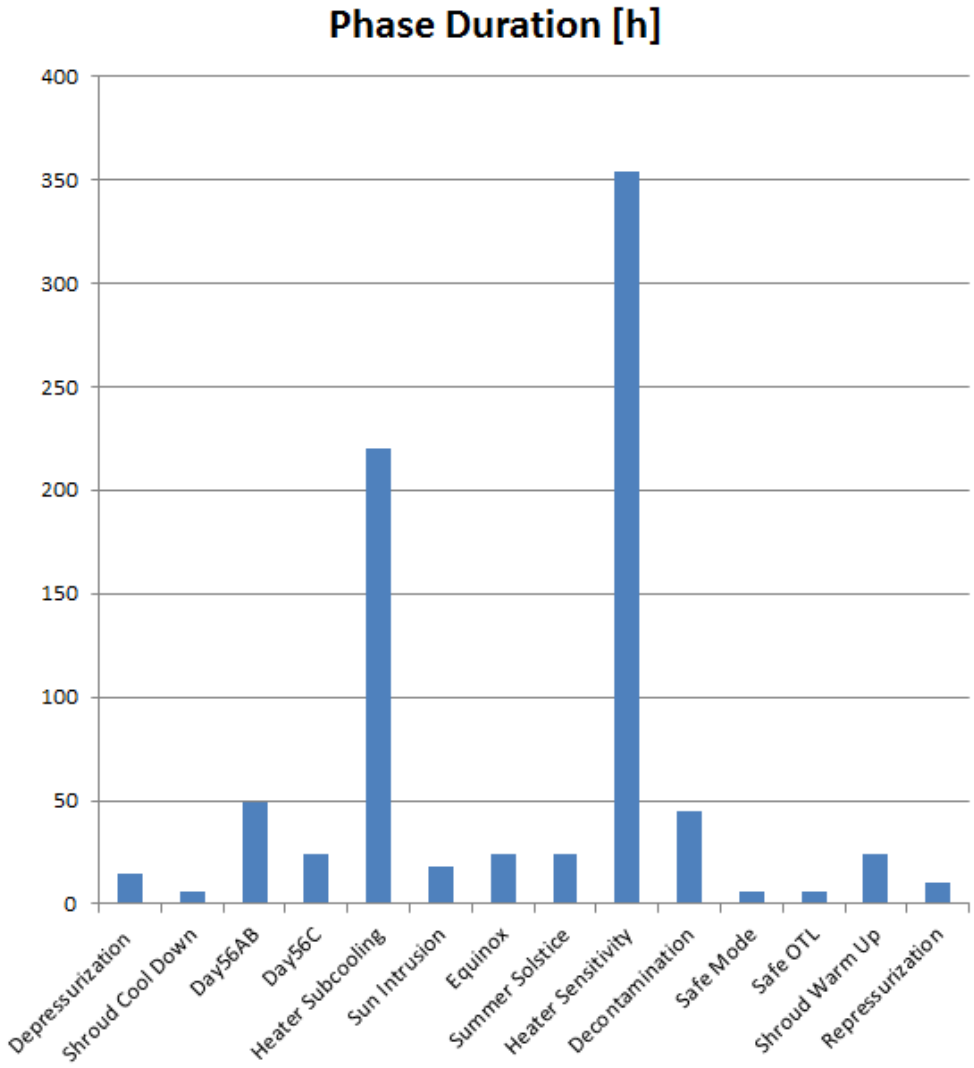

Figure 8.1: Phases Duration

It is therefore natural to ask ourselves if it could be possible to save some time. It must be said that Heater Sensitivity already underwent a compression process of its duration, introduced by choosing to deactivate the heaters by independent groups rather than singularly: a reduction of these phase would necessarily mean a loss of accuracy in establishing the power needed for the set point of the heaters. The same consideration is true for the Heater Subcooling phase, where the groups of heaters chosen did not completely satisfied their requirement of independence. If the test duration will be considered excessive, it will be a duty of the thermal department to carry out a trade-off between accuracy and quantity of informations

to be obtained, and the overall testing period of time.

8.2 Criticalities

As explained in the ϵ-effect isolation, the M1 stabilization is achieved at only 5°C from its limit temperature. This margin could be additionally increased for example by considering a lower intensity of the solar simulator, thus accepting to split this investigation from the observation of the detectors cooling down sequence and introducing an additional phase to the thermal balance test.

The study carried out on the operational hot case, Day56C, suggests that a orbital simulation comprising the observation of the characteristic spikes is theoretically feasible and presents a high degree of adherence with the orbital loads thanks to the test scan law produced. Nevertheless its execution is rather complex since it requires a synchronized control of the chamber spinbox with the instrument scanner, that has to assume the orientation dictated by the test scan law at precise relative angles between the instrument and the solar beam.

The predictions regarding the Summer Solstice shows that regardless the minimization developed on the solar fluxes impinging the optics, the temperature difference of M1 and M2 between the orbital and test cases remains pretty high (6°C-4°C), therefore the inclusion of this phase into the thermal balance test could be eventually rediscussed.

8.3 Open Points & Future Work

It is also here to underline that the work done is based on the available informations on the Large Space Simulator, and on its latest numerical model which introduces several simplifications. An eventual deeper insight into the optical model of the mirror, and on the temperatures achieved by the shrouds, could help to better simulate the chamber conditions to the real ones.

The lack of detail had on the Sun simulator shuttering mechanism did not allow to finely implement the eclipse, happening during the Equinox phase, and the

several shuttering actions taken during Day56B and Sun Intrusion.

A consistent approximation of the chamber behavior was done by considering the spectral irradiance of the solar generator as identical to that one of the Sun. This difference will have to be taken into account by considering the spectral irradiance of the LSS solar generator into the calculations, as an additional convergence to the real test conditions.

With respect to the adapter developed, an open point remains for the cryogenic plate installed below the Encoder Radiator to simulate the space conditions. This choice was done again in part due to the lack of information about the spinbox behavior, that was assumed to be controlled at $-180°C$, in part due to the presence of the adapter legs inside the field of view of the radiator. Its presence is not mandatory and strictly depends on the unverified possibility to cryogenically cool down the spinbox shroud, and on the impact that the legs of the adapter would have on the radiator cooling capacity. The interface plate design between the adapter and the instrument, that will be deeper discussed in Appendix A, will have to be refined by investigating its equilibrium temperature for the different test phases, proof that will give a measure of the margin existing for its controllability. It is left for the thermal department of OHB to verify for the qualification and availability of the thermal coating chosen for the interface plate, which have not to be taken for granted. If regions of uncontrollability of the interface plate should arise with a different coating, it is suggested to operate the shuttering mechanism to workaround the temperature increase.

As a last consideration, it would be useful to implement the possibility to execute the thermal balance phases calculation within a single run, and not through separated analysis as it was done in this thesis. Such an implementation would also fix some issues encountered in the PID regulation of the heaters, since it was not possible to store and reinsert the integrative parameters from one phase to the next one; moreover this would considerably reduce the time needed to conduct the analysis.

All in all, the thesis work on the thermal balance test does not want to definitely fix the test procedure, but is a guideline which presents pros and cons of the phases analyzed, serving as a basis for the next analysis to be conducted with a newer model of the IRS.

Bibliography

[1] David G. Gilmore et al. (2002) emphSpacecraft Thermal Control Handbook, Volume I: Fundamental Technologies, David G. Gilmore Editor

[2] J. Meseguer, I.Pérez-Grande and A. Sanz-Andrés (2012) *Spacecraft Thermal Control*, Woodhead Publishing

[3] ITP Engines UK Ltd. (2013) *ESATAN-TMS Workbench User Manual*

[4] ITP Engines UK Ltd. (2013) *ESATAN-TMS Thermal User Manual*

[5] European Cooperation for Space Standardization (2007), *Space engineering - Thermal control* (ECSS-E-31A), ECSS Standard

[6] Jakob K. Hirthammer (2014), *Umsetzung und Automatisierung einer Thermaltestvorhersage für Satelliten*, Technische Universität Dresden

[7] K. Lattner (2013), *IRS Design and Technical Description*, Internal Document

[8] M. Killian (2013), *IRS Analysis Report*, Internal Document

[9] L. Morgenroth (2014), *IRS Thermal Verification Approach*, Internal Document

[10] I. Melendo (2014), *IRS Thermal Control Hardware Design*, Internal Document

[11] S. Wolff (2015), *IRS DEA Detailed Thermal Design and Analysis Technical Note*, Internal Document

[12] P.E. Dupuis (2011), *Large Space Simulator - Facility Description*, European Space Agency Document

[13] P. Poinas, C. Gomez-Hernandez (1997), *Esarad Geometrical Mathematical Models of the Large Space Simulator Chamber*, European Space Agency Document

Appendix A

Adapter Interface Plate

Along the test prediction, the behavior of the interface plate has been observed as the simulation variables change in the different test phases. As anticipated in Chapter 6, the plate has been white painted, following the idea of minimizing its α/ϵ ratio to achieve sufficiently low temperatures for a finer thermal control. While conducting the calculations, it has been found that the initial properties considered for the white paint ($\alpha = 0.1, \epsilon = 0.9$), where satisfying the controllability requirement for the hot cases and for the safe mode, but it was also discovered that during the cold cases the plate temperature did not stabilize below the wished limit. This is explicable by considering that despite the lower solar constant acting in the cold cases, the needed temperature for the plate is lowered to $-10°C$ against the $+40°C$ of the hot cases. It is than natural that an equilibrium below the hot case limit does not guarantee a cooling down, since the equilibrium temperature of the plate could also find place between the $-10°C$ and $+40°C$. From here the decision to change the optical coating to "barium sulphate with polyvinyl alcohol" ($\alpha = 0.06, \epsilon = 0.88$), that finally led to a lower equilibrium in the plate temperature also during the cold cases.

In Table A.1 a brief summary of the interface plate control results is presented, for those phases requiring it. During the rest of the test, the plate is either controlled or uncontrolled in function of the state at which it will be needed by the next phase. During "Shroud Warm Up", the plate is brought from the ambient temperature to $+40°C$, to prepare it to the execution of Day56AB, Day56C and Heater Subcooling. In Half Cone Angle, the plate set point is brought to $-10°C$, adapting its temperature for the Equinox, Summer Solstice and Heater Sensitivity

phase. Before starting the decontamination, the plate is left cool down to $-40°C$ until the Safe OTL phase ends, falling the need of controlling the plate during Shroud Warm Up.

Test Phase	Aim Temperature	Maximum Deviation
Day56AB	$+40°C$	$0.7°C$
Day56C	$+40°C$	$0.8°C$
Heater Subcooling	$+40°C$	$0.6°C$
Equinox	$-10°C$	$0.5°C$
Summer Solstice	$-10°C$	$0.3°C$
Heater Sensitivity	$-10°C$	$0.3°C$
Decontamination	$-40°C$	$1°C$
Safe Mode	$-40°C$	$1°C$
Safe OTL	$-40°C$	$0.3°C$

Table A.1: Interface Plate Control Errors

Appendix B

Temperature Check

While the thesis work was focusing the attention on the optics and few other components, the thermal balance test is actually an occasion to observe and record the behavior of the instrument as a whole. Without having gone into the details, a final check on the maximum and minimum temperatures of the entire instrument have been carried out by considering each phases of the thermal balance test, showing that all the components did not exceed their allowed temperatures. Coherently with the treatment held during the thesis, the achieved limits for the front telescope optics (FTO) and the Entrance and Baffling Assembly (EBA) are here reported, the two subsystems analyzed the most. In Figures B.1 and B.2 the black lines represent the maximum and minimum temperatures achieved during the thermal balance test, while the gray lines represent the correspondent orbital temperatures. The red and blue areas correspond to the survival temperatures in the hot and cold case respectively.

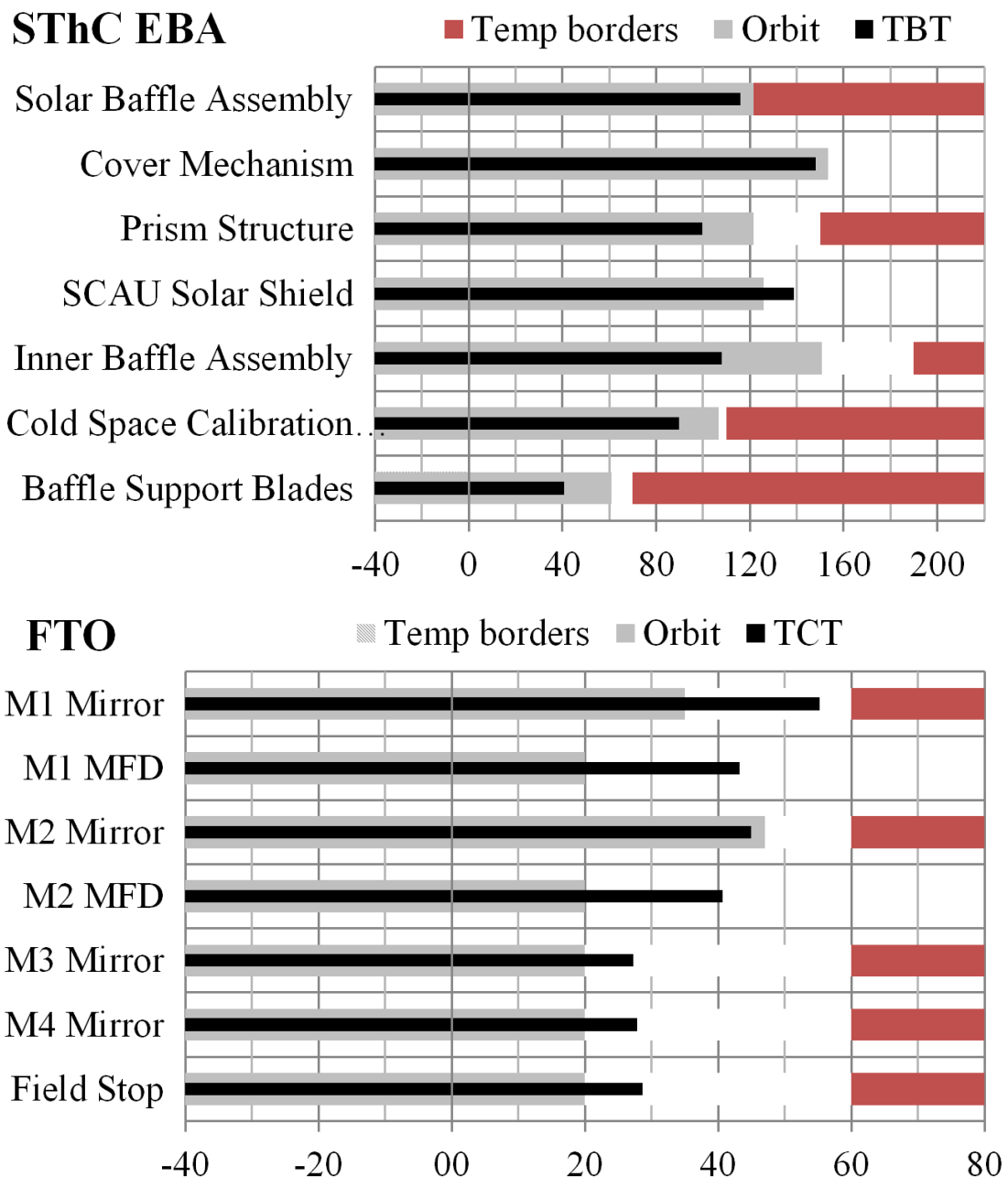

Figure B.1: Maximum Temperatures for the Entrance and Baffling Assembly (above), and the Front Telescope Optics (below) subsystems

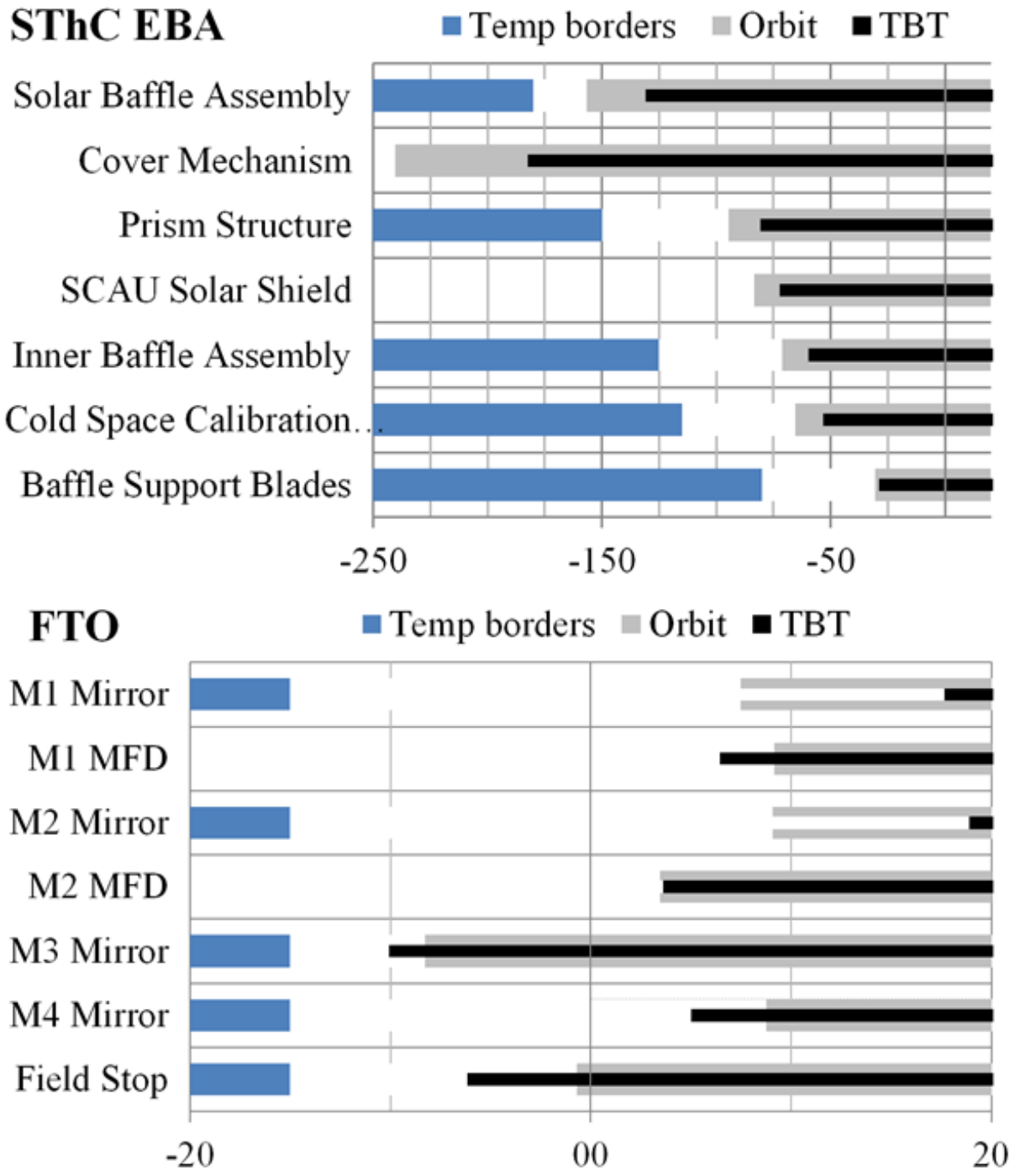

Figure B.2: Minimum Temperatures for the Entrance and Baffling Assembly (above), and the Front Telescope Optics (below) subsystems